COMPRESSIVE SENSING AND WIRELESS NETWORK CAPACITY WITH PERFORMANCE ANALYSIS

by

DAVIS KIRACHAIWANICH

Presented to the Faculty of the Graduate School of
The University of Texas at Arlington in Partial Fulfillment
of the Requirements
for the Degree of

DOCTOR OF PHILOSOPHY

THE UNIVERSITY OF TEXAS AT ARLINGTON

August 2011

To my beloved father Chaiyaporn Kirachaiwanich

who set the example and who made me who I am.

ACKNOWLEDGEMENTS

I would like to thank my supervising professor Dr. Qilian Liang for constantly motivating and encouraging me, and also for his invaluable advice during the course of my doctoral studies.

I would also like to extend my appreciation to National Electronics and Computer Technology Center, Thailand for providing financial support for my doctoral studies.

I would like to express my deep gratitude to my father Chaiyapon Kirachaiwanich and my mother Anukool Areeyakarnlert who have encouraged and sponsored me through my undergraduate and graduate studies. I am extremely fortunate to be so blessed. I am also extremely grateful to my sisters Krissana Juisiri and Apapon Rangdal, and my lovely wife Rachaya Srisurichan for their sacrifice, encouragement and patience.

Finally, I wish to thank all the teachers who taught me during the years I spent in schools in Thailand and the United States. Last but not least, I am grateful to several of my friends who have helped me throughout my career.

March 31, 2011

ABSTRACT

COMPRESSIVE SENSING AND WIRELESS NETWORK CAPACITY WITH PERFORMANCE ANALYSIS

DAVIS KIRACHAIWANICH, Ph.D.

The University of Texas at Arlington, 2011

Supervising Professor: Qilian Liang

This dissertation contains five reseach topics. In chapter 1, the performances of a noncoherent slow frequency-hopping system with M-ary frequency-shift-keyed modulation (NC-FH/MFSK) under various hostile jamming strategies are studied. Then, the knowledge obtained is used in developping a new "combined-jamming" interference model. The model can be used in analyzing the performance of NC-FH/MFSK networks, where transmissions from each network node can interfere with one another. An example application of the proposed model is the channel assignment in a multiradio FH/MFSK wireless mesh network (MR-FH/MFSK WMN).

In chapter 2, the multiradio frequency-hopping wireless mesh networks (MR-WMN) is still being considered. However, the scope of the study is wider. Instead of having each node using NC-FH/MFSK modulation only, this chapter considers the a wider variety of modulation choices, such as M-PSK or M-QAM. To improve the throughput of MR-WMN, the space-time block coding (STBC) technique is introduced in the physical layer and a MAC-layer channel management is also used to combat against two major sources of deteriorations in wireless communications,

the fading channel and cochannel interferences. With the STBC technique, both temporal and spatial diversities can be deployed; hence, the link performance can be improved in the presence of a fading channel. Then, to protect the link from cochannel interferences, an interference-aware algorithm is used to carefully bind the radio interfaces of the nodes to the frequency channels. Within the study, an additional adaptive transmission scheme is also proposed to aids in deciding an optimal number of antennas and selecting the best antenna set for the pending transmission.

In chapter 3, the capacity of wireless hybrid networks, in which a wired network of base stations is used to support very long-range communications between wireless nodes, is investigated. By allowing more than one source node to transmit simultaneously and utilizing successive interference cancellation to decode information at the destination node, a multiple access technique is being introduced to the network. The results show that, for a hybrid network containing n wireless nodes and a wired infrastructure of $b = o(\frac{n}{\log n})$ base stations, with the multiple access concept, the destination or the nearest base stations can receive information from the source nodes at the rate of $O(\frac{b}{n} \log \frac{n}{b})$. But when data is delivered to a node, because the base station is the only transmitter in the cell, it can forward the message to each node only at rate $\Theta(\frac{b}{n})$. This can be further improved by deploying an antenna array or increasing the transmission power of the base stations.

In the last two parts of the dissertation, the compressive sensing (CS) is considered. Compressive sensing can be considered as method to capture and represent compressible signals at a rate significantly below the Nyquist rate. In chapter 4, the compressive sensing scheme is considered from the information theory point of view and derive the lower bound of the probability of error for CS when length N of the information vector is large. The result has been shown that, for an i.i.d. (independent and identical) Gaussian distributed signal vector with unit variance, if the measure-

ment matrix is chosen such that the ratio of the minimum and maximum eigenvalues of the covariance matrices is greater or equal to $\frac{4}{(\frac{M}{K}+1)}$, then the probability of error is lower bounded by a non-positive value; which implies that the information can be perfectly recovered from the CS scheme. On the other hand, if the measurement matrix is chosen such that the minimum and maximum eigenvalues of the covariance matrices are equal, then the error is unavoidable and the perfect recovery can never be achieved.

One of the major challenges in the CS technique is how to design a reconstruction algorithm that can perfectly recover the compressed information. It is known that a family of algorithms using the Orthogonal Matching Pursuit (OMP) technique can offer fast reconstruction and simple geometry interpretation. However, when the compressed observation contains a great amount of noise, the performance of the OMP-based algorithms drops substantially. In chapter 5, a fuzzy forecasting reconstruction algorithm, which can help improving the OMP-based reconstruction algorithm, is proposed. Relying on a collection of the less noisy past information, the algorithm extracts the knowledge in the values of the current compressed information. Using such knowledge together with the noisy observation received, it can better extract both the values and the locations of the sparse coefficients in the information vector. The simulation results have shown that, compared to a standard OMP algorithm performance, an improvement in the ratio of signal to reconstruction error of up to 2 dB, at SNR=15 dB, can be achieved using the proposed approach.

TABLE OF CONTENTS

LIST OF ILLUSTRATIONS

LIST OF TABLES

CHAPTER 1

THE COMBINED-JAMMING MODEL FOR IEEE 802.11 FH/MFSK NETWORKS

1.1 Introduction

The performances of noncoherent slow frequency-hopping receiver with M-ary frequency-shift-keyed modulation (NC-FH/MFSK) under various hostile jamming have been widely studied in several publications in the past decades (see for example [1, 2]). The term, independent multitone jamming (IMTJ), refers to a jamming strategy in which the communication bandwidth is jammed by a pre-specified number of randomly distributed jamming tone: thus a jammed FH (frequency-hopping) band may be jammed with as few as one tone to as many as M tones. In contrary, partial-band jamming (PBJ) is the term use to represent the jamming strategy where the total jamming power is spread evenly over a portion of the bandwidth. Thus, the jamming signal is of a similar characteristic as the AWGN (additive white Gaussian noise), except that it will cover only a fraction of the communication bandwidth.

In this chapter, the exact expressions for determining the BER performance of a NC-FH/MFSK receiver in the presence of the IMTJ and the PBJ is derived. Especially with the IMTJ, a new expression, which is developed from the analysis in [1, 3], for calculating the performance of the receiver, is also proposed. This new BER expression is considered as an alternative to that presented in [4]. It predicts the same BER performance as reported in [4], but with the advantage of one numerical integration less.

Nevertheless, the main contribution in this chapter is from the different perception of the jamming signals taken when applying the expressions obtained from the previous derivations. Specifically, let us consider a data network with nodes communicating via IEEE 802.11 NC-FH/MFSK interfaces. A transmission of one node may cause interference to that of another node in its neighborhood if they occur simultaneously on the same frequency channel, so-called cochannel interference. Thus, to the receiver, the cochannel interferences from these source nodes are equivalent to several jamming tones in the IMTJ. Furthermore, when considering the interference from external networks, it is found that major source of such interferences is generally the signal from co-located IEEE 802.11 b/g networks. Interestingly, the characteristic of this external interferences are somewhat similar to that of jamming signals in the PBJ strategy. To determine the error of a given signal in the network, the two expressions for the IMTJ and the PBJ are combined to obtain a new combined-jamming formula that takes into account both the cochannel and the external interferences.

As an example application for the combined-jamming formula, consider the channel assignment problem in multiradio NC-FH/MFSK wireless mesh networks where each router node being equipped with multiple IEEE 802.11 NC-FH/MFSK interfaces. Using multiple radio interfaces in wireless mesh networks has been widely recognized as a solution for improving its throughput. However, as the number of radio interfaces increases, router nodes in the network tend to interfere more with each other. Unless the channels are carefully assigned to each interface, increasing number of interfaces could, on the other hand, reduce the mesh throughput.

Several publications have proposed different CA algorithms to manage how each interface should access to the shared medium (see for example [5, 6]). One of the most important design issues for these algorithms is how to evaluate the current amount of interferences on each frequency channel, in order to assign the most appropriate

channel to the interface being considered. To stay within the scope of the study, in this chapter, the interference-aware algorithm in [5] is modified and incorporated with the new combined-jamming formula to allow the algorithm to evaluate the amount of interferences on the frequency channels.

This chapter is organized as follows: In Section 1.2 and Section 1.3, the expression for estimating the BER performance of an NC-FH/MFSK receiver in presence of the IMTJ and PBJ is derived. In Section 1.4, the combined-jamming formula for IEEE 802.11 NC-FH/MFSK networks is developed. In Section 2.4 a MR-FH WMN is formulated as an example application for the combined-jamming formula in the channel assignment problem. Section 5.5 concludes the chapter.

1.2 NC-FH/MFSK System Under IMTJ

From Figure 1.1, let assume there are N non-overlapping FH bands, each containing $M = 2^K$ frequency bins, where K is the number of bits per transmitted symbol of the M-ary FSK modulation. Hence, there are NM possible frequency bins for a signal tone to be transmitted. If all FH bands are contiguous, the total communication bandwidth thus equals to $B_T = NB_h$, where B_h is the bandwidth of an FH band. The transmission bit rate of the system is $R_b = KR_s = K/T_s$, where $R_s = 1/T_s$ denotes the symbol rate. The FH system is assumed to be slow hopping, which means the hop period T_h is a multiple of symbol period. The average received power for a symbol, irrespective of the channels effect, is assumed to be $P_s = E_s/T_s$, where E_s is the average symbol energy. The transmitted signal and jamming tones are assumed to encounter an independent fading channel before arriving at the receiver, which uses a noncoherent detection scheme. All fading channels in this study

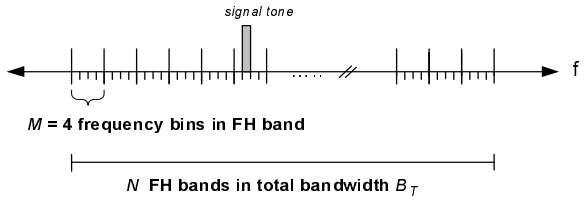

Figure 1.1. FH band setup.

are modeled as slow fading, frequency non-selective Rician processes, whose PDFs (probability density functions) are of the form

$$f_X(x) = \frac{x}{\varsigma^2} \exp\left(-\frac{x^2+\alpha^2}{2\varsigma^2}\right) I_0\left(\frac{\alpha x}{\varsigma^2}\right) u(x) \tag{1.1}$$

where $I_0(\cdot)$ denotes the zeroth order modified Bessel function and $u(\cdot)$ is the unit step function. The symbols α^2 and $2\varsigma^2$ are the average power of the LOS (Line-Of-Sight) ray and the average power of the scattering ray of the fading channel, respectively.

The total number of $q \in [1, NM]$ jamming tones is assumed to be transmitted from the jamming source. These interference tones are assumed to be uniformly distributed over the entire bandwidth B_T, and share equally the total power of P_{jT}. Thus, the received power for each jamming tone is $P_j = P_{jT}/q$.

At the receiver, the received signal will be de-hopped and noncoherently detected. The receive signal after de-hopped can be represented as

$$r(u,t) = x\sqrt{2P}\cos(\omega_m t + \phi) + n(u,t) \tag{1.2}$$

where x is a Rician random variable representing the envelope of the fading channel and its PDF can be represented as (1.1). P is the average received power of the tone, ω_m is the angular frequency for an MFSK (M-ary FSK) symbol, ϕ is unknown phase, and $n(u,t)$ is AWGN with a variance (or power) $\sigma_n^2 = N_0/T_s$.

Because there can be zero or up to $\min(q, M)$ jamming tones in a jammed FH band, hence the probability of symbol error (or symbol error rate, SER) of the NC-FH/MFSK system can be calculated by

$$P_s(e) = P_0 \cdot P_{s0}(e) + \sum_{n=1}^{\min(q,M)} P_n \cdot P_{sn}(e) \tag{1.3}$$

where P_0 and P_n are the probabilities that an FH band is jammed by zero and n jamming tones, where $1 \leq n \leq \min(q, M)$. $P_{s0}(e)$ and $P_{sn}(e)$ are the SER's corresponding to the specified number of jamming tones. Finally, the probability of bit error (Bit Error Rate, BER) can be calculated as

$$P_b(e) = \frac{M/2}{M-1} P_s(e) \tag{1.4}$$

1.2.1 The SER When No Jamming Tone is in the FH Band

The probability that a chosen FH band does not contain a jamming tone can be given by

$$P_0 = \prod_{k=0}^{M-1} (1 - \frac{q}{NM-k}) \tag{1.5}$$

The SER given there is no jamming tone (the FH band is not jammed) can be obtained from [1], [7], and [8] as

$$P_{s0}(e) = \sum_{v=1}^{M-1} \frac{(-1)^{v+1}}{1 + v(1 + \frac{2\varsigma_s^2}{\sigma_n^2})} \binom{M-1}{v} \exp\left[\frac{-v\frac{\alpha_s^2}{\sigma_n^2}}{1 + v(1 + \frac{2\varsigma_s^2}{\sigma_n^2})}\right] \tag{1.6}$$

where α_s^2 and $2\varsigma_s^2$ are the average LOS power and the average scattering power of the signal symbol.

1.2.2 The SER When n Jamming Tones are in the FH Band

The probability that an FH band will be jammed by $1 \leq n \leq min(q, M)$ jamming tones is given by

$$P_n = \prod_{k=0}^{n-1}(\frac{q-k}{NM-k}) \prod_{j=n}^{M-1}(1-\frac{q-n}{NM-j}) \tag{1.7}$$

There are two cases, in which an error can occur. The first is the case when the signal tone is jammed by one of n jamming tones in the FH band, and the probability that one of n jamming tones jam the signal tone is n/M. The second is when no jamming tones is located in the same frequency bin as the signal, i.e. the signal tone is not jammed. The probability of the second case is $(M-n)/M$. Hence, the SER when the FH band is interfered by n jamming tones can be expressed as

$$\begin{aligned} P_{sn}(e|n \text{ jamming tones}) &= (\frac{n}{M})P_{sn}(e|\text{signal is jammed}) \\ &+ (\frac{M-n}{M})P_{sn}(e|\text{signal is not jammed}) \end{aligned} \tag{1.8}$$

1.2.2.1 The Signal Tone is Jammed

When the signal tone is jammed, the average power at the detector output, in the branch where the signal is present, can be expressed as

$$\alpha_{sj}^2 = \alpha_s^2 + \alpha_j^2 + 2\alpha_s\alpha_j \cos\varphi \tag{1.9}$$

where α_j is the average LOS power of the jamming tone, and $\varphi \in [0,2\pi]$ is the random phase difference between the signal tone and the jamming tone. To evaluate the SER when the signal tone is jammed, [3] has provided a computational-efficient method based on the use of phasor representations and noncentral chi-squared PDF's. It can

be shown that, for any two Rician random variables, say R_1 and R_2, $P(R_1 > R_2) = P(R_1^2 > R_2^2)$. In (3) of [3], the probability is given as

$$\begin{aligned} P(R_1 > R_2) &= P(R_1^2 > R_2^2) \\ &= Q\left(\sqrt{\frac{2K_1}{b+1}}, \sqrt{\frac{2K_2 b}{b+1}}\right) \\ &\quad - \left(\frac{b}{b+1}\right) \exp\left(-\frac{K_1 + K_2 b}{b+1}\right) I_0\left(\frac{\sqrt{4K_1 K_2 b}}{b+1}\right) \end{aligned} \tag{1.10}$$

where $K = \alpha^2/2\varsigma^2$ is the Rician factor for the random variables, b=$\varsigma_2^2/\varsigma_1^2$, and Q(x,y) is the Marcum's Q function. Without loss of generality, let assume that the signal tone and one of the n jamming tones that jam the signal tone are present in the first output branch of the detector and the rest of the n-1 jamming tones are in the next consecutive branches. Therefore, the first to the n^{th} output branches of the envelope detector will have the PDF of the Rician distribution and the output of the rest of the $M - n$ branches will follow the Rayleigh distribution. The SER when there are $1 \leq n \leq min(q, M)$ jamming tones in the FH band and the signal tone is jammed can be calculated as

$$\begin{aligned} P_{sn}(e|\text{signal is jammed}) &= 1 - P\{(R_1 > R_2) \cap (R_1 > R_3) \cap (R_1 > R_4)...\} \\ &= 1 - P(R_1 > R_2)^{n-1} \cdot P(R_1 > R_M)^{M-n} \end{aligned} \tag{1.11}$$

The second equality in (1.11) is based on each output of the detector branches being independent of each other. Now, consider the first product term on RHS of the second equality in (1.11). The conditional probability $P(R_1 > R_2|\varphi)$ can be evaluated by substituting the following parameters into (1.10)

$$K_1 = \frac{\alpha_{sj}^2}{2\varsigma_s^2 + 2\varsigma_j^2 + \sigma_n^2}, \quad K_2 = \frac{\alpha_j^2}{2\varsigma_j^2 + \sigma_n^2}, \quad b = \frac{2\varsigma_j^2 + \sigma_n^2}{2\varsigma_s^2 + 2\varsigma_j^2 + \sigma_n^2} \tag{1.12}$$

where ς_j^2 is the scattering power of the jamming tones. Similarly, by treating a Rayleigh random variable as a special case for Rician random variable, the probability for the second product term with a condition on φ can be obtained as

$$P(R_1 > R_M|\varphi) = 1 - \frac{\sigma_n^2}{2(\varsigma_s^2 + \varsigma_j^2 + \sigma_n^2)} \exp\left[\frac{-\alpha_{sj}^2}{2(\varsigma_s^2 + \varsigma_j^2 + \sigma_n^2)}\right] \quad (1.13)$$

By substituting (1.12) in (1.10) to obtain the probability of the first product term with a condition on φ, using (1.13) for the probability of the second product term with a condition on the same variable, and integrating (1.11) over φ, the complete expression for the SER for the casecan then be obtained.

$$\begin{aligned} &P_{sn}(e|\text{signal is jammed}) \\ &= 1 - \frac{1}{2\pi}\int_0^{2\pi} \left\{ Q\left(\sqrt{\frac{\alpha_{sj}^2}{\varsigma_T^2 + \varsigma_j^2}}, \sqrt{\frac{\alpha_j^2}{\varsigma_T^2 + \varsigma_j^2}}\right) - \frac{2\varsigma_j^2 + \sigma_n^2}{2(\varsigma_T^2 + \varsigma_j^2)} \exp\left[-\frac{\alpha_{sj}^2 + \alpha_j^2}{2(\varsigma_T^2 + \varsigma_j^2)}\right] \right. \\ &\quad \left. \times I_0\left(\frac{2\alpha_{sj}\alpha_j}{\varsigma_T^2 + \varsigma_j^2}\right) \right\}^{n-1} \left\{1 - \frac{\sigma_n^2}{2\varsigma_T^2} \exp\left(-\frac{\alpha_{sj}^2}{2\varsigma_T^2}\right)\right\}^{M-n} d\varphi \end{aligned} \quad (1.14)$$

where

$$\varsigma_T^2 = \varsigma_s^2 + \varsigma_j^2 + \sigma_n^2 \quad (1.15)$$

1.2.2.2 The Signal Tone is not Jammed

If none of the jamming tones in the FH band are in signal branch, $n+1$ output branches of the envelope detector will follow the Rician distribution and the rest of the $M-n-1$ branches will follow the Rayleigh distribution. Again, assume that the signal tone is present in the first output branch and each of the n jamming tones is in the next consecutive branches. In this case, the SER can be expressed as

$$\begin{aligned} P_{sn}(e|\text{signal is not jammed}) &= 1 - P\{(R_1 > R_2) \cap (R_1 > R_3) \cap (R_1 > R_4)...\} \\ &= 1 - P(R_1 > R_2)^n \cdot P(R_1 > R_M)^{M-n-1} \end{aligned} \quad (1.16)$$

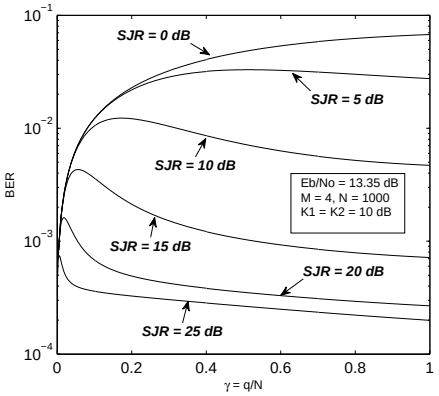

Figure 1.2. The BER performances for NC-FH/4FSK with Rician fading channels against the tone jamming ratio,$\gamma = q/N$, at various SJR values.

The probability $P(R_1 > R_2)$ can be calculated by substituting the following parameters into (1.10)

$$K_1 = \frac{\alpha_s^2}{2\varsigma_s^2 + \sigma_n^2},\ K_2 = \frac{\alpha_j^2}{2\varsigma_j^2 + \sigma_n^2},\ b = \frac{2\varsigma_j^2 + \sigma_n^2}{2\varsigma_s^2 + \sigma_n^2} \tag{1.17}$$

By the same means, the conditional probability for the second product term is found to be

$$P(R_1 > R_M) = 1 - \frac{\sigma_n^2}{2(\varsigma_s^2 + \sigma_n^2)}\ \exp\left[\frac{-\alpha_s^2}{2(\varsigma_s^2 + \sigma_n^2)}\right] \tag{1.18}$$

Finally, the total SER of the NC-FH/MFSK system under the IMTJ can be computed by substituting the corresponding terms into (1.3). Compared to Figure 6 of [4], Figure 1.2 illustrates the same BER performances by using the analysis provided in this section. Nevertheless, it should be noted that the probability of symbol error given that the FH band is jammed by n jamming tones in the signal branch is calculated in (19) of [4] using a numerical approach on the double-integral equation while, in (1.14), the same probability can be evaluated more efficiently using single numerical integration.

1.3 NC-FH/MFSK System Under PBJ

With the PBJ strategy, it is assumed the total jamming power, P_{jT}, is being spread evenly over a continuous bandwidth B_j. Hence, the jamming signal will have a very similar characteristic to the AWGN: thus, from this point forward, is referred to as the jamming noise.

If B_T denotes the communication bandwidth, the jamming ratio can then be represented as $\rho = B_j/B_T \leq 1$. This jamming ratio represents the fraction of bandwidth that is jammed by the jamming noise. Further, the power spectral density (PSD) of the jamming noise can be represented as

$$N_j = \frac{P_{jT}}{B_j} = \frac{P_{jT}}{B_T} \cdot \frac{B_T}{B_j} = \frac{N_{jT}}{\rho} \tag{1.19}$$

where $N_{jT} = P_{jT}/B_T$ is the equivalent PSD level of the jamming noise when spread over the bandwidth B_T.

For simplicity, it is assumed that, if an FH band is jammed, the entire M frequency bins of the FH band will be jammed. Based on this assumption, an FH band can be jammed with the probability of ρ and not jammed with the probability of $1-\rho$. When jammed, the total noise power σ_T^2 in the FH band can be expressed as

$$\sigma_T^2 = \sigma_j^2 + \sigma_n^2 = \frac{N_{jT}}{\rho T_s} + \frac{N_0}{T_s} \tag{1.20}$$

The total SER of an NC-FH/MFSK receiver under PBJ can thus be expressed as

$$\begin{aligned} P_s(e) &= P(\text{FH jammed}) \cdot P_s(e|\text{FH jammed}) \\ &\quad + P(\text{FH not jammed}) \cdot P_s(e|\text{FH not jammed}) \\ &= \rho \cdot P_s(e|\text{FH jammed}) + (1-\rho) \cdot P_s(e|\text{FH not jammed}) \end{aligned} \tag{1.21}$$

1.3.1 The SER When the FH Band is Jammed

If an FH band is jammed, the jamming noise will superimpose the AWGN and the total noise power, σ_T^2, can be found using (1.20). The SER given that the chosen FH band is jammed can be calculated from

$$P_s(e|\text{FH jammed}) = \sum_{v=1}^{M-1} \frac{(-1)^{v+1}}{1+v(1+\frac{2\sigma_s^2}{\sigma_T^2})} \binom{M-1}{v} \exp\left[\frac{-v\frac{\alpha_s^2}{\sigma_T^2}}{1+v(1+\frac{2\sigma_s^2}{\sigma_T^2})}\right] \quad (1.22)$$

1.3.2 The SER When the FH Band is not Jammed

When an FH band is not jammed, AWGN will be the only noise source corrupting the transmitted signal tone. The SER given that the FH band is not jammed can be found by replacing σ_T^2 in (1.22) with σ_n^2.

1.4 The Combined-Jamming Formula

The questions to be raised at this point are how to make use of the expressions obtained from these jamming models? Are there non-military applications to which these expressions can be applied? To answer to these questions, let us first consider a network of nodes with IEEE 802.11 NC-FH/MFSK radio as shown in Figure 1.3. If some neighbors of a receiving node are transmitting data to their engaged partners but they happen to use the same FH band occupied by the signal transmitted to it, in this case, the receiver receives not only the signal tones from the expected source, but also the unexpected cochannel interference tones from these neighbors. Except for the fact that they come from different origins (rather than a single jammer), these cochannel interference tones have, in fact, a similar characteristic to the jamming tones in the IMTJ strategy. In the presence of the cochannel interferences, it is thus possible to calculate the error rate as if the receiving node is being jammed by the IMTJ.

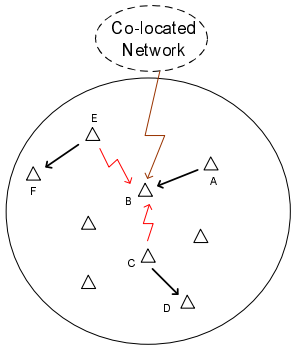

Figure 1.3. An illustration of interferences in an NC-FH/MFSK network. The signal tone from node A to node B is corrupted by the cochannel interference tones from node C and node E and by the external interference from co-located network.

Besides the interferences between nodes in the network, in most deployments, there also are external interferences from the co-located wireless networks. For the IEEE 802.11 NC-FH/MFSK network, which operates on the 2.4 GHz frequency spectrum, the most prominent interferer is, undoubtedly, the IEEE 802.11 b/g (WiFi) wireless network, which has increasingly gained its popularity over the past decade. Since WiFi devices use only one of the three non-overlapping frequency channels defined by the standard, the WiFi signals are usually spread over a fraction of the bandwidth by the direct sequence spread spectrum (DSSS) technique. When compared together, the similarity between the WiFi signal and the PBJ noise can be seen clearly. Suppose that the WiFi signal is the only interference from outside. This allows modeling the external interference for the FH network as the jamming noise in the PBJ strategy.

To determine the BER performance of an NC-FH/MFSK receiver in the presence of the cochannel interference tones and the external interference noise, a new formula that combines the effect of the IMTJ and the PBJ needs to be developed. The jamming-based expressions are, apparently, useful components to begin with.

Now, assume an external interference noise from a WiFi network is detected and spread over a bandwidth B_j of the entire bandwidth B_T. For ease of presentation, $\mathcal{A}$ is defined as the event that a chosen FH band is interfered by the interference noise from a co-located WiFi network and $\mathcal{A}'$ denotes the event that a chosen FH band is not interfered by the interference noise. Clearly, $P(\mathcal{A})$ is equal to the jamming ratio $\rho = B_j/B_T$ and $P(\mathcal{A}')$ is $(1-\rho)$. Based on (1.21), the probability of symbol error can be calculated by

$$P_s(e) = P(\mathcal{A}) \cdot P_s(e \mid \mathcal{A}) + P(\mathcal{A}') \cdot P_s(e \mid \mathcal{A}') \tag{1.23}$$

Provided that there are q cochannel interference tones from the other nodes, if a chosen FH band is interfered, there can be as few as one and as many as $min(q, M)$ in the FH band. Let $\mathcal{B}_0$ denote the event that there is no interference tone in the FH band (that is, the FH band does not experience the cochannel interference) and $\mathcal{B}_n$ denotes the event that the FH band is experiencing $1 \leq n \leq min(q, M)$ interference tones. If N is the total number of FH bands in the entire bandwidth $P(\mathcal{B}_0)$ and $P(\mathcal{B}_n)$ can be calculated from (1.5) and (1.7).

Hence, to include the effect of the cochannel interferences, (1.23) can be rewritten as

$$\begin{aligned}
P_s(e) &= P(\mathcal{A} \cap \mathcal{B}_0) \cdot P_s(e \,|\, \mathcal{A} \cap \mathcal{B}_0) + \quad P(\mathcal{A}' \cap \mathcal{B}_0) \cdot P_s(e \,|\, \mathcal{A}' \cap \mathcal{B}_0) \\
&\quad + \sum_{n=1}^{min(q,M)} \Big[P(\mathcal{A} \cap \mathcal{B}_n) \cdot P_s(e \,|\, \mathcal{A} \cap \mathcal{B}_n) \quad + \quad P(\mathcal{A}' \cap \mathcal{B}_n) \cdot P_s(e \,|\, \mathcal{A}' \cap \mathcal{B}_n) \Big] \\
&= P(\mathcal{A}) \cdot \Big[P(\mathcal{B}_0) \cdot P_s(e \,|\, \mathcal{A} \cap \mathcal{B}_0) \quad + \sum_{n=1}^{min(q,M)} P(\mathcal{B}_n) \cdot P_s(e \,|\, \mathcal{A} \cap \mathcal{B}_n) \Big] \\
&\quad + P(\mathcal{A}') \cdot \Big[P(\mathcal{B}_0) \cdot P_s(e \,|\, \mathcal{A}' \cap \mathcal{B}_0) + \sum_{n=1}^{min(q,M)} P(\mathcal{B}_n) \cdot P_s(e \,|\, \mathcal{A}' \cap \mathcal{B}_n) \Big]
\end{aligned} \tag{1.24}$$

The second equality in the equation is derived based on the independency of the interference tones and the interference noise, i.e.$\mathcal{A}$ is independent from event $\mathcal{B}_0$ and $\mathcal{B}_n$.

Consider the conditional probabilities in (1.24). Under event $\mathcal{A}'$, AWGN is the only noise corrupting the signal tone: thus, the total noise power σ_T^2 is equal to σ_n^2. $P_s(e \,|\, \mathcal{A}' \cap \mathcal{B}_0)$ and $P_s(e \,|\, \mathcal{A}' \cap \mathcal{B}_n)$ can then be evaluated using (1.6) and (1.8). In contrary, if the interference noise exists in the FH band, the total noise power now becomes $\sigma_T^2 = \sigma_n^2 + \sigma_j^2$. To calculate $P_s(e \,|\, \mathcal{A} \cap \mathcal{B}_0)$ and $P_s(e \,|\, \mathcal{A} \cap \mathcal{B}_n)$, (1.6) and (1.8) are used by replacing σ_n^2 with σ_T^2.

With all these terms being substituted, the combined-jamming formula in (1.24) can then be calculated. Nevertheless, there is certain restrictions that should be pointed out in the combined-jamming formula. Recall that, in the IMTJ strategy, each jamming tone is transmitted from the same jammer and received with an equal average power because their propagation distances are the same. However, in the IEEE 802.11 NC-FH/MFSK network, the cochannel interference tones may come from different nodes; thus, their received powers may not equal, unless the interferers are equally distant from the receiver. To obtain an accurate estimation using the formula, it is required that the network of interest must contain nodes that are equally spaced. An example of such a network is the honey-grid network where nodes are placed on the hexagonal lattice.

Also, when the BER expression is derived for the IMTJ model, it was assumed no two jamming tones are transmitted on the same frequency bin. Obviously, for a single jammer, this assumption can easily be satisfied because the jammer has a complete control on every tone it transmits. However, in the FH network, the interference tones are received from different interferers, and there is no guarantee that a frequency bin used by one interferer will not be used again by another. It

is possible that more than one interference tones are located in the same frequency bin: thus, the assumption is violated. To make the IMTJ expression valid for the FH network, the FH system should be designed with a large number of FH bands so that there are several frequency bins for each interferer to choose and the probability that more than one interference tones are transmitted on the same frequency bin is negligibly small.

1.5 Channel Assignment in Multiradio NC-FH/MFSK Wireless Mesh Networks

A multiradio wireless mesh network (MR-WMN) usually refers to an infrastructure network formed by a set of wireless routers, each with multiple radio interfaces, to provide a backbone network access for the mesh clients, [9]. Due to the numbers of radio interfaces on each router node, the data received at a given node can be forwarded through several destinations simultaneously. This increases the mesh throughput. The most challenging question in MR-WMN is, however, the channel assignment, i.e., how to bind each radio interface to a radio channel so that a reasonable gain in throughput can be achieved.

In general, the channel assignment (CA) is performed at the beginning phase of the network by a CA algorithm, then the procedure is repeated periodically to take into account dynamic changes in the network. To be able to determine appropriate channels, a crucial task for the CA algorithm is to assess the condition of each frequency channel or estimate the amount of interferences on each channels, [5]-[10]. In [5], an interference-aware channel assignment algorithm has been proposed for multiradio IEEE 802.11 a/b/g WMN. This centralized algorithm is designed by taking into account both the cochannel interferences and the external interference from co-located networks. To estimate and model the cochannel interferences, the authors have developed the Multiradio Conflict Graph (MCG) while, for the exter-

nal interference, the inherited IEEE 802.11 radio-sensing mechanism was adopted to periodically monitor for unrecognized radios.

In this section, the interference-aware algorithm in [5] is reconsidered. The combined-jamming formula is incorporated to the algorithm and allows it to assign the frequency channels (later known as hopping patterns) to radio interfaces in multiradio NC-FH/MFSK wireless mesh networks (MR-FH WMNs).

1.5.1 Network Model

The following assumptions and definitions are provided for modeling the mesh network

(i) A backbone MR-FH WMN is constructed with nodes that are equipped with at least two IEEE 802.11 NC-FH/MFSK radio interfaces used for sending and receiving information and an additional control interface, which operates on a different spectrum than the first interface and is used for control and signalling purposes.

(ii) The network is deployed in a rural area and the operational spectrum is contaminated by only one co-located WiFi network. To acquire the optimal coverage, every node is equally spaced from each other and they are perfectly aware of their own locations.

(iii) The MR-FH WMN is assumed to be centralized. There is only one gateway node at the center of the mesh, which is connected to the internet network. The location and ID of the gateway node are known to every other node.

(iv) *Transmission range* is defined as the circular distance around the source node, within which reliable communication can be achieved, assuming that there is no interferences from other radios. Assume every node has the same transmission

range, which approximately equals the distance from a node to its first-tier neighbors, so-called one-hop distance.

(v) *Interference range* is the circular distance around the transmitting node, beyond which the power received at the receiving node is negligible. The interference range for each node is assumed homogeneous and equal to the distance from a node to its second-tier neighbors, so-called two-hop distance.

According to the standard, the IEEE 802.11 NC-FH/MFSK interface is operated in the ISM 2.4 GHz band. A bandwidth of 83.5 MHz is divided into 79 FH bands to support the FH technique. To allow multiple access, three hopping patterns (or patterns, for short) are further established with 26 FH bands per pattern [11]. Because the FH bands of these patterns are interleaving and non-colliding, simultaneous transmissions can be enabled. Notice that these hopping patterns is, in fact, the counterpart of the frequency channels in the WiFi standard. With proper modification, the CA algorithms used for the WiFi network can thus be applied to the FH one.

Irrespective of the standard values mentioned, to generalize this study, parameters are used, instead, to denote these values. That is the entire bandwidth B_T Hz is divided into N FH bands, which are further grouped into p interleaving and non-colliding hopping patterns. Each hopping pattern contains $N_p = N/p$ FH bands. Therefore, the total of frequency bins is equal to N_pM. Because these patterns are interleaving and non-colliding, each node can support concurrent data links, if the links are performed on different patterns.

1.5.2 The CA Procedure and Algorithm

Algorithm 1.1 illustrates the CA algorithm, which is a modified version of that in [5], for assigning hopping patterns in the MR-FH WMN. At the setup of the

network, each router node must instantly forward its information, e.g. node IDs, locations, noise floor level, and number of interfaces, to the gateway node, using the control radio. After the information is received, the gateway creates the map and the Multi-radio Conflict Graph (MCG) of the network. The MCG is defined as a graph G with vertices and edges. A vertex V in the MCG denotes a possible link between any two nodes in the network that are within the distance of one hop from each other, according to the transmission range previously defined. Also, an edge E between two vertices of the MCG exists if the links represented by the two vertices are within the two-hop interfering distance from each other (see [5] for more detail).

Once the MCG is available, the gateway starts the algorithm by listing all vertices in the MCG into list V (Line 1). It will visit and assign patterns to vertices in MCG by starting from the links that are fanning out from the gateway (Line 3-4). The smallest hop count in the MCG is determined first in line 3 and, in line 4, all vertices with distance from the gateway equal to smallest hop count are listed into the waiting list L. In line 5, the vertices in list L are then sort according to their distance to give priority to link closer to the gateway.

Next, the algorithm visits each vertex in L (Line 7-11). It searches all the vertices that interfere with the current vertex v_c and places them into the list V_n (Line 12). Then, for each pattern, the algorithm finds the number of vertices using the pattern and calculates the cost (BER) for the pattern (Line 15-17). In line 18, the algorithm then compares the costs and assign the pattern k with minimum cost to the current vertex.

In line 16, all vertices containing either radio from current vertex are placed into a list R and being removed from the MCG in line 17 to assure that only one pattern is assigned to each link. The radios in the list of vertices that do not belong to the current vertex are temporarily assigned to next pattern number in Line 18.

Algorithm 1.1: The CA algorithm for MR-FH WMN

Parameters: p = Total number of hopping patterns
N_p = Total number of sequences per pattern

1: $V = \{v \mid v \in MCG\}$
2: **while** *NotAllVerticesVisited* (V) **do**
3: $h =$ *SmallestHopCount*(V)
4: $L = \{v_l \mid v_l \in V$ & *NotVisited*(v_l) & $HopCnt(v_l) = h\}$
5: *Sort*(L)
6: **while** *Size*$(L) > 0$ **do**
7: $v_c =$ *RemoveHead*(L)
8: *Visit*(v_c)
9: $V_n = \{v_n \mid v_n \in MCG$ & *EdgeInMCG*(v_n, v_c)=True$\}$
10: **for** m =1 to p
11: $V_n^m = \{v_n^m \mid v_n^m \in V_n$ & *Pattern*(v_n)=$m\}$
12: $q_m =$ *Cardinality* (V_n^m)
13: $Cost_m = f(q_m, V_n^m)$
14: **end for**
15: Choose pattern k with min. cost for v_c
16: $R = \{v_r \mid v_r \in MCG$ & has either radio from $v_c\}$
17: *RemoveVerticesInListFromMCG*(R)
18: Temporarily assign pattern k' to radios in R that are not of v_c
19: Let r_f be router node with interface in v_c that is farthest away from the gateway
20: Let $Tail$ be list of all active $v \in MCG$ such that v contains an interface from r_f
21: *Sort*$(Tail)$
22: *AddToList*$(L, Tail)$
23: **end while**
24: Permanently assign patterns to radios yet assigned with permanent patterns
25: **end while**

Then, in line 19-22, the vertices in the next level are attached to the waiting list L and the algorithm continues until all vertices in MCG are visited. In line 24, the radios that have not been assigned by the algorithm because the vertices containing it were deleted in line 17 are permanently assigned to the patterns temporarily assigned to them in line 18.

1.5.3 Example Assignment

An example of the MR-FH WMN that satisfies the previous assumption is shown in Figure 1.4. Here, six router nodes are used to form a simple mesh network with node A as the gateway node. Each node is labeled corresponding to name and number of FH interfaces. For example, A-2 means node A is equipped with two NC-FH/MFSK interfaces. Also, the total of $N = 78$ FH bands are divided just $p = 2$ hopping patterns, as seen in Figure 1.5, so that there are $N_p = 39$ FH bands in each pattern.

The power of jamming noise received at each node depends on how far the node is from the co-located WiFi network. The parameter σ_{jk}^2 is defined as the power of the jamming noise being received at router node k. Because two hopping patterns are formed by interlacing FH bands, N_J jammed FH bands are equally partitioned to each pattern. Consequently, the jamming ratio in hopping pattern i, ρ_i, is the same as the entire-bandwidth jamming ratio, ρ. It is assumed that σ_{jk}^2 at any node k and ρ_i are known to the gateway after a pre-install site survey.

Assume the gateway node A has run the algorithm for a period of time and some of the links have already been assigned with hopping patterns; A↔B (the link between node A and node B) and C↔E are assigned to pattern 1 while A↔C and B↔D are allocated to pattern 2. For the time being, both node C and node F have one radio interface available and it will be used to create a link C↔F. The algorithm is now considering an appropriate pattern for the link. Figure 1.6 shows the current MCG of the network.

Because, in this centralized network, the priority should be given to the nodes that are closest to the gateway, when consider an appropriate hopping pattern for C↔F, the algorithm must choose one that minimizes the interferences received at node C. Hence, node C should be considered as a reference receiver and every link

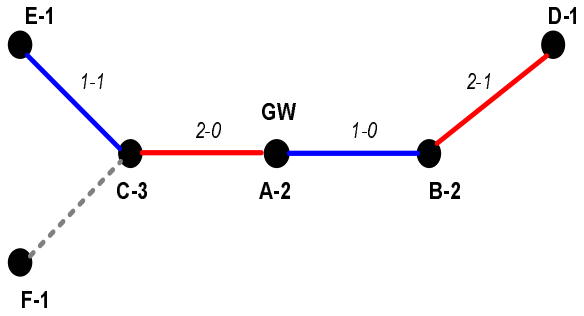

Figure 1.4. An MR-FH WMN for the example assignment.

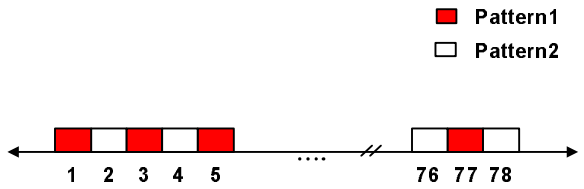

Figure 1.5. By interlacing $N = 78$ FH bands, hopping pattern 1 and 2 are formed by 39 odd-number FH bands and 39 even-number FH bands, respectively.

within its two-hop radius is considered a conflict/interfering link to C↔F; namely A↔B, A↔C, and C↔E.

From the loop in line 10-14, the algorithm must consider both pattern 1 and 2 when determining an appropriate for C↔F. However, to make this chapter concise, let us consider only the case when pattern 1 is being considered and note that the same logic is applied for the other pattern. If C↔F is to be assigned to pattern 1, A↔C, which is already assigned to pattern 2, is no longer considered as its interference: hence, the cost or BER calculation at node C should take into account only A↔B and C↔E. Also, to consider the extreme case, the algorithm assumes $q_1 = 2$ cochannel interference tones are sent from node A and node E, which are closer to node C. The received powers of the signal from node F and the interference tones from node A and node E can be found using the free-space pathloss model, [12],

$$P_{kl} = K\frac{P_T}{d^2} \tag{1.25}$$

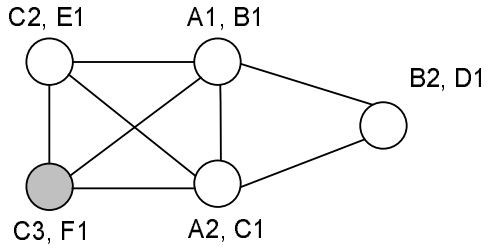

Figure 1.6. The current MCG of the network with some vertices already been removed by the algorithm in line 16-17. The grey vertex representing C↔F is being considered in the algorithm.

where d is the distance between transmitting and receiving node, P_{kl} is the received power of the signal from node k to node l, and P_T is the transmitted power. The constant K can be determined by the transmitting and receiving antenna gains. Since the nodes are assumed to be equally spaced, P_{AC} and P_{EC} are almost equal. The average of these powers can be used as the power of each interference tone received at node C (P_{jC}).

Table 1.1 illustrates the values for some important parameters used in (1.24) to calculate the SER when C↔F is to be assigned with pattern 1. Note that, in the table, the scattering ray powers for signal and interference tones are set to zero because no fading channel is assumed in this example. In general, the parameters can be set accordingly to reflect the actual characteristic of the fading channel.

1.5.4 Simulation Results

In this subsection, SIR (signal-to-interference-noise ratio) is defined as the ratio of signal power to interference noise power from the co-located network and SNR (signal-to-noise ratio) as the ratio of signal power to AWGN power. Mathematically, these ratios can be expressed as

$$SIR = \frac{P_s}{\sigma_{jk}^2 log_2 M} \ , \quad SNR = \frac{P_s}{\sigma_n^2 log_2 M} \tag{1.26}$$

Table 1.1. Parameters for calculating SER when C↔F is assigned to the pattern 1

Variable	Definition	Value
N	Total FH bands	$N_p = 78/2$
P_s	Received power of signal tone	P_{FC}
P_j	Received power of int. tone	$\frac{P_{AC}+P_{EC}}{2}$
q	Total number of int. tones	$q_1 = 2$
α_s^2, α_j^2	LOS signal/int. power	P_s, P_j
ς_s^2, ς_j^2	Scattering signal/int. power	0
ρ	Jamming ratio in the pattern	ρ_1
σ_j^2	Int. noise power at node C	σ_{jC}^2

For the scenario in Figure 1.4 with NC-FH/4FSK modulation, SIR equals $P_{FC}/2\sigma_{jC}^2$ and SNR equals $P_{FC}/2\sigma_n^2$. In the simulation, it is assumed that the router node F is the closest node to node C, then node A, and node E, respectively. But, because these nodes are spaced equally. Thus, their distances from node C are not so different, and, consequently, the powers of the tones received at node C are set to $P_{FC} = 1.1P_{AC} = 1.2P_{EC}$. Furthermore, it is assumed that the co-located IEEE 802.11 b network is operating on one of the three non-overlapping channels in 2.4 GHz band. So, ρ is set to approximately 0.3 and $\rho_1 = \rho_2 = \rho = 0.3$ because the hopping patterns are interlacing.

From Figure 1.7, it can be observed that, regardless of the SIR value, the BER obtained when C↔F is assigned to the hopping pattern 1 always larger than that when assigned to the hopping pattern 2. Thus, the CA algorithm assigns the hopping pattern 2 to C↔F. It can be observed that the interference noise contributes a very little effect on the selection for the most appropriate pattern. This is because it was assumed that the hopping patterns are interlacing. Hence, the effect of the interference noise appears as a constant offset on every pattern and get cancelled when the BER's for each pattern are compared.

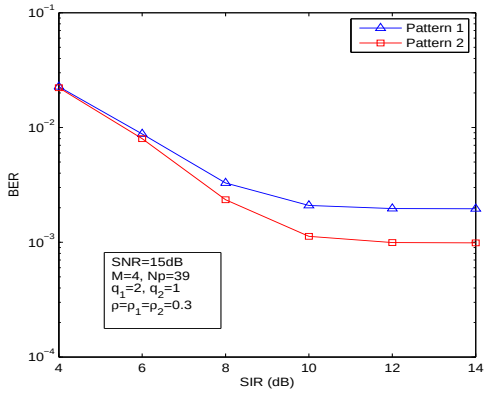

Figure 1.7. The BER performances of C↔F with interlacing hopping patterns.

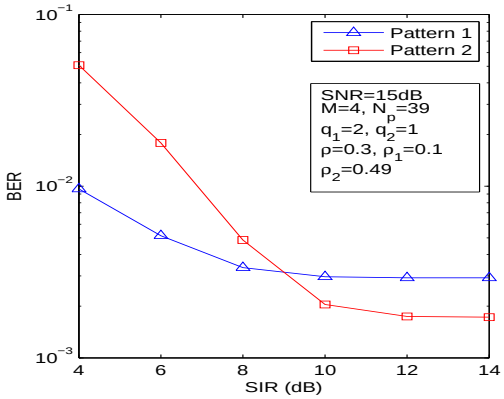

Figure 1.8. The BER performances of C↔F with non-interlacing hopping patterns.

Now, if the FH bands are randomly partitioned then the hopping patterns will no longer be interlacing. Each pattern is corrupted differently by the interference noise. In this case, the selection can be made more accurately if the interference noise is, as well, considered. Figure 1.8 illustrates the BER performances for the same example, but with non-interlacing hopping patterns. In the simulation, it is assumed there are $N_J = \rho N = 0.3 \times 78 \approx 23$ total jammed FH bands; 4 of 23 jammed FH bands are in pattern 1 and the rest 19 are in pattern 2. It can be observed that the choice of the appropriate pattern is now depending not only on the interference tones

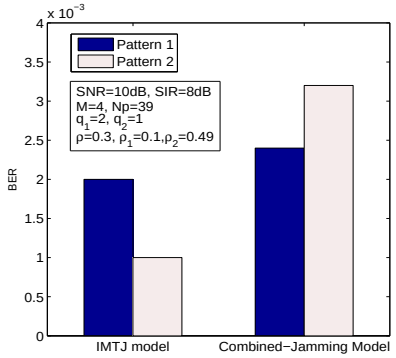

Figure 1.9. The comparison between the performances obtained from the combined-jamming model and the ITMJ model with non-interlacing hopping patterns.

but also on the external jamming noise received at node C. Unless the SIR is lower than 8 dB, pattern 2 will be the most appropriate choice for C↔F. Comparing with the result from Figure 1.7, it can seen clearly the influence of the external jamming noise on the choice of the appropriate pattern when non-interlacing patterns are used.

Next, to emphasize the advantage of the proposed formula, Figure 1.9 illustrates the comparison between the BER performances estimated by the new model and the conventional IMTJ model for non-interlacing hopping patterns. Because the IMTJ formula only considers the cochannel interferences, thus the hopping pattern 2, which has only one cochannel interference tone, is appraised as the most appropriate pattern for C↔F. However, with the effect of the coexisting network being considered, the combined-jamming model could provide more accurate estimation and suggests, in contradict, that hopping pattern 1 is, in fact, the more suitable pattern for C↔F. Clearly, if the combined-jamming formula is not used, the CA algorithm would have assigned C↔F to pattern 2 –though pattern 1 is the more proper choice– and the capacity of C↔F would have been lost unnecessarily.

1.6 Conclusions

In this chapter, the BER expressions for determining the performance of an NC-FH/MFSK receiver under the IMTJ and the PBJ strategy have been derived. Then, by viewing the jamming as interferences in IEEE 802.11 NC-FH/MFSK network, these expressions are combined to create a combined-jamming formula, which can be used for determining the performance of a node in the NC-FH/MFSK network, in the presence of the cochannel interference and the external interference from a co-located WiFi network. However, to obtain an accurate estimation from the combined-jamming formula, it is required that each node in the network be equally spaced and the number of FH bands in the system must be large enough. As an example, the usefulness of the combined-jamming formula have been illustrated through the channel assignment problem in multiradio IEEE 802.11 MR-FH/MFSK WMNs. Since the developed formula has taken into account the most common interferences for such FH network, it can be incorporated in a CA algorithm to evaluate the amount of interferences in each frequency channel and assists the algorithm in determining the most appropriate channel for each link.

CHAPTER 2

IMPROVING PERFORMANCE OF MULTI-RADIO FREQUENCY-HOPPING WIRELESS MESH NETWORKS

2.1 Introduction

Multi-radio wireless mesh network (MR-WMN) usually refers to an infrastructure network formed by a set of wireless routers, each with multiple radio interfaces, to provide backbone network access for the mesh clients. Due to the numbers of radio interfaces on each router node, the data received at a given node can be forwarded through several destinations simultaneously: hence, increases in the mesh throughput. The most challenging question in MR-WMN is, however, the channel assignment, i.e., how to bind each radio interface to a frequency channel so that a reasonable gain in throughput can be achieved.

Several publications, see [5, 6, 13, 14, 15] for example, have proposed the algorithms in the MAC-layer, which is called the channel assignment (CA) algorithms, to carefully manage how each radio should access the shared medium. In [5], an interference-aware channel assignment algorithm has been proposed for multi-radio IEEE 802.11 a/b/g WMNs. This centralized algorithm is designed by taking into account both the cochannel interferences and the external interference from co-located networks. To estimate and model the cochannel interferences, the authors have developed the Multi-radio Conflict Graph (MCG) while, for the external interference, the inherited IEEE 802.11 radio-sensing mechanism was adopted to periodically monitor for unrecognized radios.

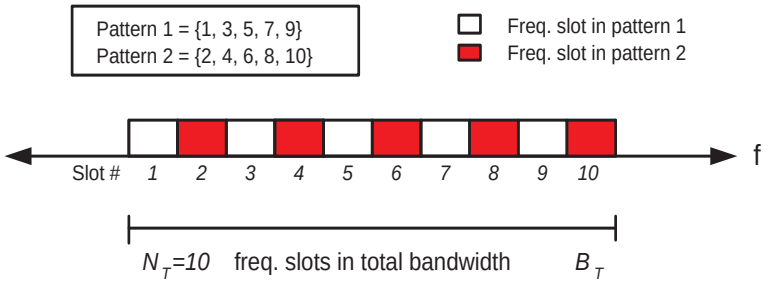

Figure 2.1. An example of the frequency spectrum B_T with $N_T = 10$ frequency slots and two hopping patterns ($p = 2$).

In this chapter, a multi-radio frequency-hopping wireless mesh network (MR-FH WMN) is studied. To accommodate the FH technique, the entire bandwidth is, first, divided into frequency slots as shown in Figure 2.1. Then, to allow multiple access to the shared medium, the frequency slots are further grouped to form hopping patterns, similar to those defined by the IEEE 802.11 (FH) standard [11]. At this point, it is noted that the hopping pattern concept here closely resembles the non-overlapping frequency channels in the WiFi standard: thus, to assign hopping patterns to the radio interfaces, the same CA algorithms for the WiFi networks can then be applied to the MR-FH WMN. Nevertheless, while the existing studies on WMNs have merely focused on improving the mesh capacity by reducing cochannel interferences, in this chapter, the improvement from the fading channel by introducing the space-time block coding (STBC) technique to the mesh is also considered. The STBC has long been recognized as a very practical and powerful technique to combat against fading channels. Using the STBC physical technique along with the MAC channel assignment, the MR-FH WMN acquires two-folded immunity against two important sources of deteriorations.

The performance of an isolated STBC link has been investigated in several publications. In the absence of the interference from other users (cochannel interference),

[16] and [17] have illustrated that the STBC can provide remarkable performance at the expense of almost no extra processing. However, under the influence of cochannel interference, the improvement provide by the STBC still remains questionable.

The chapter begins by investigating the degradation of the STBC link performance caused by cochannel interferences in the network. In Section 2.2, the mathematical model for the received signal in the STBC MIMO networks is introduced. To provide the theoretical background for the STBC, the coding and decoding processes for the STBC are described in Section 2.2.2. In Section 2.3, the simulation results are presented to illustrate the BER performances of an STBC MIMO link under various interference environments. Then, in Section 2.4, an STBC MR-FH WMN is modeled and a CA algorithm is used to assign hopping patterns to links in the mesh. In Section 2.5, an adaptive transmission scheme that allows the transmitting node (TX node) to determine the optimal number of antennas and choose the best antenna set for the pending transmission is proposed. Section 5.5 concludes the chapter.

2.2 Signal Modeling and Space-Time Block Coding

2.2.1 MIMO Signal and Interference Modeling

Consider a wireless link between two nodes in a MIMO network. Assume that the TX (transmitter) node and the RX (receiver) node use n antennas and m antennas, respectively, to establish the communication. Also, the TX power is assumed to be constant and equally allocated to each TX antenna used. During the transmission, it is further assumed there are Q other nodes accessing the channel simultaneously –hence cochannel interference is introduced– and each of these nodes uses n_q TX antennas, where $q \in 1, 2, .., Q$, for transmission. Hence, at the RX node, the total of Q interferences are being received.

Each antenna is assumed to undergo independent fading channel. Every channel is assumed to be slow frequency-nonselective fading complex channel, whose envelope is a Rayleigh random variable (rv). The complex channel gain for the path between TX antenna i and RX antenna j is represented as $h_{i,j}$, where $i \in 1, 2, .., n$ and $j \in 1, 2, .., m$, and the gain in each dimension of $h_{i,j}$ is modeled as independently and identically distributed (IID) Gaussian rv with zero mean and the variance of 0.5 per dimension. During the frame of length l, the channel gain is assumed to be constant, but it varies from one frame to another (quasi-static channel).

At the time slot t, the desired signal c_t^i is transmitted from antenna i=1,2,..,n and the received complex baseband samples at a receive antenna j of the receiver can be represented as

$$\begin{aligned} r_t^j &= \sum_{i=1}^{n} h_{i,j}\ c_t^i + \sum_{q=1}^{Q} \sum_{k=1}^{n_q} \sqrt{\frac{n}{n_q \gamma_q}} g_{q,k,j}\ z_t^{q,k} + n_t^j \\ &= \sum_{i=1}^{n} h_{i,j}\ c_t^i + I_t^j + n_t^j \end{aligned} \tag{2.1}$$

where $g_{q,k,j}$ represents the complex channel gain of the path between TX antenna k of node q and the receive antenna j and $z_t^{q,k}$ is the TX symbol at time t from TX antenna k of interfering node q. Because $g_{q,k,j}$ and $z_t^{q,k}$ are unknown to the receiver, I_t^j is thus the rv denoting the sum of all interferences received at time t in antenna j. γ_q denotes the ratio between the average received power of the desired signal and the average received power of signal from an interfering node q. The symbol n_t^j represents the noise at the received antenna j at time t and can be modeled as a complex Gaussian rv with zero mean and variance $\frac{n}{\gamma_0}$, where γ_0 is the signal-to-noise ratio (SNR) or the ratio between the average received signal power and the total noise power.

2.2.2 Space-Time Block Code Encoding

In the STBC, the generator matrix (G_{nkp}) is defined as a matrix of size $p \times n$, where n is the number of TX antennas used in the transmission, k is the number of symbols transmitted per block code, and p is the time slots required in transmitting the coding block. For a given number of TX antenna, there are so many block code designs that one can choose. In this chapter, the following generator matrices G_{222}, G_{348}, and G_{448} proposed in [16] and [17] are used for transmitting with two, three, or four TX antennas, respectively;

$$G_{222} = \begin{pmatrix} s_1 & s_2 \\ s_2^* & -s_1^* \end{pmatrix} \tag{2.2}$$

$$G_{348} = \begin{pmatrix} s_1 & s_2 & s_3 \\ -s_2 & s_1 & -s_4 \\ -s_3 & s_4 & s_1 \\ -s_4 & -s_3 & s_2 \\ s_1^* & s_2^* & s_3^* \\ -s_2^* & s_1^* & -s_4^* \\ -s_3^* & s_4^* & s_1^* \\ -s_4^* & -s_3^* & s_2^* \end{pmatrix} \tag{2.3}$$

$$G_{448} = \begin{pmatrix} s_1 & s_2 & s_3 & s_4 \\ -s_2 & s_1 & -s_4 & s_3 \\ -s_3 & s_4 & s_1 & -s_2 \\ -s_4 & -s_3 & s_2 & s_1 \\ s_1^* & s_2^* & s_3^* & s_4^* \\ -s_2^* & s_1^* & -s_4^* & s_3^* \\ -s_3^* & s_4^* & s_1^* & -s_2^* \\ -s_4^* & -s_3^* & s_2^* & s_1^* \end{pmatrix} \tag{2.4}$$

2.2.3 Space-Time Block Code Decoding

As an example of the STBC decoding/detection process, let us consider the receiver for the Alamouti's STBC shown in Figure 2.2, where only two RX antennas are assumed at the receiver.

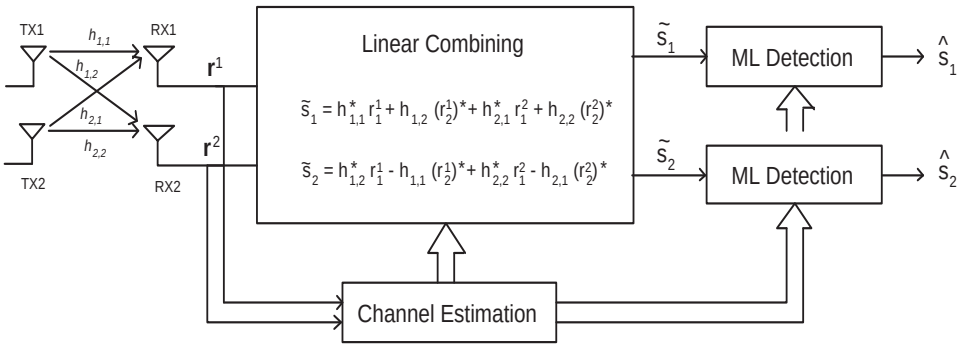

Figure 2.2. Alamouti's space-time block code decoder with two receiving antenna.

At time slot 1, the transmitting node simultaneously transmits s_1 from antenna 1 and s_2 from antenna 2 and r_1^j has been received at the received antenna j. Then, at time slot 2, s_2^* and $-s_1^*$ are simultaneously transmitted from antenna 1 and antenna

2 and the received signal at antenna j is r_2^j. With cochannel interference being considered, r_1^j and r_2^j can be expressed using (2.1) as

$$\begin{aligned} r_1^1 &= h_{1,1}\ s_1 + h_{1,2}\ s_2 + I_1^1 + n_1^1 \\ r_2^1 &= -h_{1,1}\ s_2^* + h_{1,2}\ s_1^* + I_2^1 + n_2^1 \\ r_1^2 &= h_{2,1}\ s_1 + h_{2,2}\ s_2 + I_1^2 + n_1^2 \\ r_2^2 &= -h_{2,1}\ s_2^* + h_{2,2}\ s_1^* + I_2^2 + n_2^2 \end{aligned} \tag{2.5}$$

To detect the transmitted symbols, the receive signals can be passed to the linear combiner to construct the following two combined signals for a soft decision

$$\begin{aligned} \tilde{s}_1 &= h_{1,1}^*\ r_1^1 + h_{1,2}\ (r_2^1)^* + h_{2,1}^* r_1^2 + h_{2,2}\ (r_2^2)^* \\ \tilde{s}_2 &= h_{1,2}^*\ r_1^1 - h_{1,1}\ (r_2^1)^* + h_{2,2}^* r_1^2 - h_{2,1}\ (r_2^2)^* \end{aligned} \tag{2.6}$$

By using (2.5) in (2.6), it can be shown that

$$\begin{aligned} \tilde{s}_1 &= (\sum_{j=1}^{2}\sum_{i=1}^{2} |h_{i,j}|^2) s_1 + h_{1,1}^*\ I_1^1 + h_{1,2}\ (I_2^1)^* + h_{2,1}^* I_1^2 + h_{2,2}\ (I_2^2)^* \\ &+ h_{1,1}^*\ n_1^1 + h_{1,2}\ (n_2^1)^* + h_{2,1}^* n_1^2 + h_{2,2}\ (n_2^2)^* \\ \tilde{s}_2 &= (\sum_{j=1}^{2}\sum_{i=1}^{2} |h_{i,j}|^2) s_2 + h_{1,2}^*\ I_1^1 - h_{1,1}\ (I_2^1)^* + h_{2,2}^* I_1^2 - h_{2,1}\ (I_2^2)^* \\ &+ h_{1,2}^*\ n_1^1 - h_{1,1}\ (n_2^1)^* + h_{2,2}^* n_1^2 - h_{2,1}\ (n_2^2)^* \end{aligned} \tag{2.7}$$

Then the soft decision $\tilde{s}_1$ and $\tilde{s}_2$ are sent to two separate ML (maximum likelihood) detections, which will select any symbol $s_k \in S$, where S is the set of all possible symbols in the constellation, as the estimated symbol $\hat{s}_1$ if s_k minimizes the following decision metric

$$|\tilde{s}_1 - s_k|^2 + (-1 + \sum_{j=1}^{2}\sum_{i=1}^{2} |h_{i,j}|^2)\, |s_k|^2 \tag{2.8}$$

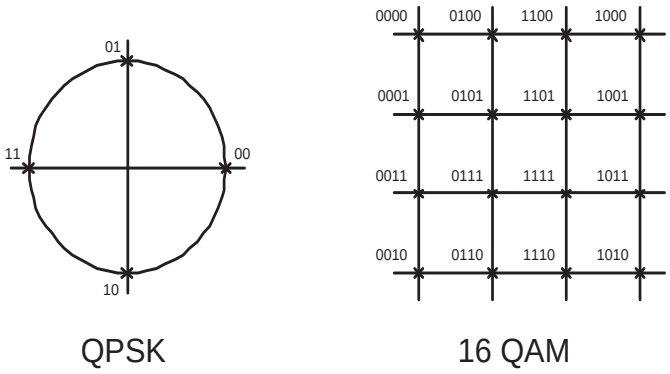

Figure 2.3. Gray Mapping for QPSK and 16QAM.

and select $s_l \in S$ as the estimated symbol $\hat{s}_2$ if s_l minimizes

$$|\tilde{s}_2 - s_l|^2 + (-1 + \sum_{j=1}^{2} \sum_{i=1}^{2} |h_{i,j}|^2) |s_l|^2 \tag{2.9}$$

For some other STBC designs, the detection scheme will be very similar to that described here. The ML decision metrics for the STBC with three or four TX antennas with different transmission rates are provided in [17].

2.3 Performance Simulations

In this section, the BER performances of MIMO communication are investigated. Throughout the section, the BER performances with different TX antennas will be presented, based on a given transmission bit rate at 2 bit/sec/Hz and assuming that there are four receiving antennas used. Table 2.1 describes the transmission scheme used for achieving the data rate required. For transmission with one antenna, the STBC technique is applicable, hence the detection is performed using MRC and ML scheme.

Table 2.1. Investigated transmission schemes

Rate	1 TX ant.	2 TX ant.	3 TX ant.	4 TX ant.
2 bit/s/Hz	QPSK	QPSK $\&G_{222}$	16QAM $\&G_{348}$	16QAM $\&G_{448}$

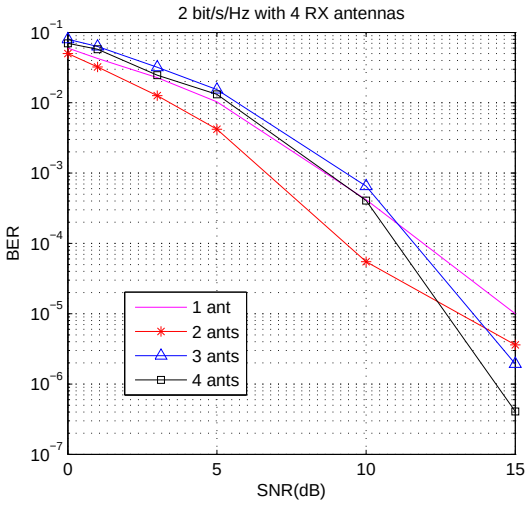

Figure 2.4. Performance of an STBC MIMO link at rate 2 bit/sec/Hz without cochannel interference (four RX antennas).

2.3.1 Transmission without Cochannel Interference

Figure 2.4 illustrates a benchmark performance for an STBC link without cochannel interference. It can be seen that, at a SNR lower than 10 dB, the transmissions with QPSK with one and two antennas outperform the transmissions with 16QAM with three or four antennas, which have higher degree of diversity. This is because the QPSK modulation is less vulnerable to noise than 16QAM modulation. The improvement achieved via spatial and temporal diversities can be easily observed when the transmission schemes that use the same constellation is considered. For example, in the transmissions with three or four antennas, 16QAM is used, but with different generator matrices, to achieve the transmission rate at 2 bit/sec/Hz. It

is observed that the performance with four TX antennas always outperforms that of three antennas because more diversity gain is achieved. The same is true when comparing the transmissions with one and two antennas.

2.3.2 Transmission with Cochannel Interference

To take into account interference, a signal-to-interference ratio (SIR) is defined as the ratio between the average received signal power and the average of aggregated received power from every interfering node;

$$SIR = \frac{1}{\sum_{q=1}^{Q} \frac{1}{\gamma_q}} \tag{2.10}$$

where γ_q is the ratio between the average received power of the desired signal and the average received power of signal from interfering node q.

2.3.2.1 One interferer

First consider when $Q = 1$ and assume that the interferer is using G_{222} and QPSK for transmission. Figure 2.5 illustrates the BER performance of a 2x4 link (two TX antennas and four RX antennas) with the rate of 2 bit/sec/Hz at different SIR levels.

Compared to the BER for AWGN channel, Figure 2.5 clearly illustrates how cochannel interferences degrade the performance of the link. At the same SNR level, the BER values at SIR = 5 and 15 dB are higher that of the AWGN channel due to the effect of the interference introduced. Besides, it can be observed that, high SNR values, both curves become horizontal lines and the BER values appear constant, despite the change in SNR. This is because, at high SNR, the interference becomes the dominating source of error and, since interference power is fixed in each curve, the BER remains unchanged.

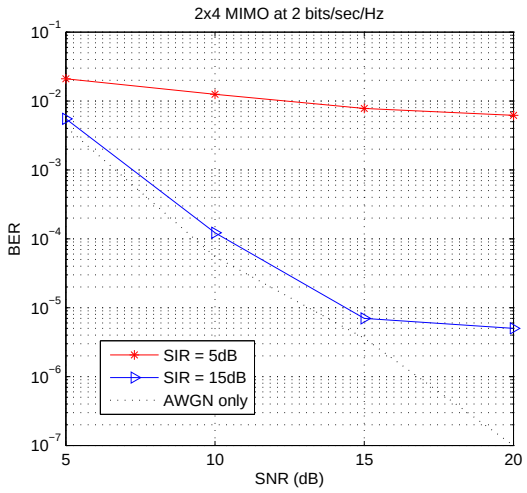

Figure 2.5. Performance of an STBC 2x4 link at rate 2 bit/sec/Hz with different SIR levels, assuming $Q = 1$.

Figures 2.6 and Figures 2.7 illustrate the BER performances for transmission rate 2 bit/sec/Hz with different number of TX antennas at SIR = 5 and 15 dB, respectively. For SIR = 5 dB in Figures 2.6, the effect of the cochannel interference can be seen clearly in high SNR region as the BER curves get flattened irrespective of the SNR change. Also, it can be observed that the transmission with one TX antenna always outperform the transmission with three TX antennas because the QPSK modulation is less vulnerable to noise and interference than 16QAM modulation. Thus, no further benefit can be achieved by increasing number of TX antennas from two to three when the interference is high.

Besides the G_{222} with QPSK, in the study, extensive simulations are performed and different type of transmission scheme listed in Table 2.1 is assigned to the interferer. Apparently, this would generally change the distribution of the interference. However, the numerical results have indicated that, irrespective of the transmission scheme used by the interferer, the BER performance obtained is quite similar to that when G_{222} with QPSK is being assigned to the interferer. This implies that the type

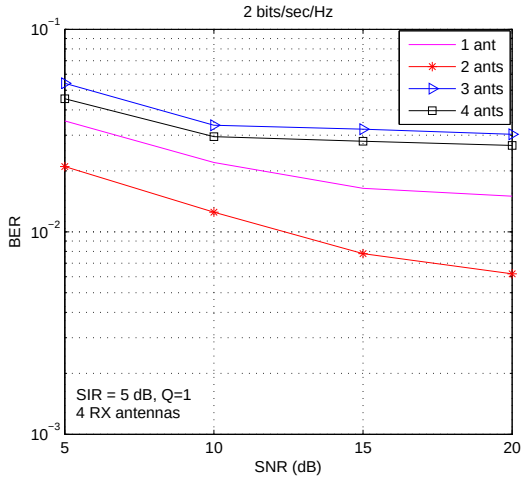

Figure 2.6. Performance of an STBC MIMO link at rate 2 bit/sec/Hz with $Q = 1$ and SNR=5dB.

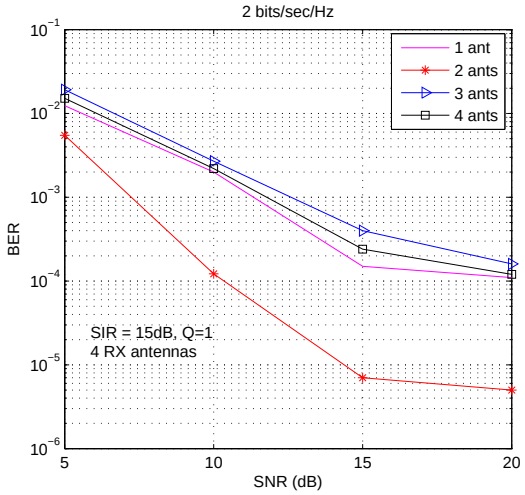

Figure 2.7. Performance of an STBC MIMO link at rate 2 bit/sec/Hz with $Q = 1$ and SNR=15dB.

of transmission scheme used by the interferer is probably not an important factor in determining the BER performance.

2.3.2.2 Five equal-power interferers

In the study, the cases when there are more than one interferer are also considered. First, assume there are five interferers and the interference from each interferer reaches the RX node with the same power. The total sum of the interference power is defined by SIR. The simulations have been performed for the case when all interferers are assigned with a fixed transmission, G_{222} with QPSK, and the case when each interferer is assigned with a transmission scheme randomly chosen from those listed in Table 2.1. From the results obtained, it can be observed that, with the total interference power being fixed by SIR, the BER values obtained for both cases are nearly the same and very similar to that of the previous case when $Q = 1$.

For example, the BER performances obtained at a transmission rate of 2 bit/sec/Hz for 1x4, 2x4, 3x4, and 4x4 MIMO links with five interfering nodes ($Q = 5$) are listed in Table 2.2, Table 2.3, Table 2.4, and Table 2.5, respectively. The results in these tables were obtained by assuming that interferences are received with equal powers and the transmission scheme used by each interferer is randomly chosen; hence, the characteristics of the total interference received is random.

Observe that the BER performances obtained when more than one equal-power interferers ($Q = 5$) are introduced are nearly the same as those obtained with the same number of TX antennas used when there is only one interferer.

2.3.2.3 Five interferers with dominant interferers

Instead of having each equal-power interferences, a case when the power received from D interferers are larger than the others is also considered, i.e. the SIR measured is dominated by D interferers. Every dominant interferer is assigned with a power which is twice as large as that of a regular interferer but the sum of all interferer's

Table 2.2. The BER values for the STBC links at rate 2 bit/sec/Hz using 1x4 MISO with five equal-power interferers

SNR	$SIR = 5dB$		$SIR = 15dB$	
	$Q = 1$	$Q = 5$	$Q = 1$	$Q = 5$
5 dB	0.0353	0.0331	0.0124	0.0105
10 dB	0.0220	0.0195	0.0025	0.0011
15 dB	0.0164	0.0139	1.3e-4	1.5e-4
20 dB	0.0150	0.0124	1.1e-4	1.3e-4

Table 2.3. The BER values for the STBC links at rate 2 bit/sec/Hz using 2x4 MIMO with five equal-power interferers

SNR	$SIR = 5dB$		$SIR = 15dB$	
	$Q = 1$	$Q = 5$	$Q = 1$	$Q = 5$
5 dB	0.0210	0.0251	0.0055	0.0058
10 dB	0.0125	0.0130	1.22e-4	2.23e-4
15 dB	0.0078	0.0068	7e-6	6.5e-6
20 dB	0.0062	0.0069	5e-6	2.81e-6

Table 2.4. The BER values for the STBC links at rate 2 bit/sec/Hz using 3x4 MIMO with five equal-power interferers

SNR	$SIR = 5dB$		$SIR = 15dB$	
	$Q = 1$	$Q = 5$	$Q = 1$	$Q = 5$
5 dB	0.0541	0.0602	0.0192	0.0191
10 dB	0.0336	0.0354	0.0027	0.0028
15 dB	0.0321	0.0330	4e-4	3.6e-4
20 dB	0.0303	0.0311	1.6e-4	2.2e-4

Table 2.5. The BER values for the STBC links at rate 2 bit/sec/Hz using 4x4 MIMO with five equal-power interferers

SNR	$SIR = 5dB$		$SIR = 15dB$	
	$Q = 1$	$Q = 5$	$Q = 1$	$Q = 5$
5 dB	0.0454	0.0505	0.0172	0.0177
10 dB	0.0295	0.0303	0.0022	0.0028
15 dB	0.0280	0.0295	2.4e-4	3.17e-4
20 dB	0.0267	0.0250	1.2e-4	1.6e-4

powers is still restricted by the total interference power defined by the SIR. In the simulations, the cases when $D = 1$ and $D = 3$ are considered. Based on previous observations, the case when each interferer is assigned with a transmission scheme randomly chosen from those listed in Table 2.1 is considered here.

The BER performances obtained at a transmission rate of 2 bit/sec/Hz for 1x4, 2x4, 3x4, and 4x4 MIMO links with a different number of dominant interferers, i.e.,$D = 1$ and $D = 3$, are listed in Table 2.6, Table 2.7, Table 2.8, and Table 2.9, respectively. From the results obtained, it can be observed that, with the total interference power fixed by SIR, the BER values obtained for both when $D = 1$ and $D = 3$ are nearly the same and they are also close to those values obtained in the previous case when five interferers are of equal power ($D = 0$).

In summary, it can be observed from the results in this section that, even with interferences, the temporal and spatial diversities deployed in the STBC can still help improving the performance against fading channel. As previously observed, the transmissions with one or two TX antennas both require QPSK modulation to achieve the given rate of 2 bit/sec/Hz. But, with two TX antennas, G_{222} is deployed and higher diversity gain is obtained, the performance with two TX antennas is thus always better than that with one antenna. Similarly for the transmissions with three or four TX antennas, both require 16QAM modulation and the performance with four antennas is always better.

However, because the transmissions with three or four TX antennas require more aggressive modulation scheme to achieve the given data rate, the performances achieved by the transmissions with three or four TX antennas can be worse than those with one or two TX antennas, especially when the interference power is high. This means using the STBC technique with multiple antennas can improves the link performance but, depending on the operating SIR and SNR levels, one must carefully

Table 2.6. The BER values for the STBC links at rate 2 bit/sec/Hz using 1x4 MISO with different number of dominant interferers

SNR	$SIR = 5dB$			$SIR = 15dB$		
	$D = 0$	$D = 1$	$D = 3$	$D = 0$	$D = 1$	$D = 3$
5 dB	0.0331	0.0345	0.0360	0.0105	0.0098	0.0111
10 dB	0.0195	0.0212	0.0267	0.0011	0.0017	0.0020
15 dB	0.0139	0.0155	0.0169	1.5e-4	1.39e-4	1.22e-4
20 dB	0.0124	0.0138	0.0124	1.3e-4	9.6e-5	1.6e-4

Table 2.7. The BER values for the STBC links at rate 2 bit/sec/Hz using 2x4 MIMO with different number of dominant interferers

SNR	$SIR = 5dB$			$SIR = 15dB$		
	$D = 0$	$D = 1$	$D = 3$	$D = 0$	$D = 1$	$D = 3$
5 dB	0.0251	0.0250	0.0254	0.0058	0.0062	0.0068
10 dB	0.0130	0.0148	0.0150	2.23e-4	2.81e-4	1.82e-4
15 dB	0.0068	0.0069	0.0080	6.5e-6	1.2e-5	4.13e-6
20 dB	0.0069	0.0055	0.0078	2.81e-6	4.13e-6	3.2e-6

Table 2.8. The BER values for the STBC links at rate 2 bit/sec/Hz using 3x4 MIMO with different number of dominant interferers

SNR	$SIR = 5dB$			$SIR = 15dB$		
	$D = 0$	$D = 1$	$D = 3$	$D = 0$	$D = 1$	$D = 3$
5 dB	0.0602	0.0610	0.0630	0.0191	0.0191	0.0194
10 dB	0.0354	0.0375	0.0380	0.0028	0.0035	0.0037
15 dB	0.0330	0.0342	0.0356	3.6e-4	1.81e-4	2.2e-4
20 dB	0.0311	0.0316	0.0328	2.2e-4	1.6e-4	1.13e-4

Table 2.9. The BER values for the STBC links at rate 2 bit/sec/Hz using 4x4 MIMO with different number of dominant interferers

SNR	$SIR = 5dB$			$SIR = 15dB$		
	$D = 0$	$D = 1$	$D = 3$	$D = 0$	$D = 1$	$D = 3$
5 dB	0.0505	0.0532	0.541	0.0177	0.0180	0.0192
10 dB	0.0303	0.0354	0.0385	0.0028	0.0032	0.0035
15 dB	0.0295	0.0310	0.0330	3.17e-4	4.81e-4	4e-4
20 dB	0.0250	0.0285	0.0310	1.6e-4	1.81e-4	2.17e-4

consider not to use too many TX antennas, which could result in a worse performance than a simple transmission with one antenna. Yet, when SIR is high or when there is no cochannel interferences, it is observed that the transmission with the STBC technique via multiple TX antennas always provide better or nearly the same performance as when transmitting with one antenna without the STBC. Hence, to always achieve the benefit of the STBC technique, one must, again, try to avoid having cochannel interferences on the link.

With further investigation on the effect of interference characteristic on the link performance, it has been observed that, for a given sum of interference power or for a given SIR, the factors like what type of the transmission schemes used by the interferers, how many interferers, or whether there are dominant interferers are not exactly significant factors in determining the link performance.

2.4 Multi-Radio Frequency-Hopping Wireless Mesh Network with the STBC

2.4.1 Network Model

The following assumptions and definitions are provided for modeling the mesh network

(i) A backbone MR-FH WMN is constructed with nodes that are equipped with at least two FH radio interfaces designated for sending and receiving information and an additional control interface, which operates on a different bandwidth than that of the FH interface and is used for controlling and signalling purposes.

(ii) Every FH interface uses an array of four antennas and has the same RF parameters, e.g., transmission power and antenna gain. Every node knows and keeps monitoring its own noise floor level.

(iii) The network is deployed such that every node is equally spaced from each other and they are perfectly aware of their own location.

(iv) The MR-FH WMN is assumed to be centralized. There is only one gateway node at the center of the mesh, which is connected to the internet network. The location and ID of the gateway node are known to every other node.

(v) *Transmission range* is defined as the circular distance around the source node, within which reliable communication can be achieved, assuming that there is no interferences from other radios. Assume every node has the same transmission range, which approximately equals the distance from a node to its first-tier neighbors. This is called one-hop distance.

(vi) *Interference range* is the circular distance around the transmitting node, beyond which the power received at the receiving node is negligible. The interference range for each node is assumed homogeneous and equal to the distance from a node to its second-tier neighbors, so-called two-hop distance.

2.4.2 Frequency Hopping Parameters

Within the entire frequency bandwidth B_T designated for data, let assume there are N_T FH bands with bandwidth $B_h = \frac{B_T}{N_T} = \frac{1}{T_s}$ per FH band (B_h is determined by the coherent bandwidth of the channel, i.e. channel bandwidth). To achieve the greatest benefit with a node having multiple data interfaces, N_T FH bands are then partitioned into p interleaving and non-colliding hopping patterns, as shown in Figure 2.1, to enable concurrent transmissions. Thus, each hopping pattern equally contains $N_p = \frac{N_T}{p}$ FH bands. The order of the N_p slots in each pattern forms a hopping sequence (or sequence for short) for the the carrier frequency of the FH interface to hop through. Assume that the frequency carrier is hopping slowly and the hopping period T_h is an integer multiple of the time required to transmit one

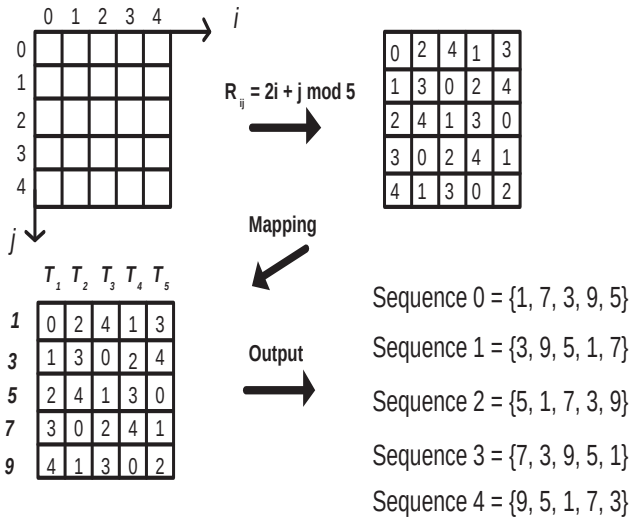

Figure 2.8. The Latin square with $N_p = 5$ and $a = 2$ and the output hopping sequences obtained after mapping frequency slots in hopping pattern 1.

frame of data. That is, within one data frame, which is composed of several channel estimation symbols and many STBC data coding blocks, the signals will remain in the same frequency slot, hence the channel estimation performed at the beginning of the data frame is still valid throughout the entire data frame and the frequency hopping is blind to the coding and decoding scheme.

Since only one frequency slot in the pattern will be occupied by the modulated signal, more than one node can be allowed to share the same pattern if their hopping sequence are different during each hopping period. In other words, this means the number of frequency channels can be increased by forming different sequences in each pattern. Now, let consider the Latin square in Figure 2.8 with $N_p = 5$ and $a = 2$. The (i, j) element of the N_pxN_p Latin square matrix R^a is defined as, [18],

$$R^a_{i,j} = (a \cdot i + j) \ \ mod \ \ N_p \tag{2.11}$$

where $a \in 1, 2, ..., N_p - 1$ is an arbitrary number. To create N_p non-overlapping sequences, the slots in each pattern can be mapped to the rows of the square and let

the columns represent the hopping periods. For example, in Figure 2.1, the pattern 1 is assigned with slots number 1, 4, 7, 10, 13 and the lower left illustration of Figure 2.8 shows the mapping of these slots to the rows of the Latin square matrix. After the mapping process, $N_p = 5$ different subpatterns can then be obtained for the first pattern.

2.4.3 The Channel Assignment Procedure and Algorithm

For wireless mesh networks with multiple radio interfaces, it is widely known that, as the number of interfaces increases, router nodes also tend to interfere more with each other. Unless the channels are carefully assigned to each interface, increasing the number of interfaces could, on the other hand, reduce the mesh throughput. To mitigate the problem, in this subsection, an interference-aware CA algorithm is proposed to assign hopping patterns to links in the STBC MR-FH WMN.

Algorithm 2.1 illustrates the CA algorithm, which is a modified version of that in [5]. At the setup of the network, each router node must forward its information, e.g. node IDs, locations, noise floor level, and number of interfaces, to the gateway node, using the control radio. After the information is received, the gateway creates the map and the Multi-radio Conflict Graph (MCG) of the network. The MCG is defined as a graph G with vertices and edges. A vertex V in the MCG denotes a possible link between any two nodes in the network that are within the distance of one hop from each other, according to the transmission range previously defined. Also, an edge E between two vertices of the MCG exists if the links represented by the two vertices are within the two-hop interfering distance from each other (see [5] for more detail).

Once the MCG is available, the gateway starts the algorithm by listing all vertices in the MCG into list V (Line 1). It will visit and assign patterns to vertices in MCG by starting from the links that are fanning out from the gateway (Line 3-4).

Algorithm 2.1: The CA Algorithm for the STBC MR-FH WMN

Parameters: p = Total number of hopping patterns
N_p = Total number of FH bands per pattern

$V = \{v \mid v \in MCG\}$
while *NotAllVerticesVisited* (V) **do**
  h= *SmallestHopCount*(V)
  L=$\{v_l \mid v_l \in V$ and *NotVisited*(v_l) and *HopCount*$(v_l) = h\}$
  Sort(L)
  while *Size*$(L)> 0$ **do**
    v_c=*RemoveHead*(L)
    if *Visited*(v_c) **then**
      continue
    end if
    Visit(v_c)
    $V_n = \{v_n \mid v_n \in MCG$ and *EdgeInMCG*(v_n,v_c)=TRUE$\}$
    for m =1 to p
      $V_{n,m} = \{v_{n,m} \mid v_{n,m} \in V_n$ and *Pattern*(v_n)=$m\}$
      Q_m=*Size*$(V_{n,m})$
      $Cost_m = f(Q_m, V_{n,m})$
    end for
    Choose hopping pattern k with the minimum cost and assign to v_c
    for h =1 to N_p
      $V_{n,k,h} = \{v_{n,k,h} \mid v_{n,k,h} \in V_n$ & *Pattern*(v_n)=k & *Subpattern*$(v_{n,k})$=$h\}$
      Q_h=*Size*$(V_{n,k,h})$
      $Cost_h = f(Q_h, V_{n,k,h})$
    end for
    Choose subpattern j in pattern k with the minimum cost and assign to v_c
    $R = \{v_r \mid v_r \in MCG$ and v_r has either radio from $v_c)\}$
    RemoveVerticesInListFromMCG(R)
    Temporarily assign pattern k' and subpattern j' to radios in R
    Let r_f be router node with interface in v_c that is farthest away from PAC
    Let $Tail$ be list of $v \in MCG$ such that v contains an interface from r_f
    Sort$(Tail)$
    AddToList$(L, Tail)$
  end while
  Permanently assign pattern to radios that are yet assigned
end while

The smallest hop count in MCG is determined first in line 3 and, in line 4, all vertices with distance from the gateway equal to smallest hop count are listed into the waiting list L. In line 5, the vertices in list L are then sort according to their distance to give priority to link closer to the gateway.

Next, the algorithm visits each vertex in L (Line 7-11). It searches all the vertices that interfere with the current vertex and places them into the list V_n (Line 12). Then, for each hopping pattern, the algorithm finds the number of vertices that uses the same hopping pattern and calculates the costs associated with the hopping pattern (Line 15-17). In line 18, the algorithm then compares the costs for each pattern and assigns the pattern k with minimum cost to the current vertex. Similarly, in line 19-24, the algorithm finds subpatern j in the chosen pattern k that gives minimum cost and assigns it to the current vertex.

In line 25, all vertices containing either radio from current vertex are placed in to a list R and removed from the MCG in line 26 to assure that only one hopping pattern is assigned to each radio. The radios in the list of vertices that do not belong to the current vertex are temporarily assigned to the next pattern and subpattern number (Line 27). Then, in line 28-31, the vertices in the next level are attached to the waiting list L and the algorithm continues until all vertices in MCG are visited. In line 33, the radios that have not been assigned by the algorithm because the vertices containing it were deleted in line 26 are permanently assigned to the hopping patterns and subpatterns temporarily assigned to them in line 27.

2.4.4 SER-Based Cost Function

It is noted that, to determine the most appropriate pattern for a link, the CA algorithm must first evaluate and then compare the cost, or the amount of interference, associated with each hopping pattern (Line 13-24). One of the most prominent can-

didates for the cost function is undoubtedly one related with the link BER. However, since nodes are free to use any transmission scheme that is proper to their operating conditions, the characteristic of the interference from each node is diverse and it is nearly impossible to capture such dynamic factors mathematically.

Fortunately, because the estimated costs are eventually compared together to provide a binary decision as to which pattern provides better BER, as long as the differences between patterns can be identified, whether an individual cost is correctly estimated or not is obviously not at the highest concern. The results from the previous chapter have shown that the error rate is most likely determined by large-scale parameters like the interference power, rather than its characteristic. Hence, to derive an appropriate cost function, it is better to ignore how each interference is characterized and try just to capture its large-scale behavior instead.

In this chapter, the cost function developed from the SER (symbol error rate) of a link with two TX antennas is used. To derive such a cost function, let first consider the soft decision outputs from the linear combiner in the STBC decoding like those in (2.7). With the STBC, a MIMO link can be transformed to several SISO (single-input single-output) links and the decisions for each transmitted symbol can be made independently from these soft decision outputs. It can be shown that instantaneous SNR for each of the soft decision outputs will be equal to $\frac{1}{n}\sum_{i=1}^{n}\sum_{j=1}^{m}|h_{i,j}|^2\,\gamma_0$. Variables n and m are number of TX antennas and RX antennas used in the link. γ_0 represents the average SNR of received signal.

It can be observed that the same instantaneous SNR value can be obtained by transmitting one symbol with a SNR equal to γ_0/n over $n \times m$ channels and using MRC for detection. Therefore, the performance over each of these transformed SISO channels will be the same as the performance of a system transmitting one symbol over $n \times m$ channels and using MRC (maximum ratio combiner) for detection. In general,

the average symbol error rate (SER) can be calculated using the instantaneous SNR and then the result is averaged over the channel distribution.

For Rayleigh fading channel. The average SER for M-PSK with SNR equal $\frac{\gamma_0}{n}$ can be obtained as, [19] and [20],

$$\begin{aligned} P_s(e) &= \frac{M-1}{M} - \left(\frac{1}{\pi}\sqrt{\frac{\frac{1}{n}\gamma_0 \sin^2\frac{\pi}{M}}{1+\frac{1}{n}\gamma_0\sin^2\frac{\pi}{M}}}\right)\left\{\left(\frac{\pi}{2}+\tan^{-1}\alpha\right)\sum_{k=0}^{d-1}\frac{\binom{2i}{i}}{\left[4\left(1+\frac{1}{n}\gamma_0\sin^2\frac{\pi}{M}\right)\right]^i}\right. \\ &\left. +\sin(\tan^{-1}\alpha)\sum_{u=1}^{d-1}\sum_{v=1}^{u}\frac{T_{uv}}{(1+\frac{1}{n}\gamma_0\sin^2\frac{\pi}{M})^u}\left[\cos(\tan^{-1}\alpha)\right]^{2(u-v)+1}\right\} \end{aligned} \tag{2.12}$$

where

$$\begin{aligned} \alpha &= \sqrt{\frac{\frac{1}{n}\gamma_0\sin^2\frac{\pi}{M}}{1+\frac{1}{n}\gamma_0\sin^2\frac{\pi}{M}}}\cot\left(\frac{\pi}{M}\right) \\ T_{uv} &= \frac{\binom{2i}{i}}{\binom{2(u-v)}{u-v}4^v[2(u-v)+1]} \end{aligned}$$

and $d = n \times m$ is the number of independent channel paths between transmitting and receiving nodes or the number of MRC branches. Then, by assuming that every node is using G_{222} with BPSK modulation ($M = 2$), the SER for a link with one RX antenna ($m = 1$) can be obtained from (2.12) as

$$P_s(e) = \frac{1}{2}\left\{1-\sqrt{\frac{\gamma_0}{2+\gamma_0}}\left(1+\frac{1}{2+\gamma_0}\right)\right\} \tag{2.13}$$

This BER expression considers only the effect of AWGN on a particular transmission with G_{222} and BPSK. Yet, because it depends only on the SNR, this expression is useful in determining appropriate pattern when the transmission scheme is different. The next task is just to introduce the effect of interference into the expression. Now, consider a special case when all Q interfering nodes transmit using one

TX antenna with QPSK modulation. Recalled from (2.1), the sum of all interferences received at time t in antenna j, defined as I_t^j, can be expressed as

$$\begin{aligned} I_t^j &= \sum_{q=1}^{Q} \left[\sqrt{\frac{n}{n_q \cdot SIR_q}} \cdot \sum_{k=1}^{n_q} g_{q,k,j} \; z_t^{q,k} \right] \\ I_t &= \sum_{q=1}^{Q} \sqrt{\frac{2}{SIR_q}} \cdot g_q \; z_t^q \end{aligned} \tag{2.14}$$

where the second equality is due to the fact that there is only one antenna at the RX node and all interfering nodes using one antenna to transmit. Consider the product $g_q \; z_t^q$ for certain interfering node q at time t. The rv g_q represents the complex channel gain between the TX antenna of node q and the RX antenna and can be modeled as IID Gaussian rv with zero mean and the variance of 0.5 per dimension, i.e. $\mathcal{N}(\mu$=0, σ^2=0.5). The rv z_t^q is the transmitted symbol from node q at time t and can be modeled as a complex discrete rv. Therefore, if $X = \Re\{g_q\}$ and $Y = \Re\{z_t^q\}$, and $Z = XY$ then, for a certain node q and time t, the conditional PDF of Z given Y can be shown as,[21],

$$f_Z(z \,|\, y) = \frac{1}{|y|} \; f_X(\frac{z}{y} \,|\, y) = \mathcal{N}(\mu_z = 0, \sigma_z^2 = y^2 \sigma_x^2) \tag{2.15}$$

Thus, $f_Z(z)$ can be calculated by summing over the set of Y. For any QPSK symbol, the real part of the symbol is chosen from $\{\sqrt{\frac{P_q}{2}}, -\sqrt{\frac{P_q}{2}}\}$, where P_q is the average power for node q;

$$\begin{aligned} f_Z(z) &= \sum_{y_i \in \mathcal{Y}} f_Z(z \,|\, y_i) P(y_i) \\ &= \frac{1}{2} \left[\frac{1}{\sigma_x \sqrt{P_q \pi}} \cdot exp\left(\frac{-z^2}{P_q \sigma_x^2} \right) + \frac{1}{\sigma_x \sqrt{P_q \pi}} \cdot exp\left(\frac{-z^2}{P_q \sigma_x^2} \right) \right] \\ &= \frac{1}{\sigma_x \sqrt{P_q \pi}} \cdot exp\left(\frac{-z^2}{P_q \sigma_x^2} \right) \end{aligned} \tag{2.16}$$

Obviously, these PDF's are Gaussian distributions. This means the product between $\Re\{g_q\}$ and $\Re\{z_t^q\}$ for QPSK modulation is a Gaussian rv. Similarly, it can be shown

that the product between the complex numbers g_q and z_t^q is just the summation of these Gaussian rvs, it is hence a complex Gaussian rv with zero mean and variance equal to $P_q\sigma_x^2 = \frac{P_q}{2}$ per dimension. Therefore, the signal received from all Q interfering nodes at time t or I_t is also a zero-mean complex Gaussian rv.

Furthermore, since only one antenna is used on each interfering node, I_1, I_2,..., I_t or the total sum of interferences at each time t are IID and their joint PDF is a zero-mean multivariate Gaussian PDF, similar to that of the AWGN. Hence, from (2.13), the cost function for the algorithm can be easily obtained by replacing the average SNR (γ_0) with the average signal-to-interference and noise ratio (SINR). The required cost function can then be expressed as

$$f(SINR) = \frac{1}{2}\left\{1 - \sqrt{\frac{SINR}{2+SINR}}\left(1 + \frac{1}{2+SINR}\right)\right\} \tag{2.17}$$

where

$$SINR = \frac{P_s}{\sum_{q=1}^{Q} P_q + N_0} = \frac{1}{\sum_{q=1}^{Q} \frac{1}{\gamma_q} + \frac{1}{\gamma}} \tag{2.18}$$

P_s is the average power of signal from the TX node and N_0 is the one-sided power spectral density of AWGN. If the TX powers and locations of nodes are known, $\frac{1}{\gamma_q}$ can then be easily estimated by the free-space propagation model.

2.4.5 Example of Channel Assignment in the STBC MR-FH WMN

An example of the STBC MR-FH WMN that satisfies the previous assumptions is shown in Figure 2.9. Here, six router nodes are used to setup a simple backbone mesh network with node A as the gateway node. Each node is labeled corresponding to its name and number of its information interfaces, for example A-2 means node A is equipped with two FH interfaces. Assume that the entire bandwidth is divided into $p = 2$ hopping patterns, each with $N_p = 5$ FH bands. The Latin square in (2.11)

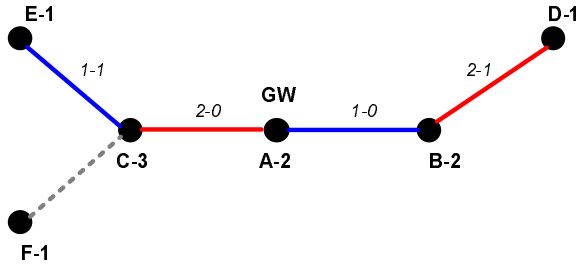

Figure 2.9. An MR-FH WMN for the example assignment.

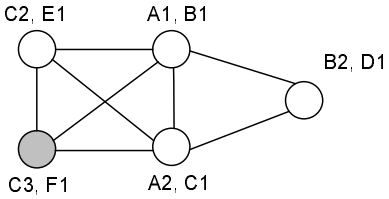

Figure 2.10. The current MCG of the network with some vertices being removed by the algorithm in line 26 to assure only pattern is assigned to each link. The grey vertex denoting C↔F is being considered by the algorithm.

with $a = 2$ was used to create five subpatterns for each hopping pattern as shown in Figure 2.8.

Suppose the gateway node A has run the algorithm for a period of time and some of the links have already been assigned with hopping patterns; A↔B (the link between node A and node B) and C↔E are assigned to pattern 1-0 (subpattern0 of hopping pattern1) and pattern 1-1 while A↔C and B↔D are allocated to pattern 2-0 and pattern 2-1. At the time being, both node C and node F have one radio interface available and going to be used to create a link C↔F. The algorithm is now considering an appropriate pattern for the link. Figure 2.10 shows the current MCG of the network.

Because, in this centralized network, the priority should be given to the nodes that are closest to the gateway, when consider an appropriate hopping pattern for C↔F, the algorithm must choose one that minimizes the interferences received at

node C. Hence, node C should be considered as a reference receiver and every link within its two-hop radius is considered a conflict/interfering link to C↔F; namely A↔B, A↔C, and C↔E.

From the loop in line 13-23, when determining an appropriate pattern for C↔F, the algorithm must consider both pattern 1 and pattern 2, as well as their associating subpatterns. However, to make this chapter concise, let consider only the case when pattern 1 is being considered and note that the same logic is applied for the other pattern. If C↔F is to be assigned to pattern 1, A↔C, which already assigned to pattern 2, will no longer interfere with it; hence, the cost function should take into account only A↔B and C↔E. Note that, regardless of the subpattern number assigned to them, the algorithm always consider two links interfering with each other if they use the same hopping pattern.

Then, to consider the extreme case, the algorithm assumes $Q_1 = 2$ cochannel interferences are sent from node A and node E, which are closer to node C. The received powers of the signal from node F and the interference tones from node A and node E can be found using the free-space pathloss model;

$$P_{kl} = K\frac{P_T}{d^2} \tag{2.19}$$

where P_{kl} is the received power of the signal transmitted from node k and received at node l, P_T is the TX power, and d is the distance between the nodes. The constant K can be determined by the TX and RX antenna gains and the wavelength of the transmitted signal.

Since all these RF parameters are already known, the received signal power from node F can easily be calculated, P_{FC}, and the received interference powers from node A, P_{AC}, and node E, P_{EC}. Subsequently, $\gamma_1 = \frac{P_{FC}}{P_{AC}}$ and $\gamma_2 = \frac{P_{FC}}{P_{EC}}$ can be computed. Furthermore, because the noise floor level at node C is already known

to the gateway, the SNR level γ_0 at node C can be easily calculated. Once, all the parameters obtained, the SINR and the cost associated with pattern 1 can be found by using (2.18) and (2.17).

Once a pattern is chosen, the algorithm then repeat the entire over to search for an appropriate subpattern that provide the minimum cost. Finally, by using the CA algorithm, patterns and subpatterns can be assigned to links in the network.

In practice, there are numbers of literatures proposing to improve the performance of MIMO systems by introducing an additional filter process to suppress the cochannel interferences in the received signal, before passing it to the decoding block. For example, in [22], an additional MMSE (minimum mean square error) filter is proposed and the authors have shown that the proposed method can effectively suppress cochannel interference while preserving the space-time structure, thereby significantly improving the systems interference suppression ability without significant bit error rate performance degradation.

However, when being applied to the STBC, such pre-filtering processes would inevitably damage the symmetry inherited in the received signals, making it impossible for the transmitted symbols to be detected independently; hence, discouraging the use of the STBC technique. With the CA algorithm and the multi-radio frequency hopping technique used in this chapter, the cochannel interference can be avoided by assigning different channels to different links in the network. Because no additional process is introduced for suppressing interference in the detection scheme, the symmetry in the received STBC signal is preserved. Compared to the MMSE filtering technique, the channel assignment technique can be considered as another solution for mitigating cochannel interference in the STBC MIMO networks while maintaining the complete advantage of deploying the STBC technique.

2.5 Adaptive Transmission Scheme with Channel Set Selection

From the results obtained in Section 2.3, it can be observed that using more transmitting antennas does not always guarantee better BER performance. To decide the best transmission scheme one must consider also the parameters such as SNR and, especially, SIR levels at the RX node. Since the errors occurred in a transmission depend mostly on the total interference power, a pre-estimated performance curve can thus be used to determine the transmission scheme that provides the best performance. Such pre-estimated BER curves can be obtained accurately by a test under control environment at various SNR and SIR values.

In practice, it can be seen that the BER performance, though important, is not the only goal to achieve in a data transmission. The amount of system resources that are consumed within the processing of the transmitted symbols is also of equally important consideration. Instead of achieving the best performance, when possible, can more errors be tolerated by using a scheme with less TX antennas to make data processing less complex and cut down the processing power and time? So, the challenging question is whether or not the link performance can be compromised to spare the processing resources.

In most wireless equipments, the BER threshold is usually defined in specifying the effective data rate of the system. If base on the threshold value and select a transmission scheme that provides the best trade-off between the error rate and the number of TX antennas required, then the optimal point where the target data rate can be achieved and system resources can be efficiently deployed is thus reached. Figure 2.11 illustrates the adaptive transmission. Once a node (TX node) has data designated for transmission to another node (RX node), it sends a service message to *notify* the designated RX node. This service message is considered equivalent to the RTS (request-to-send) message used in IEEE 802.11. Assume every node is well aware

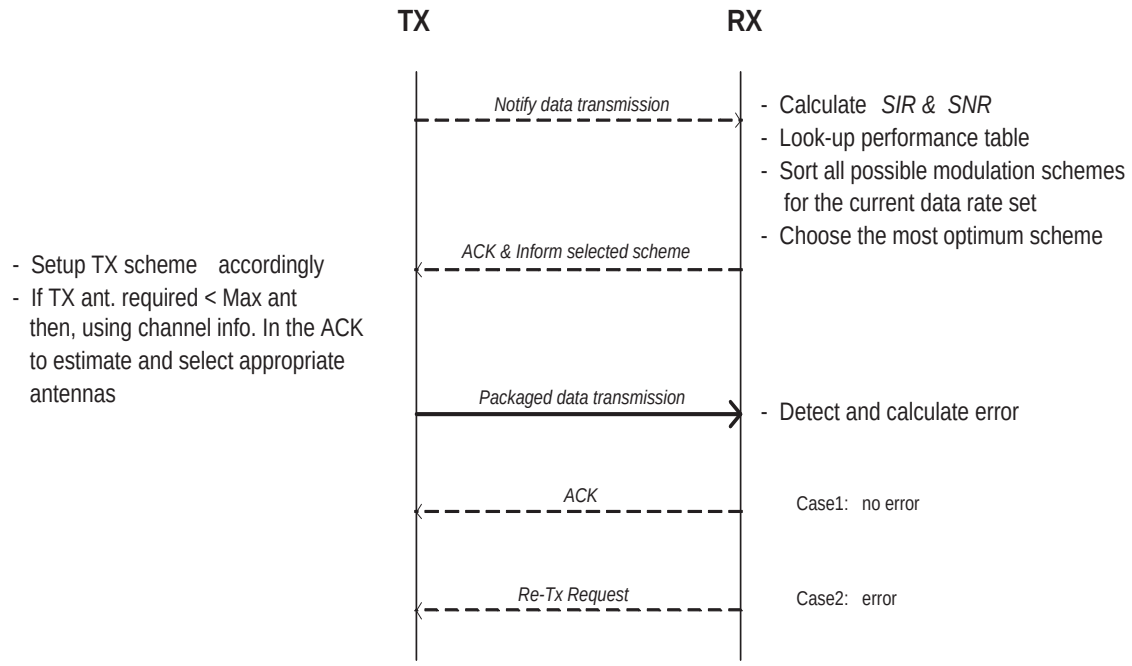

Figure 2.11. The adaptive transmission protocol for optimizing number of transmitting antennas.

of its own noise floor energy. Thus, when the RX node received the *notify* message, it will calculate the current SNR level and start measuring the current amount of cochannel interference to evaluate the SIR level. It is noted that, after the channel assignment is performed, every radio interface of a node will communicate only to its specific link partner (another interface of a neighbor node) assigned by the algorithm. Therefore, to measure the interference amount, the receiving interface must measure the power of every package received, but not originated from its designated partner.

Once the SNR and SIR are known, the RX node then uses these parameters and the BER threshold for the current preset data rate, to look-up a pre-estimated performance table. Next, it chooses the optimal transmission scheme that satisfies the BER criteria, and reply to the TX node with an *ACK* service message to acknowledge the transmission and to inform the TX node of the proper choice of transmission

scheme. Hence, the data transmission can be executed accordingly. It can be observed that, in the described protocol, the RX node will be the one choosing the transmission scheme that is matched with its own settings and environments. In fact, the decision can also be made at the TX node itself, but more signaling overheads may be required. Furthermore, it is noted that the service messages must be transmitted using a default transmission scheme to provide a way for both ends of the link to communicate during the association stage when the exact choice of transmission scheme has yet been finalized. Though relatively short, these messages are quite important to the protocol. Hence, the default transmission that is used to transmit these messages must be the transmission scheme that can achieve the best performance.

With the adaptive scheme, it is possible that some antennas may not be used for the transmission. If, by some means, the TX node can acquire the knowledge about the channels prior to the transmission, another degree of freedom is then acquired to select the antenna set that best benefits the transmission. From Figure 2.11, it can be observed that, before the actual data transmission, the RX node must send *ACK* message to the TX node to acknowledge the data transmission request and inform the optimal transmission scheme. Thus, if some known symbols are attached at the end of every service message, including the *ACK* message, the TX node can then use these symbols to estimate the most-updated channel gains.

Figure 2.12 illustrates an example structure of service message with the known symbols at the end of service packets, so-called tail words. Though the default transmission is chosen to be two TX antennas with the rate of 2 bit/sec/Hz, G_{222}, and QPSK modulation, but, in the tail word, four TX antennas will be used for channel estimation purpose. The symbol S in the tail words represents a symbol in QPSK constellation. At each time slot of the tail words, only one antenna of RX node will

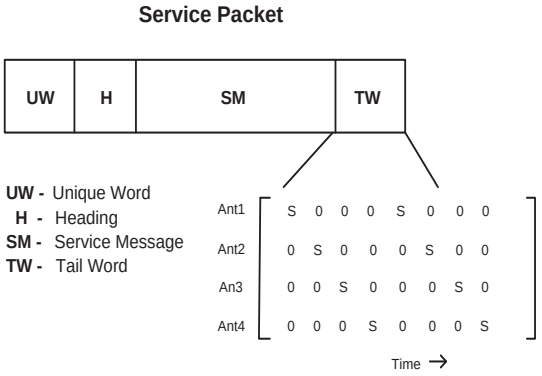

Figure 2.12. The service message structure with tail words for channel estimation.

transmit a known symbol S so that the TX node can estimate the channel gains on the paths between each antenna pair.

By using the tail words, it is assumed that the most-updated channel gains can be known to the transmitting node prior to the data transmission. Now, to select the appropriate antennas, let consider the soft decision in (2.7) for a transmission with two TX and two RX antennas using Alamouti's G_{222}. Due to the symmetry in $\tilde{s}_1$ and $\tilde{s_2}$, just the soft decision $\tilde{s}_1$ is considered, which can be expressed as;

$$\begin{aligned}\tilde{s}_1 &= (\sum_{j=1}^{2}\sum_{i=1}^{2}|h_{i,j}|^2)s_1 + h_{1,1}^{*}\ I_1^1 + h_{1,2}\ (I_2^1)^* \\ &\quad + h_{2,1}^{*} I_1^2 + h_{2,2}\ (I_2^2)^* + h_{1,1}^{*}\ n_1^1 + h_{1,2}\ (n_2^1)^* \\ &\quad + h_{2,1}^{*} n_1^2 + h_{2,2}\ (n_2^2)^* \end{aligned} \tag{2.20}$$

In this equation, $|h_{i,j}|$ is the envelope of channel between TX antenna i and RX antenna j. The parameter I_t^j and n_t^j are the interferences and noises received at time slot t and RX antenna j. At different time t or different RX antenna j, The rvs n_t^j are IID zero-mean complex Gaussian and the rvs I_t^j are zero mean and variance $\sigma_I^2 = \sum_{q=1}^{Q} P_q$. By nature, the rvs I_t^j and n_t^j are independent. Suppose the rvs I_t^j for

different time t or RX antenna j are all independent, the average power of $\tilde{s}$ can be expressed from (2.20) as

$$\sigma^2_{\tilde{s_1}} \;=\; \alpha^2 \left|s_1\right|^2 + \alpha\ \sigma^2_I + \alpha\ \sigma^2_n \tag{2.21}$$

where $\alpha = \sum_{j=1}^{2}\sum_{i=1}^{2} |h_{i,j}|^2$. It can be observed that the instantaneous SIR and SNR in $\tilde{s}_1$ are both equal to α, assuming I_t^j for different time t or antenna j are independent. If α is maximized, then the performance of the ML detection in which the soft decision is used is also maximized or, in other word, the $\sum_{j=1}^{2}\sum_{i=1}^{2} |h_{i,j}|^2$ shall be maximized to improve the link BER.

Obviously, the maximization can be performed just by choosing the first two TX antennas that have the largest envelope sum over all RX antennas. This means, among n TX antennas of the TX nodes, the antenna u and v that maximize the goal must be chosen such that $\sum_{j=1}^{2} |h_{u,j}|^2 , \sum_{j=1}^{2} |h_{v,j}|^2 \geq \sum_{j=1}^{2} |h_{i,j}|^2$ for i=1,2,..n and $i \neq u, v$. Similar conclusion can also be drawn for more than two RX antennas or for the cases of three TX antennas with G_{348} and four TX antennas with G_{448}.

Note that, in (2.21), I_t^j for different time t or antenna j were assumed to be independent. In practice, with the STBC technique, these rvs are usually correlated (highly correlated) and this will make the SIR of the soft decision be somewhat different from α. However, because the SNR remains unchanged, the error rate can still be improved by the antenna selection criteria.

Figure 2.13 illustrates the performance improvement obtained by selecting the best antenna set at SIR= 10 dB. It was assumed that there are four antennas at the TX node but only two are used for the transmission at rate 2 bit/sec/Hz, QPSK, G_{222}. Also, it is assumed that there is only one interfering node, which uses the same transmission scheme as the TX node. It is obvious that transmission with the best antenna set (in this case, the best antenna set is the first two antennas with the

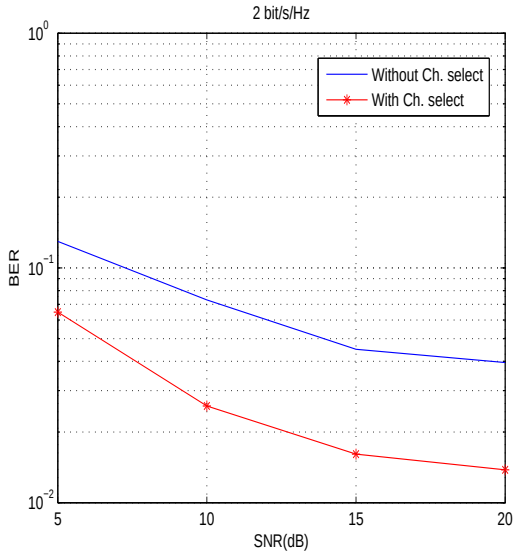

Figure 2.13. Comparison between transmissions with and without the best antenna set at SIR=10dB.

largest channel envelope sum over four RX antennas) can provide at least 5 dB gain in SNR when compared to that without.

2.6 Conclusions

In this chapter, the performances of the STBC MIMO link under the influence of cochannel interference have been investigated. Since there are various kinds of generator matrices for the STBC, in this chapter, only the G_{222}, G_{348}, and G_{448} matrices are considered with widely used modulations, like QPSK, and 16QAM. The simulation results have shown that, once the SIR is known, the factors such as the number of interfering nodes, whether or not there are dominating interference sources, or what transmission schemes are used in the interfering nodes are not important factors in determining the error rate. Based on this observation, if the SIR and SNR levels are given, the pre-estimated BER curves can then be plotted and used for predicting the performance of the STBC link in practical situations.

To further improve the STBC performance, an interference-aware CA algorithm, similar to those used for IEEE 802.11 a/b/g networks, has been applied to properly manage how radio interfaces in the STBC MR-FH WMN should access to the shared media. This CA algorithm can be considered as a MAC-layer approach, which is used to enhance the performances of the STBC links , while still achieving the full benefits of the space-time code.

Based on the previous simulation results, it have been found that using more antennas does not always guarantee a better performance; thus, to decide the optimal number of antennas required and select the best antenna set, an adaptive transmission scheme is proposed. The simulation results have illustrated that, for transmission with G_{222} selecting the best antenna set can be improved the link performance by at least 5 dB, compared to that with arbitrarily chosen antennas.

CHAPTER 3

CAPACITY OF WIRELESS HYBRID NETWORKS WITH SUCCESSIVE INTERFERENCE CANCELLATION

3.1 Introduction

In wireless networks, nodes are allowed to exchange information with each other over a common wireless channel. Under different traffic scenarios and different constraints (bandwidth, and power, for example), the amount of data that are exchanged between the wireless nodes may vary. A key question that arises in such systems is how the throughput capacity changes with a different network setup and how it grows with the number of nodes in the network.

Wireless networks without support from fixed infrastructure is commonly known as ad-hoc networks. Due to the lack of an infrastructure, data needs to be forwarded to the destination via a multi-hop fashion. A well-known study in [23] has illustrated that, when nodes are placed optimally, the per-node capacity decreases at $\Theta(1/\sqrt{n})$ as n tends to infinity. On the other hand, if nodes are randomly located, the per-node capacity will decay faster at $\Theta(1/\sqrt{n \log n})$. Nevertheless, with a more general information theoretic setting, the authors of [24] have proved that the rate higher than $\Theta(1/\sqrt{n \log n})$ is achievable. Subsequently, in [25], the authors have applied the percolation theory and provided a lower bound of $1/\sqrt{n}$ for the per-node capacity of a network with randomly placed nodes; hence closing the gap in the capacity of wireless networks.

Notice that the mentioned literature is focused mostly on *static* (immobile) wireless nodes with typical communication scenarios. In fact, there are numbers of

references that pay special attention to different aspects of the networks. In [26], the authors have shown that the mobility of nodes can increase network capacity and the per-node throughput of *mobile* ad-hoc networks is bounded by a constant, even as the number of nodes (n) increases. Nevertheless, in [27], it has later been illustrated that the use of more intelligent node cooperation and distributed MIMO communication on static nodes can also achieve the same per-node throughput. Other than that, there are also a large number of studies that considers different types of data traffic, such as multicast. Examples can be seen in [28, 29].

In some scenarios, a set of base stations may be connected together by wired links and placed within the ad-hoc network to form a wired infrastructure for enhancing the throughput performance of the ad-hoc network. The resulting network is usually referred to as a hybrid wireless network. The capacity of the hybrid networks has also been studied widely in the literature, for example [30, 31]. In [30], the benefit of the infrastructure is shown to be dependent on the number of base stations in relation to the number of wireless nodes, and, for two-dimensional hybrid network with b base stations, the maximum per-node capacity scales as $\Theta(b/n)$ if base stations are added at a speed asymptotically faster than $\sqrt{n}$, i.e. $b = \Omega(\sqrt{n})$. Similarly, in [31], it has been shown that, if $b = \omega(\sqrt{n})$, the maximum per-node capacity of $\Omega(\min(b/n, 1/\log b))$ is achievable by delivering data through the wired infrastructure. Otherwise, the percolation highway as in [25] must be used instead, in order to achieve the maximum capacity.

In this chapter, the per-node throughput capacity that can be achieved in the hybrid wireless networks of n wireless nodes and b base stations is investigated. Two different transmission strategies, the infrastructure mode and inter-cell mode, are considered. To determine which mode is proper, a *scheduled* source node will decide on the location of the destination it selected. If the chosen destination is outside the

coverage of the base station in which it is located, the infrastructure mode will be selected. The *scheduled* source node will, first, send data to the base station in its cell. The data is then transport through the infrastructure link to the base station grid in which the destination is located and forwarded to the destination by the base station. On the other hand, if the chosen destination is under the same cell as the source, inter-cell mode will be activated and the data will be transmitted directly (point-to-point) to the destination.

Unlike the previous studies in [23, 24, 25, 26, 27, 28, 29, 30, 31, 32, 33, 34, 35, 36, 37], the study in this chapter will also apply an information theoretic technique for multiple access channel to increase the throughput capacity of the network. Specifically, within each routing strategy, a set of nodes in the same cells as the *scheduled* source node is allowed to simultaneously transmit to the destination if such transmissions do not impair the achievable transmission rate of the scheduled source. These nodes are referred to in this chapter as the *(*opportunistic) sources. At the reception, the destination deploys a successive interference cancellation (SIC) technique, as detailed in [18] and [38]. That is, the signals from the opportunistic sources are decoded in the order of their signal powers received, and then subtracted from the received signal to obtain only the signal of the scheduled source plus noise. Because the interference from the opportunistic sources is eliminated, the data from the scheduled source can then be decoded perfectly as in the case when it was the only transmitting source.

Similar to [27], the key idea behind the decoding scheme chosen is the believe that the *physical model* used by many references, for example [23] and [30], is somewhat strict. In particular, the model assumes that the signals received from nodes other than the designated transmitter are interference to be regard as noise. Based on this assumption, long range point-to-point communication between nodes is not

preferable. The optimal strategy is to resort to the multi-hop scheme to confine the communications to nearest neighbors and rely on a spatial reuse to maximize the number of simultaneous transmissions. In this chapter, however, a slightly looser restriction is taken by allowing nodes to transmit data directly to their destinations. By doing so, a set of nodes is allowed to transmit simultaneously, and, using the SIC decoding technique, the interference from these nodes can then become valuable information, rather than just noise. Hence, the spatial multiplexing gain can then be achieved. Furthermore, to inherit the benefit of the spatial reuse, very long range communications are confined by letting such traffics being transported via the wired infrastructure network.

Because the main focus of this chapter mostly concerns with the asymptotic behavior of the wireless hybrid network, then will adopt the asymptotic notations as discussed in [39], i.e. $O(g(n))$, $\Omega(g(n))$, $\Theta(g(n))$, $o(g(n))$, and $\omega(g(n))$.

3.2 Network Modeling

3.2.1 Network Model

The following assumptions are made for the random wireless network model

1. The *random extended network* model is constructed by placing n wireless nodes uniformly over a square area of $[0, \sqrt{n}] \times [0, \sqrt{n}]$ with unit density ($\lambda = 1$). Nodes are assumed static and let assume every node knows its own location X_i, $1 \leq i \leq n$.
2. By regularly placing a total number of b base stations as a grid in Figure 3.1, the network is then partitioned into square cells of side length $c = \sqrt{n/b}$. Each cell contains one base station and base stations are linked together by a wired network to form an infrastructure. Assume the bandwidth of the wired network

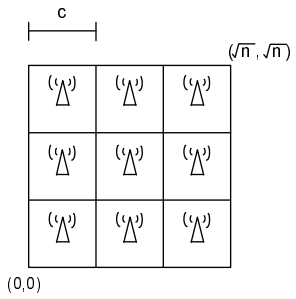

Figure 3.1. The square network of size $\sqrt{n} \times \sqrt{n}$ is partitioned into b cells of size $\sqrt{\frac{n}{b}} \times \sqrt{\frac{n}{b}}$.

is large enough so that there is no bandwidth constraint on the infrastructure. In contrast to the nodes, base stations neither generate nor consume data. They serve purely as relays for the traffic between nodes. The number b tends to infinity as $n \to \infty$, but at a much slower rate.

3. Each node i transmits signals with the same power P, and the signal is received at node j with power $Pl(|X_i - X_j|)$. Here, $l(|X_i - X_j|) = \min(1, |X_i - X_j|^{-\alpha} e^{-\gamma|X_i - X_j|})$ is the large-scale radio attenuation function, and $|X_i - X_j|$ indicates the Euclidean distance between the two nodes. The parameter $\alpha > 2$ denotes the path loss exponent and $\gamma > 0$, unless transmission is over a vacuum, represents the channel absorbtion.
4. The wireless channel is a Gaussian channel model with bandwidth W Hz and additive white Gaussian noise with power spectral density $N_0/2$.

3.2.2 Transmission Strategies

Assume each node has data to be sent to every other node in the network and these data are readily stored in a node's memory. In a particular cell, nodes will be scheduled to transmit in a round robin fashion so that, every fixed amount of time, each node will be scheduled for transmission once (timesharing). In this chapter, the

scheduled node is referred to as the *scheduled source* node or *source* for short. When being slotted for transmission, the source will randomly choose a destination, which can be any particular node in the network. Then, it retrieve the corresponding data from the memory and begins to transport the data to the chosen destination.

There are two types of transmission modes used in a hybrid network: intra-cell mode and infrastructure mode. When the source node chooses a destination located in the same cell, the intra-cell transmission mode will be in effect. Data are sent directly from the source to the destination through a single hop and without using any infrastructure. On the other hand, if the two nodes are located in different cells, the infrastructure mode will be used instead, and the transmission protocol is divided into three separate phases. The first uplink phase occurs when the data enters the infrastructure by having the source directly transmit to the base station in the cell. Subsequently, the data is transported via the wired infrastructure network in transport phase and reaches to the base station, in which the destination is located. Finally, the data is downlinked from the base station to the destination.

The channel bandwidth of W Hz is split into two orthogonal sub-channels with W_1 and W_2 Hz, respectively. The W_1 sub-channel will be assigned for the data transmitted from the source to the destination, which can either be the destination (intra-cell mode) or to the base station (uplink phase), and the bandwidth W_2 will be assigned to base stations for delivering the data to the destinations (downlink phase). From the perspective of nodes, it can be said that W_1 is allocated to the outgoing traffics of nodes while W_2 to the incoming traffics.

3.3 Main Results

In this chapter, the upper bounds and lower bounds for the throughput capacity of a hybrid network with the SIC technique are derived, based on the two transmission

modes. Before proceeding, it is noted that, in many references, the throughput capacity is usually specified via the transmitter perspective as the average rate at which every node can transmit data to its destination. In this chapter, since the scheduled and opportunistic sources are allowed to transmit simultaneously to a common destination, at any time slot in a cell, there will be more than one transmitter, but only one receiver. Further, from (3.3), the achievable rate of individual opportunistic source is always lower than that of the scheduled one. If the similar definition of throughput was adopted, the rate achieved by the scheduled source may decrease when being averaged over every transmitter. Hence, the benefit of having multiple transmitters is obscured. To clearly illustrate the advantage of the multiple access technique, the feasible throughput of the hybrid network model is defined as:

Definition 1: For a hybrid network of n nodes and b base stations, a throughput of $T(n, b)$ bit/sec for each node is feasible if there is a spatial and temporal scheme for scheduling transmissions such that every node can *receive* $T(n, b)$ bit/sec on average.

Note that if only the scheduled source is allowed to transmit at any time slot, the number of bits transmitted from the source will be equal to the number of bits the destination received. The throughput measured at the destination will be the same as that measured at the source. However, when opportunistic sources are allowed, their benefit is better illustrated through the measurement specified in Definition 1.

Now, the results for the hybrid network model mentioned are provided. It can be shown that, for a hybrid network with n wireless nodes and $b = o(n/\log n)$ base stations under the intra-cell transmission mode, the per-node throughput capacity is

$$T_{intra}(n, b) = O\left(\frac{b}{n} \log \frac{n}{b} W_1\right)$$

When the infrastructure mode is used, the base station of the cell in which the destination locates will be the only transmitter downlinking data to the destination:

hence, the SIC technique is not applied. Therefore, a bottleneck occurs and the per-node throughput capacity is

$$T_{infra}(n, b) = \Theta\left(\frac{b}{n} W_2\right)$$

Compared to the well-known result of $\Theta(1/\sqrt{n})$ from Gupta and Kumar work, it is not surprising that the capacity bounds of this chapter predict a higher throughput per node, especially when $b = o(n/\log n)$. This is because a portion of the inter-cell traffics in this chapter is transported through the wired infrastructure network. Therefore, the burden of long multi-hop relay can be avoided. Consequently, more bandwidth resources are left available for some other nodes to communicate. Furthermore, this chapter also encourages the spatial multiplexing by allowing multiple nodes to transmit simultaneously (using SIC technique), so the capacity is improved even more.

To make the comparison much fairer, the definition of network *transport capacity* in [23] should be adopted. It is clear that, for a hybrid network, when b increases, the cell size decreases and, consequently, the distance over which the information bits are transported decreases. Hence, to make up with the use of the infrastructure network, the throughput capacity in this chapter should be scaled down by the square root of cell area, instead of the square root of network area. Therefore, the transport capacities of $O(\sqrt{\frac{b}{n}} \log \frac{n}{b})$ and $\Theta(\sqrt{b/n})$ are obtained for the intra-cell mode and the infrastructure mode, respectively. Compare with the transport capacity of $\Theta(\frac{1}{\sqrt{n}} \times \sqrt{n}) = \Theta(1)$ obtained by the result from [23], the transport capacities found, which decreases as n increases, are now much lower because the average distance over which information is carried is much shorter.

Note also that when $b = o(\sqrt{n})$, the per-node capacities presented drop and the rates obtained are much less than that of Gupta and Kumar. The reason is that

the transmission strategies in this chapter depend largely on point-to-point communication between a source and a destination. Consider, for example, the throughput capacity of the intra-cell mode. When base stations are scarcely deployed, the cell size increases and the average distance between any source-destination pair increases. Because the transmission power P of these nodes is fixed, the average rates at which they transmit drop dramatically, so as the overall throughput. Therefore, it is clear that the benefit of adding base stations and adopting the SIC technique becomes significant when the investment in the wired infrastructure is high enough.

The rest of this chapter is organized as follows. In Section 3.4.4 and Section 3.5, related lemmas are discussed then the proofs for the proposed asymptotic capacity bounds is provided. In Section 4.3, the results are analyzed and compared with related literatures. Finally, Section 4.4 concludes the chapter.

3.4 Capacity of the Intra-cell Mode

3.4.1 The Number of Nodes Per Cell

Since nodes are placed randomly within the network, it is not necessary that every cell contains a wireless node. However, based on the following lemma, it can be shown that every cell in the network is not empty and there are $\Theta(n/b)$ nodes within each cell.

Lemma 1: For $b = o(n/\log n)$ and $n \to \infty$, there is at least one wireless node contained within the square cell of side length $c = \sqrt{n/b}$. Furthermore, the number of nodes, n_c, in each cell is bounded by $\Theta(n/b)$.

Proof: The proof is similar to that of Lemma 5.7 in [40]. Let event A denote a Bernoulli event that a particular node i, $1 \leq i \leq n$, will fall into a particular cell of area c^2. Because nodes are placed uniformly on the network, it is clear that

probability of event A is $P_A = (n/b)/n = 1/b$. Therefore, the probability that a cell is empty is $(1 - P_A)^n$. The probability that at least one cell in the network is empty is upper-bounded by

$$b(1 - P_A)^n = b(1 - \frac{1}{b})^n \leq b \exp(-\frac{n}{b})$$

where the last inequality is obtained from the fact that $1 - x \leq \exp(-x)$. If $b = o(n/\log n)$, $b \exp(-n/b) \to 0$ as $n \to \infty$ because the exponential term drops at faster rate. Therefore, the first part of the lemma is proved.

Next, consider the upper bound for the number of nodes, n_c, in a particular cell. The number of nodes has a binomial distribution with parameters (P_A, n). Using the Chernoff bound, it can be shown that

$$\Pr(n_c > k_1 \frac{n}{b}) \leq \frac{E\{\exp(n_c)\}}{\exp(k_1 n/b)} \tag{3.1}$$

where k_1 is a constant. Since $E\{\exp(n_c)\} = (1 + (e-1)P_A)^n \leq \exp[(e-1)n/b]$ (because $1 + x \leq \exp(x)$), it can be shown that

$$\Pr(n_c > k_1 \frac{n}{b}) \leq \exp\Big\{ - \frac{n}{b} [k_1 - (e-1)] \Big\}$$

As long as $k_1 > e - 1$, it can be shown by the union bound that Pr(some cells have more than $k_1 n/b$ nodes) $\leq b \exp\{-[k_1 - (e-1)]n/b\}$. The probability converges to zero as n tends to infinity and $b = o(n/\log n)$.

Next, using the Chernoff bound, it can be shown that

$$\Pr(n_c < k_2 \frac{n}{b}) \leq \frac{E\{\exp(-n_c)\}}{\exp(\frac{-k_2 n}{b})} \tag{3.2}$$

where k_2 is another constant. Since $E\{\exp(-n_c)\} = (1 + (e^{-1} - 1)P_A)^n \leq \exp[(e^{-1} - 1)n/b]$, it can be shown that

$$\Pr(n_c < k_2 \frac{n}{b}) \leq \exp\Big\{ - \frac{n}{b} [(1 - e^{-1}) - k_2] \Big\}$$

As long as $k_2 < 1 - e^{-1}$, it is known by the union bound that Pr(some cells have less than $k_2 n/b$ nodes) converges to zero as n tends to infinity and $b = o(n/\log n)$. Hence, it is concluded that each cell, in fact, contains $\Theta(n/b)$ nodes and the proof is completed.

3.4.2 Multiple-Access Channel with SIC

In a particular cell, nodes are time-sharing and transmit in a round robin fashion. When being slotted, the scheduled source node i at X_i will receive a bandwidth W_1/n_c Hz for the transmission. If the chosen destination node j is at X_j, from the information theoretic point of view, node i can transmit to node j at the achievable rate R determined by

$$R = \log\left[1 + \frac{Pl(|X_i - X_j|)}{\mu W_1 N_0}\right] \quad bit/sec/Hz$$

where μ represents the fraction of bandwidth W_1 that are assigned to the source and will be described in the sequel. Note that the rate R is achieved by assuming a single source transmits to the destination. Can one do better?

Let assume, for any scheduled source, there are a set of κ nodes in the same cell, whose Euclidean distance away from X_j is greater than $d_{ij} = |X_i - X_j|$. If the set of nodes is allowed to be *opportunistic* sources and transmit data simultaneously to the destination node j, the channel thus becomes a Gaussian multiple-access channel and there exists a sequence of codes, with which these sources can transmit data to the common destination with arbitrarily low probability of error. Therefore, the total number of bits transported to the receiver could be increased, in proportion to growth rate of κ.

Let $X_{i,q}$, where $q = 0, 1, ..., \kappa$, denote the locations of these sources. $X_{i,0} = X_i$ is the location of the scheduled source node i and $X_{i,q}$ for $q \neq 0$ is the location of the opportunistic source q of the scheduled source node i. Without loss of generality, assume $|X_{i,1} - X_j| < |X_{i,2} - X_j| < ... < |X_{i,\kappa} - X_j|$ and, by the previous criteria, $|X_{i,q} - X_j| > d$ if $q \neq 0$.

Chapter 14.3 of [38] and Chapter 6.1 of [18] show that, if every destination uses the SIC technique to decode the received data, the individual rate, R_q, that each node can achieve and the total sum rate are

$$\begin{aligned} R_q &< \log\left[1 + \frac{Pl(|X_{i,q} - X_j|)}{\mu W_1 N_0 + \sum_{v=0}^{q} Pl(|X_{i,v} - X_j|)}\right] \\ \sum_{q=0}^{\kappa} R_q &< \log\left[1 + \frac{\sum_{q=0}^{\kappa} Pl(|X_{i,q} - X_j|)}{\mu W_1 N_0}\right] \end{aligned} \tag{3.3}$$

It can be observed from (3.3) that the achievable rate R_0 of the scheduled source is $\log(1 + \frac{Pl(|X_i - X_j|}{\mu W_1 N_0})$, as before. Thus, the data traffic from the scheduled source remains intact but the total number of transmitted bits is growing with the number of opportunistic sources.

For simplicity, it was assumed in the previous statement that, in a cell, there are κ nodes that are at a distance farther away from the node j than node i. In the following lemma, it is proved that κ is linearly proportional to the number of nodes per cell.

Lemma 2: For a given source and destination pair in any cell, there are $\kappa = \Theta(n/b)$ nodes in the same cell that have greater distances from the destination than the source node.

Proof: For the intra-cell mode to be selected, the source must have chosen a particular node in the same cell as its destination. The Euclidean distance between

a source-destination pair is determined only by the locations of the nodes and is independent of n.

Now, assume a source node i chooses a particular node j in its cell as a destination and the Euclidean distance between these two nodes is equal to $d_{ij} = |X_i - X_j|$. If a disk of radius d_{ij} around the destination j is constructed as shown in Figure 3.2, certainly, any random point located inside the disk must be closer to node j than node i. Thus, the opportunistic sources of node i must be located outside the disk. The goal is to estimate the remaining cell area that are outside the disk and provide the bounds for the number of nodes in this area.

Depending on the locations of node i and j, sometimes a portion of the disk may fall outside the cell boundary, so they should not be taken into account when considering the events that occur to nodes in the cell. If A_d denotes the area of the disk of radius d_{ij} that is inside the cell domain, then A_d can always be represented as υc^2, where $\upsilon \in (0, 1]$ as shown in Figure 3.2. Also, it is noted that υ is determined only by the distance d_{ij} and, thus, independent of n.

Given that there are n_c nodes in the cell where node i and node j are located, let node q, $1 \leq q \leq n_c - 2$, be another node in the cell, excluding node i and j, and Z_q be a random variable that represents whether node q is located outside A_d. The random variable Z_q can be expressed as

$$Z_q = \begin{cases} 1\,, & \text{node } q \text{ is outside the area } A_d \\ 0\,, & \text{otherwise} \end{cases} \tag{3.4}$$

Since the probability that the a random node q is located outside in A_d is $1 - \upsilon$, therefore $E[Z_q] = 1 - \upsilon$. Clearly, $\kappa = \sum_{q=1}^{n_c-2} Z_q$ is the total number of nodes in the

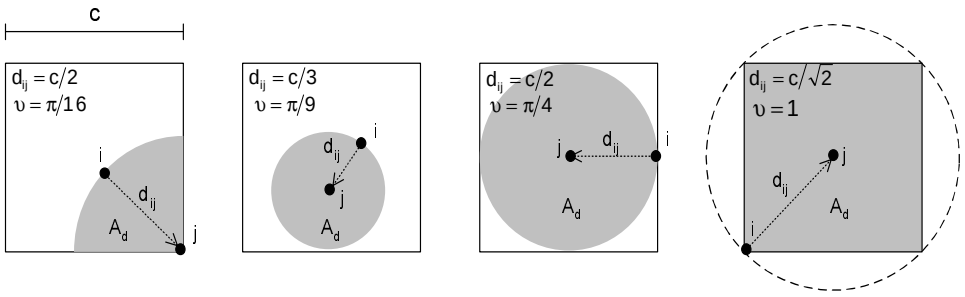

Figure 3.2. For a given source node i with distance d_{ij} away from its destination j, the opportunistic sources should be located outside (white area) the disk of radius d_{ij} centered at the destination.

cell, excluding node i and the receiver j, that are located outside A_d. By the Strong Law of Large Numbers, with probability equal to 1,

$$\frac{\kappa}{n_c - 2} = \frac{1}{n_c - 2} \sum_{q=1}^{n_c - 2} Z_q \to 1 - \upsilon \tag{3.5}$$

Since $\upsilon \in (0, 1]$ is independent of n and $n_c = \Theta(n/b)$, then $\kappa = \Theta(n/b)$. The proof is completed.

It have been shown that, when a source and its destination are located within the same cell, there exist $\kappa = \Theta(n/b)$ eligible nodes for serving as the opportunistic sources. However, because the destination for a scheduled source is chosen randomly every time, the set of these eligible nodes changes for a different source and destination pair. It is not so obvious how these κ eligible nodes can be aware of their roles as the opportunistic sources. Thus, it is important that the source has to inform every node about the chosen destination.

Note that, in the intra-cell mode, the source should be able to transmit to any chosen destination in the same cell. When it transmits, every node in the cell will always hear. Thus, if τ denotes a transmission time allocated to a source, then it can be further partitioned into two sections. The first section consumes a fraction $\theta \in [0, 1]$ of τ and is used for the source to inform every node about its chosen

destination. The second section of $(1-\theta)\tau$ is for the source and the opportunistic sources to transmit data to the common destination. Assume θ, $(0 < \theta < 1)$, remains constant, irrespective to the transmission rate.

3.4.3 Frequency Reuse

Because the outgoing and the incoming traffics of node is assigned to different different orthogonal sub-channels, there is no interference between the two types of traffic. However, within the same sub-channel, interference still exists between the same type of traffic in different cells. Fortunately, the effect of such interference can be minimized by applying the frequency reuse concept as in [31] and [25]. Specifically, the cells are first grouped together to form a certain number of clusters. Then, different frequency bands are assigned to cells in the same cluster. However, over different clusters, the same set of these frequency bands is reused. Hence, the transmissions in the cells (in different clusters) with the same frequency can be carried out simultaneously without causing excessive interference only if there is sufficient distance between these cells.

Lemma 3: For an integer $a > 0$ representing the distance of a cells within which transmissions in an arbitrary cell can be successfully received, there exists a reuse policy with M^2 frequency bands, where $M = 2(a+1)$, such that every cell in the network can transmit concurrently with a bounded interference.

Proof: The proof of this lemma is similar to that of Theorem 4 in [25]. When transmissions in an arbitrary cell can be received also by a node at a distance of a cells away, cells can be grouped into square clusters of side length $M = 2(a+1)$ cells, as depicted in Figure 3.3. Then, a reuse set of M^2 frequency bands, $\{f_1, f_2, ..., f_{M^2}\}$, can be assigned to the M^2 cells of each cluster. Now, let consider a given cell o as marked in Figure 3.3. Notice that, for a given cell o, there will always be one cell in every

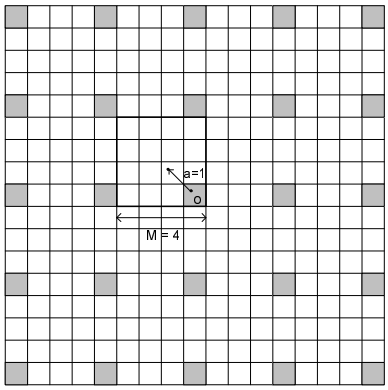

Figure 3.3. The frequency reuse scheme for the case $a = 1$. The shaded squares are cells that use the same frequency and may interfere with each other when transmitting simultaneously.

cluster that uses the same frequency. Any transmissions within these cells will cause interferences to the traffic within cell o. The maximum interference can be considered by observing in Figure 3.3 that the first-tier ($i = 1$) interferers are the transmitters in eight closest cells located at the distance of at least $[2(a + 1) - 1]c$ away from the receiver in cell o. Then, the second-tier ($i = 2$) interferers are the transmitters in the next 16 closest cells located at the distance of at least $[4(a + 1) - 1]c$.

Note each interfering cell in the i-th tier also has $\kappa_j + 1$ nodes, where $j = \{1, 2, ..., 8i\}$, that are transmitting simultaneously. Among every cell in the network, if a set of opportunistic sources in cell k has the maximum number of opportunistic nodes at a particular transmission round then $\kappa_{max} = \kappa_k$ and $\kappa_{max} \geq \kappa_l$, where $l = \{1, 2, ..., b\}$. Similarly, among every cell in the network, if a set of opportunistic sources in cell m has the minimum number of opportunistic sources then $\kappa_{min} = \kappa_m$ and $\kappa_{min} \leq \kappa_l$, where $l = \{1, 2, ..., b\}$. The κ_{max} and κ_{max} is $\Theta(n/b)$ because they are sets of opportunistic sources in two different cells. Thus, it is clear that the total numbers of simultaneous transmitters in the entire i-th interfering tier is in the interval of $[8i(\kappa_{min} + 1), 8i(\kappa_{max} + 1)]$.

By extending the sum of interferences to the entire plane transmitters in each cell, the upper bound of this sum is

$$\begin{aligned} I(c,d) &\leq \sum_{i=1}^{\infty} 8i(\kappa_{max}+1)P[2ci(a+1)-c]^{-\alpha}e^{-\gamma(2ci(a+1)-c)} \\ &\overset{(a)}{\leq} 8(\kappa_{max}+1)P\sum_{i=1}^{\infty} i\left[2ci\left(a+\frac{1}{2}\right)\right]^{-\alpha}e^{-2\gamma ci(a+\frac{1}{2})} \\ &= 8(\kappa_{max}+1)P\left[2c\left(a+\frac{1}{2}\right)\right]^{-\alpha}\sum_{i=1}^{\infty} i^{-\alpha+1}e^{-2\gamma ci(a+\frac{1}{2})} \end{aligned} \tag{3.6}$$

where (a) is due to the fact that $2ci(a+1)-c \geq 2ci(a+1/2)$. Next, to consider the minimum interference, it is observed that the first-tier and second-tier interferers are at the distance of at most $[2(a+1)+1]\sqrt{2}c$ and $[4(a+1)+1]\sqrt{2}c$ cells away, respectively. The lower bound of the interference sum can be expressed as

$$\begin{aligned} I(c,d) &\geq \sum_{i=1}^{\infty} 8i(\kappa_{min}+1)P(2\sqrt{2}ci(a+1)+\sqrt{2}c)^{-\alpha}e^{-\gamma(2\sqrt{2}ci(a+1)+\sqrt{2}c)} \\ &\overset{(b)}{\geq} 8(\kappa_{min}+1)P\left[2\sqrt{2}c\left(a+\frac{3}{2}\right)\right]^{-\alpha}\sum_{i=1}^{\infty} i^{-\alpha+1}e^{-2\sqrt{2}\gamma ci(a+\frac{3}{2})} \end{aligned} \tag{3.7}$$

where (b) results from $2\sqrt{2}ci(a+1)+\sqrt{2}c \leq 2\sqrt{2}ci(a+3/2)$. Evidently, if $\alpha > 2$ and $\gamma > 0$, the summation terms in (3.6) and (3.7) converge and the values of the bounds are defined by $\kappa_{max}c^{-\alpha}$ or $\kappa_{min}c^{-\alpha}$. Therefore, the interference decreases at the rate of $\Theta\big((n/b)^{1-\frac{\alpha}{2}}\big)$.

3.4.4 Throughput Capacity of the Intra-cell Mode

Use is made of every spatial and temporal schemes described, to find that the bandwidth allocated to a schedule source as $\mu W_1 = [(1-\theta)/(M^2 n_c)]W_1$. Consequently, the throughput per node $T(n,b)$ can be determined from the product between the bandwidth allocated to the scheduled source and the sum of the transmission rates for the scheduled and opportunistic sources, i.e. $\mu W_1 \sum_{q=0}^{\kappa} R_q$.

Lemma 4: For source node i and destination node j in an arbitrary cell with distance d_{ij} apart, as $n \to \infty$, the sum of the transmission rate of the scheduled and opportunistic sources in the cell is $O(\log(n/b))$.

Proof: Certainly, the sum rate is always greater than or equal to the rate at which the source (alone) transmits to the destination. Thus, when there is no opportunistic node for the source or if the opportunistic sources are sending at relatively small rates, compared to the source, the sum rate can be lower bounded as

$$\begin{aligned} \sum_{q=0}^{\kappa} R_q &\geq \log\left[1 + \frac{Pl(|X_i - X_j|)}{\mu W_1 N_0 + I}\right] \\ &\overset{(c)}{\geq} \log\left[1 + \frac{P \ \min(1, d_{ij}^{-\alpha} e^{-\gamma d_{ij}})}{W_1 N_0 + I_{max}}\right] \end{aligned} \tag{3.8}$$

where (c) is obtained by assuming the maximum interference and the maximum Gaussian noise power. The maximum interference is the upper bound of the interference sum in (3.6): as $n \to \infty$, the interference converges to zero. Thus, the minimum sum rate varies with the distance, which is independent of n. Therefore, the sum rate is lower bounded by a constant as $n \to \infty$.

By the selection criteria, the opportunistic sources must be located outside or on the disk of radius d_{ij} around the destination j. Thus, the sum rate is maximized if each opportunistic source has minimum distance away from the destination node j: that is, the opportunistic sources are located at the disk around node j. Under this circumstance, the maximum sum rate can be expressed as

$$\begin{aligned} \sum_{q=0}^{\kappa} R_q &\leq \log\left[1 + \frac{\sum_{q=0}^{\kappa} Pl(|X_{i,q} - X_j|)}{\mu W_1 N_0 + I}\right] \\ &\overset{(d)}{\leq} \log\left[1 + \frac{\sum_{q=0}^{\kappa} P \ \min(1, d_{ij}^{-\alpha} e^{-\gamma d_{ij}})}{\mu W_1 N_0 + I_{min}}\right] \\ &= \log\left[1 + \frac{(\kappa+1) P \ \min(1, d_{ij}^{-\alpha} e^{-\gamma d_{ij}})}{\mu W_1 N_0 + I_{min}}\right] \end{aligned} \tag{3.9}$$

where (d) is obtained by applying the minimum interference sum in (3.7). Because $\mu = (1-\theta)/M^2 n_c = \Theta(b/n)$ and $I_{min} = \Theta((n/b)^{1-\frac{\alpha}{2}})$, it is easy to show that, with $\kappa = \Theta(n/b)$, the maximum sum rate is $\Theta(\log(n/b))$. Compared to the minimum rate previously obtained, the maximum sum rate increases by a factor of $\log(n/b)$, due to the contribution of the opportunistic sources. Lastly, by taking in account the max and min values of the sum rate, it is concluded that the sum rate is $O(\log(n/b))$.

Now, it is time to consider the per-node capacity T_{intra} for the intra-cell mode.

Theorem 1: For a hybrid network with n nodes and b base stations under the intra-cell transmission mode, if $b = o(n/\log n)$, the per-node throughput capacity is

$$T_{intra}(n,b) = O\left(\frac{b}{n}\log\frac{n}{b}\,W_1\right)$$

Proof The proof is quite straightforward. By multiplying $\mu W_1 = \Theta((b/n)W_1)$ to the sum rate in Lemma 4, the per-node capacity for the intra-cell mode can be obtained directly. It is also noted that, by multiplying μ to the lower bound of the sum rate, the lower bound of T_{intra} is obtained as $\Omega((b/n)W_1)$.

3.5 Capacity of the Infrastructure Mode

If available, the opportunistic sources can also be allowed to simultaneously transmit the data to the common destination via the infrastructure mode. Specifically, in the uplink phase, the source and the opportunistic sources must, first, relay all of their traffics to the base station in the cell. Then, in the transport phase, the base station decodes the transmitted data from each source, using the SIC decoding technique, and send them through the wired network to the base station in the destination cell. Subsequently, the data is transported to the common destination in the downlink phase.

Theorem 2: For a hybrid network with n nodes and b base stations under the infrastructure transmission mode, if $b = o(n/\log n)$, the per-node throughput capacity is

$$T_{infra}(n, b) = \Theta\left(\frac{b}{n} W_2\right) \tag{3.10}$$

Proof The proof is from the fact that the throughput of the uplink and downlink when transmitted in the infrastructure mode are equal. Apparently, the uplink traffic is very similar to the traffic in the intra-cell mode. The only difference between the two types of traffic is that the receiver of the uplink transmissions is the base station in the middle of the cell, while, for the intra-cell mode, the receiver is the destination itself. Hence, the per-node throughput T_{infra}^{UL} for the uplink phase is $O((b/n)\log(n/b)\, W_1)$, which is obtained by extending the results for the intra-cell mode.

For the downlink traffic, based on the same frequency reuse technique in Lemma 3, every base station receives a bandwidth share of W_2/M^2 to simultaneously transmit to the destination in the cell. However, because there is only one base station in a cell, the multiple access technique is not applicable and each base station should equally divide its own bandwidth share for servicing every node within the cell. Therefore, the base stations before the destinations must transmit data through a bandwidth of $W_2/M^2 n_c$, and this becomes the bottleneck of the throughput.

Based on a similar proof of the minimum sum rate in Lemma 3, it can easily be shown that the rate at which the base station transmits to the destination is a constant rate k_3, which is determined by the distance between the base station and the destination: these are independent of n. Consequently, the per-node throughput T_{infra}^{DL} for the downlink phase can be obtained as $k_3 W_2/M^2 n_c = \Theta((b/n)\, W_2)$. Nevertheless, due to the downlink bottleneck, it is concluded the per-node throughput of the infrastructure mode is $\Theta((b/n)\, W_2)$.

3.6 Analysis

3.6.1 Implication from the Results

It can be observed that, regardless of how many base stations are placed in the network, T_{infra} is always lower than T_{intra} by a factor of $\log \frac{n}{b}$, due to nonexistence of the opportunistic transmitters in the downlink phase. Consequently, the per-node capacity of the network is optimized if nodes are encouraged to communicate only with the nodes in the same cell by letting $W_1 = W$. Surprisingly, this implication makes a fairly good correspondence with the "smart home" scenario of [23], in which the achievable throughput is maximized by having nearby sensors and actuators in each home communicate together. The difference is that the intra-cell communication is encouraged to avoid passing data through the bottleneck, but the smart-home network is used to restrain the distances between source-destination pairs.

3.6.2 Comparison to Related Works

For a square network of size $\sqrt{n} \times \sqrt{n}$, it was shown in [31] that the per-node throughput capacity of the infrastructure mode is

$$T'_{infra}(n,b) = \begin{cases} \Omega(\frac{W_2}{\sqrt{n}}) & \text{if } b = O(\sqrt{n}) \\ \Omega(\min(\frac{b}{n}, \frac{1}{\log b})W_2) & \text{if } b = \omega(\sqrt{n}) \end{cases} \tag{3.11}$$

where the capacity of $\Omega(W_2/\sqrt{n})$ is achieved by using the *percolation highway* to deliver the data from source to destination, instead.

In comparison, the per-node capacity T_{infra} of the infrastructure mode is given by Theorem 2 as $\Theta((b/n)\, W_2)$, when $b = O(\sqrt{n})$. The capacity becomes $O(W_2/\sqrt{n})$, which is somewhat smaller than $\Omega(W_2/\sqrt{n})$ obtained from (3.11). Also, for $b = \omega(\sqrt{n})$ and $b = o(n/\log n)$, Theorem 2 provides $T_{infra} = \omega(W_2/\sqrt{n})$, which is slightly weaker

than that obtained from (3.11). Clearly, this is because no percolation highway is formed in this study.

Because the intra-cell mode transmission is not available in [31], to perform a similar comparison for the intra-cell capacity, let consider the results from another related work. The study on a circular wireless hybrid network of a unit area in [30] has shown that the per-node capacity of the intra-cell mode is

$$T'_{intra}(n,b) = \begin{cases} \Theta(\frac{W'_1}{\sqrt{N_k}\log N_k}) & \text{if } b = o(\sqrt{n}) \\ O(\frac{W'_1}{\sqrt{N_k}}) & \text{if } b = \Omega(\sqrt{n}) \end{cases} \tag{3.12}$$

where $N_k = n/b^2$. Note that W'_1 is used to denote the bandwidth assigned for the intra-cell mode, instead of W_1, because the entire bandwidth W is differently partitioned in [30]. To be able to provide a fair comparison, a few changes are made to this study.

Instead of having a bandwidth of W_1 being used for both the intra-cell and the uplink traffics, it is now divided into two sperate bands. The first W'_1 is assigned for intra-cell transmission and the rest W''_1 is for the uplink traffic. Now, following the proof for Theorem 1 of [30], it can be shown that the number of source and destination pairs within any cell k that are communicating using the intra-cell mode is N_k. Therefore, the bandwidth W'_1 is shared among these N_k nodes only, rather than being shared by every node in the cell. Then, by using $\mu = 1/M^2N_k$ in the proof of Lemma 4, the sum rate is upper bounded with $O\big(\log(bN_k^2)\big)$. Consequently, by multiplying the upper bounded sum rate with the bandwidth W'_1/M^2N_k allocated to the scheduled source, a new upper bound for T_{intra} can be obtained as

$$T_{intra}(n,b) = O\left(\frac{\log(bN_k^2)}{N_k} W'_1\right) \tag{3.13}$$

Yet, it is not so obvious how large this capacity is when compared to one in (3.12). So, let consider the region where T_{intra} and T'_{intra} are both upper bounded,

specifically when $b = \Omega(\sqrt{n})$ and $b = o(n/\log n)$. For example, if assume $b = \Theta(\sqrt{n}\log n)$, the upper bounds of T'_{intra} and T_{intra} can be obtained from (3.12) and (3.13) as $O(\log n\, W_1)$ and $O\big((\log n)^2 \log(\frac{\sqrt{n}}{(\log n)^3})W_1\big)$, respectively. Because $\sqrt{n}/(\log n)^3 > 1$, for the given region of b, the per-node capacity T_{intra} is larger than T'_{intra} of [30] by at least a factor of $\log n$, due to the contribution of the opportunistic sources.

3.6.3 Base Stations with Antenna Array

To improve the throughput capacity of the infrastructure mode, the capacity bottleneck can be eliminated by deploying an array of antennas on every base station. Specifically, let m be the number of antennas on each base station. During the downlink phase. these antennas will cooperate and transmit data to a common destination. This is equivalent to having m transmitters situated at the same location and transmit data to a receiver; thus the channel becomes a MISO (multiple-input, single-output) channel. Furthermore, by allowing each antenna to transmit at the same power P as in the single antenna case, the interference range of the base stations remains intact, the frequency reuse scheme is still applicable, though the interference power is m times larger. By using an information-theoretic formula,the rate at which data from base station i are delivered to the destination node j can be calculated by

$$R_{MISO} = \log\left[1 + \frac{mPl(|X_i - X_j|)}{\mu W_2 N_0 + I}\right]$$

It can be shown that, with $m = \Theta(\frac{n}{b})$ and $\mu = 1/M^2 n_c$, $R_{MISO} = k_3 \log\frac{n}{b}$. Hence,

$$T^{DL}_{infra}(n,b) = \mu W_2 \cdot R_{MISO} = \Theta\left(\frac{b}{n}\log\frac{n}{b}\, W_2\right) \tag{3.14}$$

It is observed that, if the number of antennas on each base station increases at the rate of $\Theta(n/b)$, the downlink capacity becomes $\Theta((b/n)\log(n/b)\, W_2)$. The uplink traffic is now the bottleneck of the infrastructure mode, T_{infra} equals to the uplink capacity,

e.g. $O((b/n)\log(n/b)\,W_1)$, which is exactly the same as T_{intra}. Therefore, the optimal scenario is to allow nodes to communicate via both intra-cell and infrastructure modes but, because of the uncertain availability of the opportunistic sources, more bandwidth should be allocated to nodes, i.e. $W_1 > W_2$.

3.6.4 Base Stations with Increased Power

Although using multiple antennas helps achieving the multiplxing gain and increase the downlink capacity, having the number of antennas at the base station scaling with the number of nodes in the network is, however, not feasible in practice, due to the limitation in the form factor of the base station.

Nevertheless, because the base stations are line-powered and, unlike the wireless nodes, they are not power-constrained, one can also resort to an alternative solution by increasing the transmission power of the base station from P to κP. Having the base station power scales $\kappa = \Theta(n/b)$, it is easy to show that the downlink capacity will be raised to $\Theta((b/n)\log(n/b)\,W_2)$, similar to that of the multiple-antenna case. Hence, the bottleneck can be resolved. Furthermore, because κ nodes will transmit simultaneously to the base station in the uplink phase and the maximum sum of interference power is κP, by increasing the downlink transmission power to κP, the same frequency reuse scheme can be adopted in both uplink and downlink phases.

3.7 Conclusions

In this chapter, the per-node throughput capacity of the hybrid wireless networks is investigated. By allowing opportunistic sources to transmit concurrently with the source, the destination with SIC decoder can receive the data at the rate of $O((b/n)\log(n/b)\,W_1)$ via the intra-cell transmission mode. Similarly, with the base stations serving as the common destination, the uplink traffics of the infrastructure

mode can also benefit from the same multiple access technique, as a result, the uplink capacity is thus bounded to the same order as the intra-cell one. However, because the base station is the only transmitter in the cell during the downlink phase, data must be delivered to the destination in a round robin fashion, the infrastructure traffics are thus bottlenecked at the rate of $\Theta((b/n)W_2)$.

By increasing the base station power to κP, the downlink capacity can be improved by a factor of $\log(n/b)$ and the bottleneck occurs during the uplink phase, which remains at $O((b/n)\log(n/b)W_1)$, instead. Therefore, the throughput capacity of the infrastructure mode defined by the uplink traffic is on the same order as the capacity of the intra-cell mode and becomes significant to the overall network throughput.

Note that, according to Shannon theory on channel capacity, there should always be a rate at which data can be sent with arbitrarily low probability of error, regardless of the the SINR (signal-to-interference-and-noise ratio). But, in practice, the SINR level is usually required at some certain level for the nodes to maintain their connectivity (see the *physical model* in [23]). Hence, the transmission range is somewhat confined in practice. In the SIC technique, a point-to-point communication between nodes over a certain range may not be possible because the nodes are power constrained and the interference is changing with n. Fortunately, if the node power P is chosen carefully so that the asymptotic connectivity of the network is guaranteed [41], the fraction of nodes whose connectivity is lost due to the varying amount of interference can then be reduced and ignored.

CHAPTER 4

COMPRESSIVE SENSING: TO COMPRESS OR NOT TO COMPRESS

4.1 Introduction

Compressive sensing (CS) is a recently emerged method to capture and represent compressible signals at a rate significantly below the Nyquist rate. CS can be viewed as a scheme for simultaneously sensing and compression whose data acquisition rate need only be proportional to the sparsity of the signal. Mathematically, the process of compression in CS can be described by the following equation;

$$\mathbf{y} = \Phi \cdot \Psi \cdot \mathbf{x} \tag{4.1}$$

where $\mathbf{x}$ denotes a K-sparse information vector of length N, i.e. there are K non-zero entries in the vector, Ψ represents the basis matrix of size $N \times N$, $\mathbf{y}$ is the observation vector of length M, and Φ is the measurement matrix of size $M \times N$. In general, the length of $\mathbf{y}$ is far less than that of $\mathbf{x}$, i.e., $M << N$. CS can potentially provide substantial saving on data acquisition and storage.

The non-linear processing to reconstruct the signal from the measurement also plays an important role in CS. The goal of the reconstruction process is to be able to perfectly reconstruct $\mathbf{x}$ from the compressed observation $\mathbf{y}$ by solving the linear programming below

$$\min \|\hat{\mathbf{x}}\|_{l_1} \quad \text{subject to} \quad \Phi \cdot \Psi \cdot \hat{\mathbf{x}} \;=\; \mathbf{y} \tag{4.2}$$

However, as the number of measurements is below the Nyquist rate, significant ambiguity in reconstruction can occur. One of the most common problems in the re-

construction is that the estimator $\hat{\mathbf{x}}$ may not exactly equal to $\mathbf{x}$; thus the estimation error occurs.

In the last few years, the development of CS has stirred quite an amount of excitement in the signal processing community, leading to extensive research, see [42, 43]. For example, in [42], the authors discussed some interesting phenomena on the recovery of sparse signals, i.e. signals which have a few nonzero terms, from limited measurements. In[44], the authors shows that it is possible to accurately reconstruct a sparse signal from various types of random measurement ensembles, e.g. binary, Gaussian, and Fourier ensembles.

- **Binary ensemble:** the entries of Φ are identically and independently sampled from a symmetric Bernoulli distribution. That is, if X_{mn} is i.i.d. (independently and identically distributed) with $\Pr(X_{mn} = \pm 1) = 0.5$, then

$$\phi_{m,n} = X_{mn}, \quad \Pr(X_{mn} = \pm 1) = 0.5 \tag{4.3}$$

- **Gaussian ensemble:** the entries of Φ are identically and independently sampled from a normal distribution distribution.

$$\phi_{m,n} = X_{mn}, \quad X_{mn} \text{ is } N(0,1) \tag{4.4}$$

- **Fourier ensemble:** the entries of Φ are obtained by randomly sampling rows m and column n of the orthonormal N by N Fourier matrix

$$\phi_{m,n} = e^{(-i2\pi mn/N)} \tag{4.5}$$

In this chapter, the CS scheme is considered from the information theory point of view. The study will focus on the CS scheme whose measurement matrix is randomly sampled from a set of real numbers, i.e. the binary ensemble and the Gaussian ensemble[1]. The bound of the probability of error in the reconstruction process, $\Pr(\hat{\mathbf{x}} \neq \mathbf{x})$,

[1]In most CS literature the entries of Φ are drawn with variance $1/N$. The choice of the unit variance is to simplify further notation

of the CS scheme is provided, based on the Fano's inequality. This derived error bound can be used to determine if it is worth performing the compression and whether a choice of a measurement matrix Φ is proper for the certain set of input.

The remainder of this chapter is presented as follows. In Section 4.2, the Fano's inequality, which provides an information theoretic lower bound of probability of error in an estimation process, is discussed. Then, based on the inequality, the lower bound error for the CS scheme is derived. In Section 4.3, the result obtained is analyzed. Finally, the chapter is concluded in Section 4.4.

Notations Upper (lower) bold face letters denote matrices (vectors); $(\cdot)^T$ denotes transpose; $a_{i,j}$ denotes the entry at the i-th row and j-th column of matrix $\mathbf{A}$; z_n denotes the n-th entry of vector $\mathbf{z}$; $h(\cdot)$ denotes the entropy; log denotes the base-2 logarithm.

4.2 Information Theoretic Lower Bound of the Probability of Error

4.2.1 Fano's Inequality

Consider the flow of the entire CS scheme. The information $\mathbf{x}$ is first compressed, corresponding to (5.1), and the observation $\mathbf{y}$ is obtained. Then, from the observation, the algorithm of the similar form to (4.2) is executed to obtain the estimator $\hat{\mathbf{x}}$. It is observed that $\mathbf{x} \to \mathbf{y} \to \hat{\mathbf{x}} = g(\mathbf{y})$ forms a Markov chain.

Define the probability of error $\Pr(e)$ as $\Pr(\hat{\mathbf{x}} \neq \mathbf{x})$ and an error random variable E as

$$E = \begin{cases} 1\,, & \text{if } \hat{\mathbf{x}} \neq \mathbf{x} \\ 0\,, & \text{otherwise} \end{cases} \tag{4.6}$$

Then, by using the chain's rule for entropies, it is shown that

$$\begin{aligned} h(E, \mathbf{x}|\mathbf{y}) &= h(\mathbf{x}|\mathbf{y}) + h(E|\mathbf{x}, \mathbf{y}) && (4.7) \\ &= h(E|\mathbf{y}) + h(\mathbf{x}|E, \mathbf{y}) && (4.8) \end{aligned}$$

Since given $E = 0$, $\mathbf{x} = g(\mathbf{y})$ and given $E = 1$, the conditional entropy $h(\mathbf{x}|\mathbf{y}, E = 1)$ can be upper bounded by $h(\mathbf{x})$. Subsequently, $h(\mathbf{x}|E, \mathbf{y})$ can be bounded as follows:

$$\begin{aligned} h(\mathbf{x}|E, \mathbf{y}) &= \Pr(E = 0)\ h(\mathbf{x}|\mathbf{y}, E = 0) + \Pr(E = 1)\ h(\mathbf{x}|\mathbf{y}, E = 1) \\ &\leq [1 - \Pr(e)] \cdot 0 + \Pr(e) \cdot h(\mathbf{x}) && (4.9) \end{aligned}$$

Because E is a function of $\mathbf{x}$ and the estimator $\hat{\mathbf{x}}$ is a function of $\mathbf{y}$, i.e., $\hat{\mathbf{x}} = g(\mathbf{y})$, $h(E|\mathbf{x}, \mathbf{y}) = 0$. Next, because conditioning reduces entropy, $h(E|\mathbf{y}) \leq h(E)$. Also, because E is binary-valued random variable, $h(E) = h[\Pr(e)]$. Thus, by combining these results into (4.7) and (4.8), it can be shown that

$$\begin{aligned} h(\mathbf{x}|\mathbf{y}) + h(E|\mathbf{x}, \mathbf{y}) &= h(E|\mathbf{y}) + h(\mathbf{x}|E, \mathbf{y}) \\ h(\mathbf{x}|\mathbf{y}) &\leq h[\Pr(e)] + \Pr(e)\, h(\mathbf{x}) \\ h(\mathbf{x}|\mathbf{y}) &\leq 1 + \Pr(e)\, h(\mathbf{x}) && (4.10) \end{aligned}$$

Finally, the Fano's inequality, which provides the lower bound of the probability of error, can be obtained as

$$\Pr(e) \geq \frac{h(\mathbf{x}|\mathbf{y}) - 1}{h(\mathbf{x})} \qquad (4.11)$$

4.2.2 Underlying Assumptions

To calculate the lower bound, the following assumptions are made;

- The information vector $\mathbf{x} \in \Re^N$ is K-sparse. There are K non-zero coefficients in $\mathbf{x}$ and each of them is an i.i.d Gaussian random value[2] with mean μ_x and variance σ_x^2.
- The basis matrix Ψ is I_N. Thus, the projected image Θ of $\mathbf{x}$ on the basis is equal to the information vector $\mathbf{x}$ itself.
- The measurement matrix Φ is randomly generated with a binary ensemble, i.e.,$\phi_{m,n} = \pm 1$ with equal probability.
- The compression and reconstruction processes know the measurement Φ.

4.2.3 Entropies

Observe that, for the sparse information $\mathbf{x}$ with length N, its K nonzero coefficients may locate at any random entries of the vector. Therefore, each entry x_n, $n \in \{1, .., N\}$, of $\mathbf{x}$ either has a value that is randomly chosen from a Gaussian distribution with mean μ_x and variance σ_x^2 or does not have a value at all. Specifically, $\mathbf{x}$ can be expressed as a Bernoulli-Gaussian random vector in the form of

$$\mathbf{x} = \mathbf{b}^T \cdot \mathbf{z} \tag{4.12}$$

Equivalently,

$$x_n = b_n \cdot z_n \tag{4.13}$$

The random vector $\mathbf{b}$ is a Bernoulli random location vector of length N; each entry b_n can be either 0 or 1 with $\Pr(b_n = 1) = K/N$, to indicate whether the corresponding x_n has a value or not. The random vector $\mathbf{z}$ is a Gaussian random

[2]Because the information vector is specified as a Gaussian random vector, this study is not confined to a certain values of information. As long as the distribution of information vector is Gaussian, the theory developed is applied

vector of length N; each entry z_n is associating with the parameter $\mu_z = \mu_x$ and $\sigma_z^2 = \sigma_x^2$ and is used to denote the random value of the corresponding non-zero x_n.

Now, consider the entries in $\mathbf{y}$. It is observed that each entry y_m of $\mathbf{y}$ can be obtained by multiplying the m-th row of matrix Φ with the information $\mathbf{x}$. That is,

$$\begin{aligned} y_m &= \sum_{n=1}^{N} \phi_{m,n}\, x_n = \sum_{n=1}^{K} \phi_{m,n}\, z_n \\ &= Z^+ + Z^- \end{aligned} \tag{4.14}$$

where Z^+ is the random variable representing the summation of the terms in which $\phi_{m,n}$ equals $+1$ and Z^- denotes the summation of the terms in which $\phi_{m,n}$ equals -1. The second equality on the first line comes from the fact that x_n is the multiplication of b_n and z_n and there are K non-zero entries in $\mathbf{b}$.

Because $\Pr(\phi_{m,n} = \pm 1) = \frac{1}{2}$, if the length N of $\mathbf{x}$ is sufficiently large, there the Strong Law of Large Number suggests that, with high probability (w.h.p.), both Z^+ and Z^- will be the summation of $\frac{K}{2}$ multiplication terms of $\phi_{m,n}\, z_n$.

Since the measurement Φ is known to the compression process; therefore, it is easy to show that Z^+ and Z^- are also Gaussian with mean $\pm\frac{K}{2}\mu_x$ and variance $\frac{K}{2}\sigma_x^2$. Then, because y_m is the sum of Z^+ and Z^-, it is also a Gaussian random variable with zero mean and variance $\sigma_x^2 K$.

It is noted that Φ is assumed to have a binary ensemble so that each entry of $\mathbf{y}$ is obtained with identical variance and zero mean. Soon, it will be seen that this assumption helps simplifying the subsequent derivations. In general, Φ can also be Gaussian ensemble [44], and the result from this chapter still holds as long as $\mathbf{x}$ is a Gaussian distributed information vector.

To calculate the Fano's inequality, it is noted that

$$h(\mathbf{x}|\mathbf{y}) = h(\mathbf{x}, \mathbf{y}) - h(\mathbf{y}) \tag{4.15}$$

Therefore, (4.11) can be rewritten as

$$\Pr(e) \;\geq\; \frac{h(\mathbf{x},\mathbf{y}) - h(\mathbf{y}) - 1}{h(\mathbf{x})} \tag{4.16}$$

It can be shown that, for any Gaussian random vector $\mathbf{w}$ of length L, its entropy can be expressed as, [38],

$$h(\mathbf{w}) \;=\; \frac{1}{2}\,\log\Big[(2\pi e)^L |\Sigma_w|\Big] \tag{4.17}$$

where $|\Sigma_w|$ denotes the determinant of the covariance matrix of $\mathbf{w}$. However, because $\mathbf{x}$ is an N-dimension Bernoulli-Gaussian random vector, such simple formula is no longer valid. To calculate the lower bound of error, further simplification must be performed to the Fano's Inequality.

Intuitively, it is observed that the reconstruction error should be lower if the locations of the non-zero coefficients in $\mathbf{x}$ are known, compared to the case when both their locations and their values are unknown. So, the conditional probability of reconstruction error when $\mathbf{b}$ is known, $\Pr(e\,|\mathbf{b})$, is always smaller than or equal to the general probability of reconstruction error, $\Pr(e)$.

$$\begin{aligned} \Pr(e) &\geq \Pr(e\,|\,\mathbf{b}) \\ &\geq \frac{h(\mathbf{x},\mathbf{y}\,|\,\mathbf{b}) - h(\mathbf{y}\,|\,\mathbf{b}) - 1}{h(\mathbf{x}\,|\,\mathbf{b})} \end{aligned} \tag{4.18}$$

From (4.13), with the knowledge of $\mathbf{b}$, x_n is a Gaussian IID random variable, it is easy to show that the entropy of $\mathbf{x}$ can then be written as;

$$h(\mathbf{x}\,|\,\mathbf{b}) \;=\; \frac{1}{2}\,\log\Big[(2\pi e\sigma_x^2)^K\Big] \tag{4.19}$$

Also, it is clear that the knowledge of $\mathbf{b}$ does not change the previous conclusion on the PDF of $\mathbf{y}$; hence, the entropy of the Gaussian observation vector $\mathbf{y}$ can be expressed as

$$h(\mathbf{y}) \;=\; h(\mathbf{y}\,|\,\mathbf{b}) = \frac{1}{2}\,\log\Big[(2\pi e)^M |\Sigma_y|\Big] \tag{4.20}$$

where

$$\Sigma_y = \begin{pmatrix} \mathrm{COV}(y_1, y_1) & \cdots & \mathrm{COV}(y_1, y_M) \\ \vdots & \cdots & \vdots \\ \mathrm{COV}(y_M, y_1) & \cdots & \mathrm{COV}(y_M, y_M) \end{pmatrix} \tag{4.21}$$

Since each entry y_m of $\mathbf{y}$ is previously known to have zero mean and variance $\sigma_x^2 K$, the covariance $\mathrm{COV}(y_m, y_{m'})$ between the m-th and the m'-th entries of $\mathbf{y}$ can then be expressed as

$$\mathrm{COV}(y_m, y_{m'}) = \begin{cases} \sigma_x^2 K\,, & \text{if } m = m' \\ (\sigma_x^2 + \mu_x^2) \sum_{u=1}^{K} \phi_{m,u}\phi_{m',u} & \\ \quad + \ \mu_x^2 \sum_{v=1}^{K} \phi_{m,v} \sum_{\substack{w=1 \\ w\neq v}}^{K} \phi_{m',w}\,, & \text{if } m \neq m' \end{cases} \tag{4.22}$$

Next, the entropy of $\mathbf{x}$ and $\mathbf{y}$, $h(\mathbf{x}, \mathbf{y} \,|\, \mathbf{b})$, is calculated. Because $\mathbf{x}$ and $\mathbf{y}$ are joint $(K + M)$-dimensional Gaussian random variables, therefore the entropy of $(\mathbf{x}, \mathbf{y} \,|\, \mathbf{b})$ can be expressed as

$$h(\mathbf{x}, \mathbf{y} \,|\, \mathbf{b}) = \frac{1}{2}\, log\Big[(2\pi e)^{K+M} |\Sigma_{xy}|\Big] \tag{4.23}$$

where

$$\Sigma_{xy} = \begin{pmatrix} \Sigma_y & A \\ A^T & \sigma_x^2 I_K \end{pmatrix} \tag{4.24}$$

The submatrix A in Σ_{xy} denotes the matrix of the covariance $\mathrm{COV}(y_m, x_n)$ between the m-th entry of $\mathbf{y}$ and the n-th entry of $\mathbf{x}$, which can be calculated from

$$\mathrm{COV}(y_m, x_n) = \phi_{m,n}(\sigma_x^2 + \mu_x^2) + \mu_x^2 \sum_{\substack{k=1 \\ k\neq n}}^{K} \phi_{m,k} \tag{4.25}$$

Obviously, to calculate $h(\mathbf{y})$ and $h(\mathbf{x}, \mathbf{y} \,|\, \mathbf{b})$, the determinant of Σ_y and the determinant of Σ_{xy} need to be considered. suppose they are full rank, these covariance matrices are thus positive-definite matrices. Hence, the SVD technique can be

applied to decompose and find the eigenvalues of the matrices. In other word, the determinants of the covariance matrices can be expressed as

$$|\Sigma_y| = \prod_{i=1}^{M} \lambda_y^i \tag{4.26}$$

and

$$|\Sigma_{xy}| = \prod_{j=1}^{K+M} \lambda_{xy}^j \tag{4.27}$$

4.2.4 The Lower Bound of the Probability of Error

Combining every terms together, the Fano's Inequality can then be rewritten as

$$\begin{aligned}
\Pr(e) &\geq \frac{1}{K\log(2\pi e\sigma_x^2)} \cdot \left\{ \log\left[(2\pi e)^{K+M}(\prod_{j=1}^{K+M}\lambda_{xy}^j)\right] - \log\left[(2\pi e)^{M}(\prod_{i=1}^{M}\lambda_{y}^i)\right] - 2 \right\} \\
&\overset{(a)}{=} \frac{1}{K\log(2\pi e\sigma_x^2)} \cdot \left\{ \log\left[(2\pi e)^{K+M}(\prod_{j=1}^{K+M}\lambda_{xy}^j)\right] - \log\left[(2\pi e)^{M}(\prod_{i=1}^{M}\lambda_{y}^i)\right] \right\} \\
&\overset{(b)}{\geq} \frac{\log(2\pi e\lambda_{xy_min})^{K+M} - \log(2\pi e\lambda_{y_max})^{M}}{K\log(2\pi e\sigma_x^2)} \\
&= \frac{\log(2\pi e)}{\log(2\pi e\sigma_x^2)} - \left[\frac{\log(\lambda_{y_max}^{\frac{M}{K}}) - \log(\lambda_{xy_min}^{\frac{M}{K}+1})}{\log(2\pi e\sigma_x^2)}\right] \\
&\overset{(c)}{\geq} \frac{\log(2\pi e)}{\log(2\pi e\sigma_x^2)} - \left[\frac{\log(\lambda_{y_max}^{\frac{M}{K}}) - \log(\lambda_{xy_min}^{\frac{M}{K}+1})}{\log(2\pi e\sigma_x^2)}\right] - \frac{\log\lambda_{y_max}}{\log(2\pi e\sigma_x^2)} \\
&= \frac{\log(2\pi e)}{\log(2\pi e\sigma_x^2)} - \frac{\log(\frac{\lambda_{y_max}}{\lambda_{xy_min}})^{\frac{M}{K}+1}}{\log(2\pi e\sigma_x^2)}
\end{aligned} \tag{4.28}$$

where

(a) if $K >> 2$ and $\sigma_x^2 \geq 1$, $\frac{2}{K\log(2\pi e\sigma_x^2)} \approx 0$,

(b) from $\prod_{u=1}^{K+M} \lambda_{xy\_u} \geq \lambda_{xy\_min}^{K+M}$ and $\prod_{v=1}^{M} \lambda_{y\_v} \leq \lambda_{y\_max}^{M}$,

(c) from $\lambda_{y\_max} > 1$ and $\log(\lambda_{y\_max}) > 0$ (the proof is in the last section of the chapter), thus subtracting $\frac{\log\lambda_{y\_max}}{\log(2\pi e\sigma_x^2)}$ reduces the probability.

If the information is normalized to unit variance, i.e., $\sigma_x^2 = 1$, the lower bound can be written as

$$\Pr(e) \;\geq\; 1 - \frac{1}{4}\;\log(\frac{\lambda_{y\_max}}{\lambda_{xy\_min}})^{\frac{M}{K}+1} \tag{4.29}$$

This final result can be obtained by substituting $\log(2\pi e) \approx 4$ to (4.28).

4.3 Result Analysis

The question to be asked at this point is what, in general, is the relationship between λ_{xy_min} and λ_{y_max}? To answer this question, let refer to the *interlacing* property in [45].

Corollary 1 If B_r denotes the leading r-by-r principal submatrix of an n-by-n symmetric matrix B, then for $r = 1, 2, ..., n-1$ the following *interlacing* property holds:

$$\lambda_{r+1}(B_{r+1}) \leq \lambda_r(B_r) \leq \lambda_r(B_{r+1}) \leq ... \leq \lambda_2(B_{r+1}) \leq \lambda_1(B_r) \leq \lambda_1(B_{r+1}) \tag{4.30}$$

In other words, the *interlacing* property suggests that the λ_{min} of the smaller square leading principal submatrix is greater than or equal to the λ_{min} of the bigger one, but its λ_{max} is smaller than or equal to the λ_{max} of the bigger one. Since the covariance matrix Σ_{xy} in (4.24) is an N-by-N symmetric matrix and Σ_y is its leading M-by-M principal submatrix. From the *interlacing* property, it is easy to show that

$$\lambda_{xy\_min} \leq \lambda_{y\_min} \leq \lambda_{y\_max} \leq \lambda_{xy\_max}$$

The logarithm term in (4.29) is always non-negative and the lower-bound value is always less than or equal to 1. Finally, for a given information vector $\mathbf{x}$, (4.22) and (4.25) suggest that the eigenvalues of the covariance matrices depend solely on the entries in the measurement matrix Φ. Consequently, one should consider the following conditions when selecting the measurement matrix Φ;

- If Φ is generated such that $\lambda_{y\_max} = \lambda_{xy\_min}$, then the error is certain, i.e., $\Pr(e) = 1$. This means the information can never be perfectly recovered from the reconstruction process.
- If Φ is chosen such that $\frac{\lambda_{y\_max}}{\lambda_{xy\_min}} \geq 2^{\frac{4}{\frac{M}{K}+1}}$, then the lower bound is non-positive; which implies that the perfect reconstruction of information is possible.

4.4 Conclusions

In this chapter, the CS scheme is considered from the information theory point of view and derived the lower bound of the probability of error for the CS scheme, using the Fano's Inequality. By assuming the information is Gaussian distributed, the lower bound can easily be computed and provides the criteria for choosing the measurement matrix Φ.

It has been shown that if the measurement matrix Φ is chosen such that $\lambda_{y\_max} = \lambda_{xy\_min}$, then the reconstruction error is inevitable: therefore, it is unwise to perform the data compression on the choice of the measurement matrix. However, if the selected measurement matrix makes $\frac{\lambda_{y\_max}}{\lambda_{xy\_min}} \geq 2^{\frac{4}{\frac{M}{K}+1}}$, the probability of error is then lower bounded by a non-positive value; which implies that there is a potential for the information to be perfectly recovered.

It is noted that, in the study, a binary ensemble is assumed for the measurement matrix Φ just to simplify the subsequent expressions. However, the result from the study also holds if the Gaussian ensemble is used to generate Φ.

4.5 Proof for the Lower Bound of the Maximum Eigenvalue of Σ_y

4.5.1 Binary Ensemble

When Φ is a binary ensemble, Σ_y can be expressed as

$$\Sigma_y = \begin{pmatrix} \sigma_x^2 K & \cdots & \mathrm{COV}(y_1, y_M) \\ \vdots & \cdots & \vdots \\ \mathrm{COV}(y_M, y_1) & \cdots & \sigma_x^2 K \end{pmatrix}$$

Assume the signal variance is normalized. This implies the diagonal entries are all equal to K. Let $\Sigma_y = B_M$ and observe that B_M is an M-by-M symmetric matrix with the leading 1-by-1 principal submatrix, say B_1, equal to K. Then, from Corollary 1, it is conclude that

$$\lambda_{min}(B_M) \leq \lambda_{min}(B_1) \leq \lambda_{max}(B_1) \leq \lambda_{max}(B_M)$$

However, because B_1 has only one eigenvalue, which is equal to K, then the above inequality can be rewritten as

$$\lambda_{min}(B_M) \leq K \leq \lambda_{max}(B_M)$$

Therefore $\lambda_{max}(B_M) = \lambda_{y\_max} > 1$ since $K >> 1$. The proof is completed.

4.5.2 Gaussian Ensemble

If Φ is a Gaussian ensemble, Σ_y can be expressed as in (4.21) with the diagonal entries

$$\begin{aligned} \mathrm{COV}(y_m, y_m) &= \sigma_x^2 \sum_{u=1}^{K} \phi_{m,u} \sum_{v=1}^{K} \phi_{n,v} \\ &= \sigma_x^2 \left[\sum_{u=1}^{K} (\phi_{u,u})^2 + \sum_{v=1}^{K} \phi_{m,v} \sum_{\substack{w=1 \\ w \neq v}}^{K} \phi_{m',w} \right] \end{aligned}$$

Assume the the signal variance is normalized. If the parenthesized term of the second equality can be proved as greater than or equal to 1, i.e. $\mathrm{COV}(y_m, y_{m'}) > 1$, then the same proof for the binary ensemble can be followed to show that $\lambda_{y\_max} > 1$.

First, let illustrate that $\sum_{u=1}^{K} (\phi_{\cdot,u})^2 > 1$ when K is sufficiently large. Define Z_u as a binary random variable representing whether $\phi_{\cdot,u}$ is greater than or equal to 1, when $u = 1$ to K. That is, the random variable Z_u is expressed as:

$$Z_u = \begin{cases} 1\,, & \phi_{\cdot,u} \geq 1 \\ 0\,, & otherwise \end{cases} \tag{4.31}$$

Since $\{\phi_{\cdot,u}\}_1^K$ is $N(0,1)$, $Pr(\phi_{\cdot,u} \geq 1) = Q(1)$ and, if K is sufficiently large, $E[Z_u] = Q(1) = 0.159$, w.h.p.

Next, let define a random variable $S = \sum_{u=1}^{K} Z_u$, representing the total number of $\phi_{\cdot,u}$ that is greater than equal to 1. Since $\{Z_u\}_1^K$ is an i.i.d. sequence of random variables with $E[Z_u] = Q(1)$. By Strong Law of Large Numbers, as $K \to \infty$,

$$\frac{S}{K} = \frac{1}{K} \sum_{u=1}^{K} Z_u \to 0.159 \tag{4.32}$$

When K is sufficiently large, w.h.p. (with high probability), there will be $S = 0.159K$ terms in $\{\phi_{\cdot,u}\}_1^K$ that are greater than or equal to 1. For example, if $K >> 10$, there is at least 1 term in $\{\phi_{\cdot,u}\}_1^K$ that is greater than or equal to 1. Thus, it is concluded that $\sum_{u=1}^{K} (\phi_{\cdot,u})^2 > 1$ w.h.p. if K is sufficiently large.

By similar procedures, it can be shown further that if K is sufficiently large, then for any $\phi_{\cdot,i} = c$, there exists its antipode pair $\phi_{\cdot,j} = -c$ so that $\phi_{\cdot,i} + \phi_{\cdot,j} = 0$. Hence, it is straightforward that, w.h.p., $\sum_{v=1}^{K} \phi_{j,v} \sum_{w=1,w\neq v}^{K} \phi_{j,w} = 0$.

Combining together, the results from the first and second parts of the proof, it can be concluded that $\mathrm{COV}(y_i, y_i) > 1$. Thus, the proof is completed.

CHAPTER 5

FUZZY FORECASTING RECONSTRUCTION FOR CORRELATED AND SPARSE INFORMATION

5.1 Introduction

Compressive sensing (CS) is a recently emerged method to capture and represent compressible signals at a rate significantly below the Nyquist rate. CS can be viewed as a scheme for simultaneously sensing and compression whose data acquisition rate need only be proportional to the sparsity of the signal. Mathematically, the process of compression in CS can be compactly described by the following equation;

$$\mathbf{v} = \Phi \cdot \mathbf{u} \tag{5.1}$$

where $\mathbf{u}$ denotes a K-sparse information vector of length N, i.e. there are K non-zero entries in the vector, $\mathbf{v}$ is the observation vector of length M, and Φ is the measurement matrix of size $M \times N$. In general, the length of $\mathbf{v}$ is far lesser than that of $\mathbf{u}$, i.e., $M << N$, then CS can potentially provide substantial saving on data acquisition and storage.

The non-linear processing to reconstruct the signal from the measurement also plays an important role in CS. The goal of the reconstruction process is to be able to perfectly reconstruct $\mathbf{u}$ from the compressed observation $\mathbf{v}$. In [46, 47, 48], the work by Candés and Donoho et. al. has shown that l_1 optimization using Linear Programming (LP) techniques yields an equivalent solution as long as the measurement matrix Φ satisfies the restricted isometry property (RIP) with a constant parameter.

Though LP techniques play an important role in CS reconstruction, their complexity is still impractically high for certain applications. For faster processing time,

several of low-complexity reconstruction algorithms, [49, 50], have been proposed as alternatives.

In addition, there is also a family of iterative greedy techniques that offer fast reconstruction and simple geometry interpretation. These techniques include the Orthogonal Matching Pursuit (OMP), the Regularized OMP, the Stagewise OMP. The complexity of these method is proven to be significantly smaller than that of the LP, but this comes with the expense of the reconstruction quality. Examples of the algorithms belonging in this family are the ROMP [51], CoSaMP [52], and Subspace Pursuit [53].

Though OMP algorithms can operate in both noiseless and noisy environment, but when the compressed observation $\mathbf{v}$ contains a great amount of noises, the reconstruction error increases substantially. For example, in wireless communication, due to the nature of the airborne channel, the operating SNR level can be as low as 10-20 dB, which is typical for many wireless systems. When the original information is reconstructed at the other end of the wireless system, a significantly high amount of error could be resulted unless the noisy measurements is pre-processed. It is , thus, called for an effective noise reduction method.

In many applications, however, a collection of the previous data points may easily be acquired. Such prior knowledge can also be used in favor of the reconstruction process. It can use as the training data to construct a forecasting system. With this concept, one can rely on the past information, usually less noisy, to predict the subsequent data points or the unknown compressed information $\mathbf{u}$ and obtain the insight of what the original information should be. This is especially the case when each of the K nonzero entries of the information vector exhibits a certain level of correlation; the relationship among the current data set is foretold by the past data points.

Forecasting is very important problem that appears in many disciplines. In [54, 55, 56], fuzzy logic forecasting systems were used in wireless sensor networks, wireless ad-hoc networks, and time-series forecast. And, to design a fuzzy logic system (FLS), there are many methods provided in [56, 57].

In this chapter the performance of an OMP-based reconstruction technique in noisy regime is investigated. In particular, the CoSaMP algorithm [52] is considered and, to help improving its performance against the influence of noise, an FLS forecaster is constructed from a set of past information and the forecasted data is used in the reconstruction process of the algorithm. Using the forecasting FLS and some modifications to the original CoSaMP algorithm, the study shows that the reconstruction error can be further improved.

The remainder of this chapter is presented as follows. In Section 5.2, an overview of the rule-based fuzzy logic system is given and followed by the discussion on how to design a FLS forecaster using back propagation method. In Section 5.3, the fuzzy forecasting reconstruction algorithm is proposed. Then, in Section 5.4, the simulation results are provided to validate the proposed approach in comparison to a standard OMP algorithm, CoSaMP. Finally, the chapter is concluded in Section 5.5.

5.2 Fuzzy Logic Forecasting System Design

Before proceeding, let first introduce a pruned information vector $\mathbf{u}_p$, which contains only the K non-zero entries in $\mathbf{u}$ indexed by $i \in I$, $I \subset \{1, ..., N\}$, and $|I| = K$. In this chapter, the case when the value of each entry of $\mathbf{u}_p$ is highly correlated to its p previous entries is studied. That is, the ith entry of $\mathbf{u}_p$ can be determined via a function of the $i-1$ th to $i-p$ th entries. Designing a FLS can then be viewed as approximating the relation between the ith entry of $\mathbf{u}_p$ and its p predecessors.

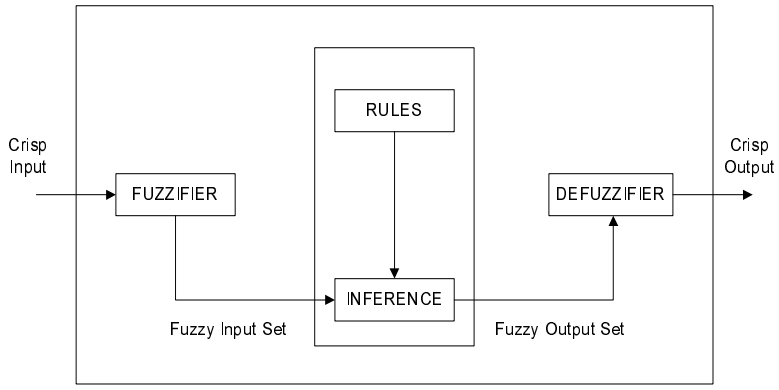

Figure 5.1. The structure of a fuzzy logic system.

Suppose that a collection of past information vector $\mathbf{u}$ or, equivalently, a set of the past $\mathbf{u}_p$ is obtainable at the reconstruction side of CS. Given these past measurements, so called the input-output data training pairs, tuning is essentially equivalent to determining a system that provides an optimal fit to the input-output pairs. The goal is to completely specify the FLS using the training data and use it as a forecaster to find the current $\mathbf{u}_p$.

5.2.1 Overview of Fuzzy Logic Systems

Figure 5.1 shows the structure of a FLS. When an input is applied to a FLS, the inference engine computes the output set corresponding to each rule. The defuzzifier then computes a crisp output from these rule output sets [56].

Consider a FLS having p inputs $x_1 \in X_1, ..., x_p \in X_p$ and one output $y \in Y$. Suppose that the FLS has L " IF-THEN " rules, where the lth rule has the form;

$$\begin{aligned} R^l \quad : \quad & \text{IF } x_1 \text{ is } F_1^l \text{ and } x_2 \text{ is } F_2^l \text{ ... and } x_p \text{ is } F_p^l \\ & \text{THEN } y \text{ is } G^l, \quad l = 1, ..., L \end{aligned} \tag{5.2}$$

where F_i is a fuzzy set whose membership function (MF), μ_{F_i}, is centered at x_i. Assuming singleton fuzzification, when an input $x' = \{x'_1, ..., x'_p\}$ is applied, the degree of firing corresponding to the lth rule is computed as

$$\mu_{F_1^l}(x'_1) * \mu_{F_2^l}(x'_2) * ... * \mu_{F_p^l}(x'_p) = T_{i=1}^{p} \mu_{F_i^l}(x'_i) \tag{5.3}$$

where $*$ denotes the t-norm operation. There are many kinds of defuzzifiers. In this chapter, the height defuzzifier is used. It computes a crisp output for the FLS by first replacing each rule fuzzy set by a singleton at the point having maximum membership in that output set. Then, it calculates the centroid of the type-1 set comprised of these singleton. The output of a height defuzzifier is given as

$$y(\mathbf{x}') = \frac{\sum_{l=1}^{M} \bar{y}^l \mu_{B^l}(\bar{y}^l)}{\sum_{l=1}^{M} \mu_{B^l}(\bar{y}^l)} \tag{5.4}$$

where $\bar{y}^l$ is the point having maximum membership in the lth output set and its membership grade in the lth output set is $\mu_{B^l}(\bar{y}^l)$. For singleton fuzzification, it can be shown that

$$\mu_{B^l}(\bar{y}^l) = \mu_{G^l}(\bar{y}^l) * \left[\mu_{F_1^l}(x'_1) * \cdots * \mu_{F_p^l}(x'_p)\right] \tag{5.5}$$

5.2.2 Designing Fuzzy Logic Systems

Because of the large numbers of possibilities for FLSs, some guidelines are necessary for their practical design. There exists a multitude of design methods that can be used to construct FLSs. In this chapter, the back-propagation (steepest descent) method [56] is used to specify the FLS. The shapes of all the antecedent and consequent MFs are fixed ahead of time and the training data is used to tune the antecedent and consequent parameters [56]. Also, the design assumes singleton fuzzification, Gaussian membership functions (GMF), *max-product* composition, *product*

implication and t-norm, and height defuzzification. It is to easy to show, using these assumptions, that (5.4) can now be written as;

$$y(\mathbf{x}') = f_s(\mathbf{x}') = \frac{\sum_{l=1}^{M} \bar{y}^l \prod_{i=1}^{p} \mu_{F_i^l}(x_i')}{\sum_{l=1}^{M} \prod_{i=1}^{p} \mu_{F_i^l}(x_i')} \tag{5.6}$$

To obtain (5.6), start with (5.4) and substitute for $\mu_{B^l}(\bar{y}^l)$ from (5.5), i.e.,

$$\mu_{B^l}(\bar{y}^l) = \mu_{G^l}(\bar{y}^l) \times \Big[\prod_{i=1}^{p} \mu_{F_i^l}(x_i') \Big] = \prod_{i=1}^{p} \mu_{F_i^l}(x_i') \tag{5.7}$$

where it have been assumed that the MFs are normalized, so that $\mu_{G^l}(\bar{y}^l) = 1$.

Given that there is a collection of T past measurements of $\mathbf{u}_p$, e.g. $u_p(1), \ldots, u_p(T)$, available at the CS reconstruction side, the past information can be partitioned into 2 subsets;

- Training subset, $R < T$ measurements from $u_p(1)$ to $u_p(R)$
- Testing subset, $T - R$ measurements from $u_p(R+1)$ to $u_p(T)$

The training subset is used in the designed FLS forecaster to establish its rules and the testing subset is used to test the accuracy of the extracted rules. Furthermore, assuming the current measurement of u_p is determined by its previous p measurements, $R - p$ input-output training pairs can be formed, $(\mathbf{x}^{(1)} : y^{(1)}), (\mathbf{x}^{(2)} : y^{(2)}), \ldots, (\mathbf{x}^{(R-p)} : y^{(R-p)})$, where $\mathbf{x}$ is the vector input and y is the scalar output of a FLS, as shown below.

$$\begin{aligned}
\mathbf{x}^{(1)} &= \begin{pmatrix} u_p(1) \\ \vdots \\ u_p(p) \end{pmatrix}, \quad y^{(1)} = u_p(p+1) \\
&\vdots \qquad\qquad\qquad\qquad\quad \vdots \\
\mathbf{x}^{(R-p)} &= \begin{pmatrix} u_p(R-p) \\ \vdots \\ u_p(R-1) \end{pmatrix}, \quad y^{(R-p)} = u_p(R)
\end{aligned} \tag{5.8}$$

Similarly, $T-R$ input-output testing pairs can be formed as

$$\begin{aligned}
\mathbf{x}^{(R-p+1)} &= \begin{pmatrix} u_p(R-p+1) \\ \vdots \\ u_p(R) \end{pmatrix}, y^{(R-p+1)} = u_I(R+1) \\
&\vdots \qquad\qquad\qquad\qquad \vdots \\
\mathbf{x}^{(T-p)} &= \begin{pmatrix} u_p(T-p) \\ \vdots \\ u_p(T) \end{pmatrix}, \quad y^{(T-p)} = u_p(T)
\end{aligned} \tag{5.9}$$

In the back propagation method, none of the antecedent or consequent parameters are fixed ahead of time. They are all tuned using a steepest decent method, which is briefly described in this section. Notice that, with Gaussian membership functions, (5.7) can be rewritten as

$$y(\mathbf{x}^{(i)}) = f_s(\mathbf{x}^{(i)}) = \frac{\sum_{l=1}^{M} \bar{y}^l \prod_{k=1}^{p} \exp\left[-\frac{\left(x_k^{(i)} - m_{F_k^l}\right)^2}{2\sigma^2_{F_k^l}} \right]}{\sum_{l=1}^{M} \prod_{k=1}^{p} \exp\left[-\frac{\left(x_k^{(i)} - m_{F_k^l}\right)^2}{2\sigma^2_{F_k^l}} \right]} \tag{5.10}$$

where $i = 1, \ldots, R-p$, and $m_{F_k^l}$ and $\sigma^2_{F_k^l}$ are the mean and the variance of the antecedent k in the lth rule, respectively. With the given the input-output training pair $(\mathbf{x}^{(i)} : y^{(i)})$, the goal is to design the FLS in (5.10) such that the following error function is minimized;

$$e^{(i)} = \frac{1}{2}[f_s(\mathbf{x}^{(i)}) - y^{(i)}]^2 \tag{5.11}$$

Using a steepest decent algorithm to minimize $e^{(i)}$, it is straightforward to obtain the following recursions to update all the design parameters of this FLS;

$$\begin{aligned}
m_{F_k^l}(i+1) &= m_{F_k^l}(i) - \alpha_m[f_s(\mathbf{x}^{(i)}) - y^{(i)}][\bar{y}^l(i) - f_s(\mathbf{x}^{(i)})] \\
&\quad \times \frac{\left(x_k^{(i)} - m_{F_k^l}(i)\right)}{\sigma^2_{F_k^l}(i)} \ \phi_l(\mathbf{x}^{(i)})
\end{aligned} \tag{5.12}$$

$$\bar{y}^l(i+1) \;=\; \bar{y}^l(i) - \alpha_{\bar{y}}[f_s(\mathbf{x}^{(i)}) - y^{(i)}]\;\; \phi_l(\mathbf{x}^{(i)}) \tag{5.13}$$

and

$$\begin{aligned} \sigma_{F_k^l}(i+1) \;&=\; \sigma_{F_k^l}(i) - \alpha_\sigma[f_s(\mathbf{x}^{(i)}) - y^{(i)}][\bar{y}^l(i) - f_s(\mathbf{x}^{(i)})] \\ &\quad \times \frac{\left(x_k^{(i)} - m_{F_k^l}(i)\right)^2}{\sigma^3_{F_k^l}(i)}\;\; \phi_l(\mathbf{x}^{(i)}) \end{aligned} \tag{5.14}$$

where $\phi_l(\mathbf{x}^{(i)})$ is the fuzzy basis function and is expressed as;

$$\phi_l(\mathbf{x}^{(i)}) = \frac{\prod_{k=1}^p \exp\left[- \frac{\left(x_k^{(i)} - m_{F_k^l}\right)^2}{2\sigma^2_{F_k^l}} \right]}{\sum_{l=1}^M \prod_{k=1}^p \exp\left[- \frac{\left(x_k^{(i)} - m_{F_k^l}\right)^2}{2\sigma^2_{F_k^l}} \right]} \tag{5.15}$$

The parameters, $\alpha_m, \alpha_{\bar{y}}$, and α_σ are the learning parameters. Frequently, they are chosen to be the same, say α. Choosing to large α can cause the algorithm not to converge, whereas choosing too small a value of α can cause the algorithm to take a very long time to converge. Evidently, the choices of the initial values for $m_{F_k^l}(0)$,$\bar{y}^l(0)$, and $\sigma_{F_k^l}(0)$ also determine the convergence speed of the algorithm. Choosing these parameters smartly will help the algorithm converging faster.

Note that, in the back propagation algorithm just described, each of the $R-p$ training pairs is used only one time and the FLS parameters are updated using an error function that depends only on a pair of training data. If an *epoch* is defined as the collection of training pairs: it is said that the tuning process occurs for only one epoch. In fact, iterative tuning can also be performed by having several epochs (or just one epoch and use it repeatedly) and using the updated parameters obtained from the current epoch as the initial parameters for the next. To ensure the convergence of the error, the updated parameters from each epoch can be tested on the set of testing pairs associating with the training data in the epoch and the iterative tuning will continue until the error requirement is met.

5.3 Fuzzy Forecasting Reconstruction Algorithm

In CS reconstruction, the exact signal recovery can be guaranteed if the measurement matrix Φ obeys a restricted isometry property (RIP) of order $2K$, i.e. there exists a universal constant δ_{2K} such that for all $2K$-sparse signal $\mathbf{z}$

$$(1-\delta)\|\mathbf{z}\|_{l_2}^2 \leq \|\Phi\mathbf{z}\|_{l_2}^2 \leq (1+\delta)\|\mathbf{z}\|_{l_2}^2 \tag{5.16}$$

If Φ has small RIP constant δ_{2K}, it approximately maintains l_2 distances between K-sparse signals. Although verifying the RIP is mathematically complex, a surprising result is that random matrices, e.g. Gaussian random matrices [44], with sufficient number of rows and columns can achieve small RIP constants with overwhelming probability.

A recent emerged body of literature provides a variety of greedy techniques and the RIP guarantees that the greedy reconstruction algorithms robustly recover the signals. An example of these greedy techniques is the Compressive Sampling Matching Pursuit (CoSaMP)[52], which is the heart of the algorithm presented in this chapter.

The concept of the fuzzy forecasting reconstruction algorithm is shown in Algorithm 1. Similar to most greedy algorithms, after each iteration j, the algorithm finds an estimate $\hat{\mathbf{u}}^j$ of the target signal and its sparse support. Each iteration refines the estimate until the halting criterion is triggered; the algorithm then stops and yields the final estimate of the target signal.

As input, the algorithm requires five pieces of information, which are the noisy observation vector, the measurement matrix, the signal sparsity, the forecasted vector, and the rough estimate. Because the first three information are the standard inputs that are common for any CS reconstruction algorithm, there is no need for further

elaboration. Therefore, the attention should be directed to the last two pieces of information, which are required only in the algorithm proposed.

In details, the forecasted vector is merely the output forecasted values of the fuzzy logic forecaster for the pruned information vector $\mathbf{u}_p$. Even though there is an error associating in the forecasting process, the forecasted vector still can provide a very good intuition about the original signal without the presence of noise. The next piece of information required is the rough estimate input, which is used in the algorithm to provides an initial approximate of the whereabouts of the nonzero entries in the signal. The rough estimate can be obtained from a few iterations of the standard CS reconstruction (for example CoSaMP). Using the rough estimate, the algorithm simply extracts a set of indices of the nonzero entries and, by substituting the FLS forecasted values on these locations, it can then obtain a very good choice of the initial seed for the reconstruction process.

Now, consider the flow of the Algorithm 1 as shown below. In Line 1, the algorithm first locates the K nonzero entries by identifying the support of the rough estimate $\mathbf{u}_r$. Then, in Line 2, it substitutes these entries by K forecasted values obtained from the FLS forecaster. Line 3-5 initializes the parameters, e.g. the counter is reset, the initial estimate $\hat{\mathbf{u}}^0$ is set to the substitution result, and the algorithm calculates the initial residual $\mathbf{r}^0$, the part of signal that has not been approximated. To perform the reconstruction process, a loop is started in Line 6. In Line 8, the residual is weighted by Φ^* to form a proxy, which is used to identifies the largest components in the residual. Then, Line 9 combines the $2K$ support of the current estimate $\hat{\mathbf{u}}^{j-1}$ with the K support of the residual. Using the least-square technique, the signal is estimated in Line 10, based on the merged support T obtained from Line 9. Here, it is noted that $\Phi_T^\dagger = (\Phi^*\Phi)^{-1}\Phi^*$ is the pseudoinverse of the measurement matrix Φ. Subsequently, in Line 11, the resulting estimate is truncated to achieve

Algorithm 5.1: The Fuzzy forecasting Greedy Reconstruction Algorithm

Inputs: noisy observation $\mathbf{v}$, measurement matrix Φ,
signal sparsity K, rough estimate $\mathbf{u}_r$, forecasted vector $\mathbf{u}_f$

1: Identify the support of the rough estimation:
$S = \text{supp}(\mathbf{u}_r|_K)$
where $\text{supp}(\cdot)$ determines the support of a vector, and $\mathbf{x}|_K$ selects the K largest components, setting all others to 0
2: Substitute with the forecasted vector:
$\mathbf{u}_r|_S = \mathbf{u}_f$
3: Initialize:
$j = 0$ {initial count}
$\hat{\mathbf{u}}^0 = \mathbf{u}_r$
$\mathbf{r}^0 = \mathbf{v} - \Phi\,\hat{\mathbf{u}}^0$
6: **while** not converged
7: Increase iteration count:
$j \leftarrow j + 1$
8: Find signal proxy:
$\mathbf{z} = \Phi^*\,\mathbf{r}^{j-1}$
9: Identify and merge the support:
$T = \text{supp}(\mathbf{z}|_{2K}) \cup \text{supp}(\hat{\mathbf{u}}^{j-1}|_K)$
10: Perform least-square estimation:
$\mathbf{b}|_T = \Phi_T^\dagger\,\mathbf{v}$ and $\mathbf{b}|_{T^c} = 0$
11: Truncate and update the estimate:
$\hat{\mathbf{u}}^j = \mathbf{b}|_K$
12: Find residual:
$\mathbf{r}^j = \mathbf{v} - \Phi\,\hat{\mathbf{u}}^j$

Output: K-sparse estimate $\hat{\mathbf{u}}^j$

the support of K and is updated as the new estimate. Finally, Line 12 calculates the new residual corresponding to the new estimate. The procedures in Line 7-12 will be repeated over and over until the error is converged or the halting criterion is triggered.

5.4 Experimental Results

To validate the performance of the fuzzy forecasting algorithm, consider an example of a time series data. Let assume the K nonzero data points in the pruned

information vector $\mathbf{u}_p$ form a group of time-series data, for example daily temperatures or stock indices. Apparently, each measurement in the time series is correlated to the previous measurements and the FLS is used to construct a set of rules that can emulate the relationship between each measurement and its predecessors.

The Mackey-Glass discrete equation in (5.17) is used to generate the set of time-series data (see Chapter 4.2.2 in [56]). The Mackey-Glass time series (for $\tau > 17$) exhibits a chaotic behavior and has become the benchmark problem for prediction in both the neural network and fuzzy logic fields.

$$u_p(i+1) = u_p(i) + \frac{0.2u_p(i-\tau)}{1+[u_p(i-\tau)]^{10}} - 0.1u_p(i) \tag{5.17}$$

With $\tau = 18$ and a random value of $u_p(0)$, a set of $1000 + K$ Mackey-Glass time series data points was generated. The first 1000 data points are used as the past pruned information (or the past $\mathbf{u}_p$) that is assumed to available at the CS reconstruction site, i.e. $T = 1000$, and the rest K points is used as the pruned information to construct a K-sparse information vector $\mathbf{u}$. Then, from the set of the past information, 500 input-output training pairs and 496 testing pairs were formed.

In designing the FLS, the size of correlation window p was set to four. That is, the current data point of the time series is presumed to be determined by its four predecessors. In other word, the FLS forecaster was designed based on the use of four antecedents. For each antecedent, two fuzzy sets, which can be characterized by a Gaussian membership function (GMF), were used. Therefore, $2^4 = 16$ rules can be setup for the fuzzy logic forecaster. Apparently, each rule is characterized by eight antecedent membership function parameters, which are the mean and the standard deviation (SD) for each of the four GMFs and one consequent parameter $\bar{y}$.

The initial location of each antecedent GMFs was chosen based on the mean m_u and the SD σ_u of the data that is used for training the FLS. Specifically, the

Table 5.1. The FLS Forecaster Design

No. of antecedents	4
No. of rules	16
No. of training pairs	500 pairs (504 data points)
No. of testing pairs	496 pairs (496 data points)
Initial means of each MF	$m_u - \sigma_u$ and $m_u + \sigma_u$
Initial SD of each MF	$2\sigma_u$
Center of the consequent MF	random in $[0, 1]$
Learning parameter	$\alpha = 0.2$

mean of each and every antecedent's two GMFs were initialized to $m_1 = m_u - \sigma_u$ and $m_2 = m_u + \sigma_u$ and their SDs were set to $2\sigma_u$. For the consequent parameter, the center of each consequent's membership function ($\bar{y}_i, i = 1$ to 16) was initialized to a random number in the range of [0,1]. Based on these initial values, the forecaster was then tuned using the back propagation method and the iterative tuning. Table 5.1 summarizes the FLS forecaster design.

As an illustration, a series of simulations were performed to compare the proposed approach with the standard CoSaMP algorithm. The experiments use the Gaussian IID random measurement matrices (see [44]) of varying dimensions M and N. Each measurement matrix satisfies the RIP in (5.16). The sparse information vector is generated by using the K time series data points and padding zeroes onto some random indices to make a length of N. The compression process is performed according to (5.1) and, to obtain a noisy observation vector, a zero-mean Gaussian noise $\mathbf{n}$ is added to the compression result. The noise power is defined through the SNR as

$$SNR = 20 \log(\frac{||\mathbf{\Phi u}||_{l2}}{||\mathbf{n}||_{l2}}) \tag{5.18}$$

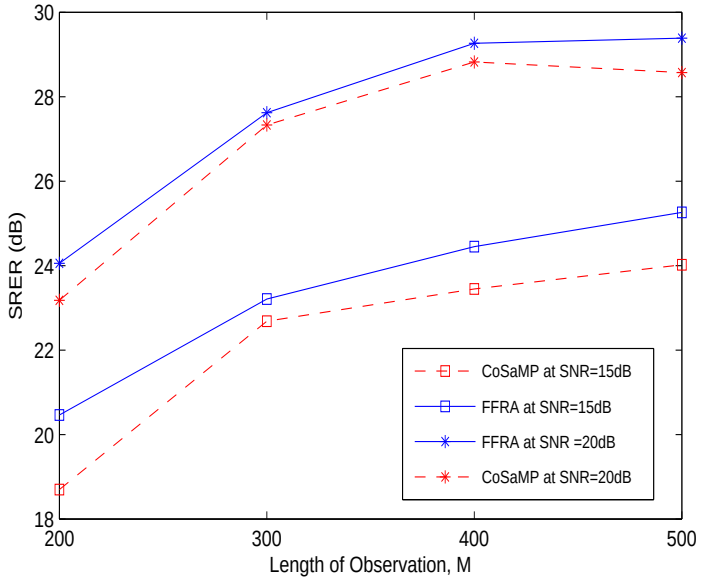

Figure 5.2. The plot of signal-to-reconstruction-error ratio for varying observation length M, with fixed $N = 1000$ and $K = 30$.

Two sets of experiments have been performed. In the first set, the sparsity and the length of the information vector are fixed to $K = 30$ and $N = 1000$ then varied the length of observation vector in four steps $M = 200, , 300, 400, 500$. In the second set of experiments, the length of the information is fixed at $N = 1000$ and the length of the observation is fixed at $M = 300$ then the information sparsity is changed in four steps $K = 20, 30, 40, 50$. For each choice of M and K, a different set of $\Phi, \mathbf{u}$, and $\mathbf{n}$, was generated; consequently, the FLS was also tuned to each data set.

To measure the performance of each algorithm, a signal-to-reconstruction-error ratio (SRER) is defined as

$$SRER = 20 \log\left(\frac{\|\Phi \mathbf{u}\|_{l2}}{\|\mathbf{u} - \hat{\mathbf{u}}\|_{l2}}\right) \tag{5.19}$$

Figure 5.2 illustrates the fuzzy forecasting reconstruction algorithm can outperform the standard CoSaMP algorithm. It can be seen that for SNR=15 dB, which is typical for many of wireless communication networks, the SRER of the proposed

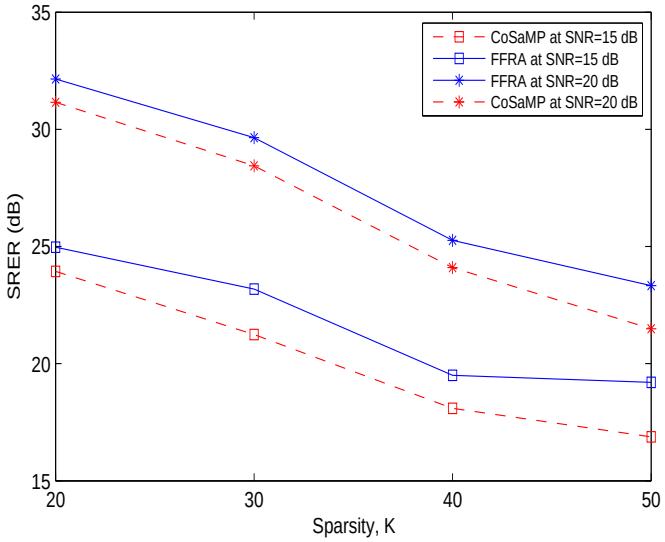

Figure 5.3. The plot of signal-to-reconstruction-error ratio for varying sparsity K, with fixed $N = 1000$ and $M = 300$.

algorithm is approximately 2 dB higher than that of the standard CoSaMP. However, the difference is lower when SNR increases to 20 dB; this is because the CoSaMP performs better at higher SNR. It is also noted that as M varies, the information becomes less compressive; thus, the reconstruction error reduces and the SRER level increases.

In contrary, Figure 5.2 displays the result when the sparsity changes. While K increases, there is more and more information contained in the original information vector $\mathbf{u}$. However, because the number of observation M is fixed, this is why the SRER decreases. However, it can be seen that the fuzzy forecasting reconstruction algorithm can still outperform the standard CoSaMP algorithm, especially when the noise power is high. Thus, from these experiments, it can be concluded that the proposed method can help improving the reconstruction process.

5.5 Conclusions

Compressive sensing is a potential choice of source encoding technique in wireless communications. However, due to small operating SNR levels of many wireless systems, the reconstructed information may become erroneous, especially when an OMP-based reconstruction algorithm is used. In this chapter, a fuzzy forecasting reconstruction algorithm, which helps improving the OMP reconstruction process, is proposed. Relying on a collection of the less noisy past information, the algorithm extracts the knowledge about the values of the current compressed information then, using such knowledge together with the noisy observation received, it can better extract both the values and the locations of the sparse coefficients in the information vector. The simulation results have shown that, compared to a standard OMP algorithm performance, an improvement in the ratio of signal to reconstruction error of up to 2 dB, depending on the noise level of the system and the compression parameters, can be achieved using the proposed approach.

REFERENCES

[1] R. Robertson and J. Sheltry, "Multitone interference of frequency-hopped noncoherent MFSK signals transmitted over Ricean fading channels." vol. 44, pp. 867–875, July 1996.

[2] A. Ali, "Worse-case partial-band noise jamming of Rician fading channels." vol. 44, pp. 974–978, June 1996.

[3] T. Tjhung and C. Chai, "Multitone jamming of FH/BFSK in Rician channels." vol. 47, pp. 974–978, July 1999.

[4] Z. Yu, T. Tjhung, and C. Chai, "Independent multitone jamming of FH/MFSK in Rician channels." vol. 49, pp. 2006–2015, Nov. 2001.

[5] K. Ramachandran, E. Belding, K. Almeroth, and M. Buddhikot, "Interference-aware channel assignment in multi-radio wireless mesh networks." in *Proc. IEEE INFOCOM'06*, Barcelona, Spain, Apr. 2006, pp. 1–12.

[6] A. Subramanian, H. Gupta, S. Das, and J. Cao, "Minimum interference channel assignment in multiradio wireless mesh networks." vol. 7, pp. 481–490, Dec. 2008.

[7] J. Proakis, *Digital Communications, 2nd ed.* New York: McGraw-Hill, 1989.

[8] I. Gradshteyn and I. Ryzhik, *Table of Integrals, Series, and Products; Alan Jeffrey, editor (translated from the Russian by Scripta Technica, Inc.* Boston: Academic Press, 1994.

[9] I. Akyildiz, X. Wang, and W. Wang, "Wireless mesh networks: A survey." *Computer Networks*, vol. 47, pp. 445–487, Mar. 2005.

[10] "Channel overlap calculations for 802.11b networks." White Paper, Cirond Technologies Inc., Feb. 2002.

[11] B. Crow, I. Widjaja, J. Kim, and P. Sakai, "Ieee 802.11 wireless local area networks." vol. 35, pp. 116–126, Sept. 1997.

[12] M. Schwartz, *Mobile Wireless Communications.* New York: Cambridge University Press, 2005.

[13] A. Mishra, V. Shrivastava, S. Banerjee, and W. Arbaugh, "Partially overlapped channels not considered harmful." in *SIGMETRICS Perform. Eval. Rev*, 2006, pp. 63–74.

[14] H. Skalli, S. Ghosh, S. Das, L. Lenzini, and M. Conti, "Channel assignment strategies for multiradio wireless mesh networks:issues and solutions." vol. 45, pp. 86–95, Nov. 2007.

[15] S. Avallone and I. F. Akyildiz, "A channel assignment algorithm for multi-radio wireless mesh networks." in *Computer Communications*, 2008, pp. 1343–1353.

[16] S. Alamouti, "A simple transmit diversity technique for wireless communications." vol. 16, pp. 1451–1458, Oct. 1998.

[17] V. Tarokh, H. Jafarkhani, and A. Calderbank, "Space-time block coding for wireless communications: Performance results." vol. 17, pp. 451–460, Mar. 1999.

[18] D. Tse and P. Viswanath, *Fundamentals of Wireless Communication.* New York: Cambridge University Press, 2005.

[19] H. Jarfarkhani, *Space-Time Coding: Theory and Practice.* New York: Cambridge University Press, 2005.

[20] M. Simon and M. Alouini, *Digital communication over fading channels, 2nd Edition.* Wiley Interscience, 2005.

[21] A. Leon-Garcia, *Probability and Random Processes for Electrical Engineering, 2nd Edition.* Addison-Wesley, 1994.

[22] J. Li, K. Letaief, , and Z. Cao, "Adaptive cochannel interference cancellation in space-time coded communication systems." vol. 50, pp. 1580–1582, Oct. 2002.

[23] P. Gupta and P. Kumar, "The capacity of wireless networks." vol. 46, pp. 388–404, Mar. 2000.

[24] L. Xie and P. Kumar, "A network information theory for wireless communication: Scaling laws and optimal operation." vol. 50, pp. 748–767, May 2004.

[25] M. Franceschetti, O. Dousse, D. Tse, and P. Thiran, "Closing the gap in the capacity of wireless networks via percolation theory." vol. 53, pp. 1009–1018, Mar. 2007.

[26] M. Grossglauser and D. Tse, "Mobility increases the capacity of ad-hoc wireless networks." vol. 10, pp. 477–486, Aug. 2002.

[27] O. L. A. Ozgur and D. Tse, "Hierarchical cooperation achieves linear capacity scaling in ad hoc networks." in *Proc. INFOCOM'07*, 2007, pp. 382–390.

[28] S. Shakkottai, X. Liu, and R. Srikant, "The multicast capacity of large multihop wireless networks." in *Proc. ACM MOBIHOC'07*, 2007, pp. 247–255.

[29] X. Mao, X.-Y. Li, and S. Tang, "Multicast capacity for hybrid wireless networks." in *Proc. ACM MOBIHOC'08*, 2008, pp. 189–198.

[30] B. Liu, Z. Liu, and D. Towsley, "On the capacity of hybrid wireless networks." in *Proc. INFOCOM'03*, 2003, pp. 1543–1552.

[31] B. Liu, P. Thiran, and D. Towsley, "Capacity of wireless ad hoc network with infrastructure." in *Proc. ACM MOBIHOC'07*, 2007, pp. 239–246.

[32] U. Kozat and L. Tassiulas, "Throughput capacity of random ad hoc networks with infrastructure support." in *Proc. MOBICOM'03*, 2003, pp. 55–65.

[33] A. Zemlianov and G. de Veciana, "Wireless networks with infrastructure support." vol. 23, pp. 657–667, Mar. 2005.

[34] X.-Y. Li, S.-J. Tang, and O. Frieder, "Multicast capacity for large scale wireless ad-hoc networks." in *Proc. ACM MOBICOM'07*, 2007, pp. 266–277.

[35] T. Le and Y. Liu, "On the capacity of hybrid wireless networks with opportunistic routing." *EURASIP Journal on Wireless Comm. and Networking*, vol. 2010, pp. 210–223, Apr. 2010.

[36] S. Weber, X. Yang, J. G. Andrews, , and G. de Veciana, "Transmission capacity of wireless ad hoc networks with successive interference cancellation." vol. 53.

[37] J. Blomer and N. Jindal, "Transmission capacity of wireless ad hoc networks: Successive interference cancellation vs. joint detection." in *Proc. ICC'09*, 2009, pp. 1–5.

[38] T. Cover and J. Thomas, *Elements of Information Theory, 2nd Edition.* New Jersey: Wiley, 2006.

[39] T. Cormen, C. Leiserson, R. Rivest, and C. Stein, *Introduction to Algorithms, 2nd Edition.* Massachusetts: MIT Press, 2001.

[40] F. Xue and P. R. Kumar, *Scaling Laws for Ad Hoc Wireless Networks: An Information Theoretic Approach.* Massachusetts: Foundation and Trends in Networking, 2006.

[41] P. Gupta and P. Kumar, "Critical power for asymptotic connectivity." in *Proc. Decision and Control*, 1998, pp. 1106–1110.

[42] E. Candés, J. Romberg, , and T. Tao, "Robust uncertainty principles: Exact signal reconstruction from highly incomplete frequency information." vol. 52, pp. 485–509, Feb. 2006.

[43] D. Donoho and X. Huo, "Uncertainty principles and ideal atomic decomposition." vol. 52, pp. 2845–2862, Nov. 2001.

[44] E. Candés and T. Tao, "Near-optimal signal recovery from random projections: Universal encoding strategies?" vol. 52, pp. 5406–5424, Dec. 2006.

[45] G. Golub and C. V. Loan, *Matrix Computations.* Maryland: John Hopkins University Press, 1983.

[46] E. Candés and T. Tao, "Decoding by linear programming." vol. 51, pp. 4203–4215, June 2005.

[47] E. Candés, T. T. R. Mark, and R. Vershynin, "Error correction via linear programming." in *IEEE Symposium on Foundations of Computr Science FOCS'05*, 2005, pp. 295–308.

[48] D. Donoho, "Compressed sensing." vol. 52, pp. 1289–1306, Apr. 2006.

[49] G. Cormode and S. Muthukrishnan, "Combinatorial algorithm for compressed sensing." in *Proceeding of the 40th Annual Conference on Information Sciences and Systems*, 2006, pp. 198–201.

[50] S. Sarvotham, D. Baron, and R. Baraniuk, "Compressed sensing reconstruction via belief propagation." *N/A.*, vol. N/A, p. N/A, July 2006.

[51] D. Needell and R. Vershynin, "Uniform uncertainty principle and signal recovery via regularized orthogonal matching pursuit." *Appl. Comp. Harmonic Anal.*, vol. 52, p. preprint, Sept. 2007.

[52] D. N. J. Tropp and R. Vershynin, "Iterative signal recovery from incomplete and inaccurate measurements." in *Information Theory and Apllications Workshop*, 2008, pp. 1–25.

[53] D. Needell and J. A. Tropp, "Cosamp:iterative signal recovery from incomplete and inaccurate samples." *Appl. Comp. Harmonic Anal.*, vol. 52, pp. 301–321, Sept. 2009.

[54] Q. Liang, "Ad-hoc wireless network traffic-self-similarlity and forecasting." vol. 6, pp. 297–299, July 2002.

[55] Q. Liang and L. Wang, "Sensed signal strength forecasting for wireless sensors using interval type-2 fuzzy logic system." in *IEEE International Conference on Fuzzy Systems, 2005*, 2005, pp. 25–30.

[56] J. M. Mendel, *Uncertain Rule-Based Fuzzy Logic Systems: Introduction and New Directions.* New Jersey: Prentice-Hall, 2001.

[57] ——, "Fuzzy logic system for engineering: A tutorial." in *Proc. IEEE, 1995*, 1995, pp. 345–377.

[58] S. Houston, "Modulation techniques for communications, part 1: Tone and noise jamming performance of spread specturm M-ary FSK and 2, 4-ary DPSK waveforms." in *Proc. IEEE NAECON'75*, Dayton, Ohio, June 1975, pp. 51–58.

[59] B. Levitt, "FH/MFSK performance in multitone jamming." vol. 3, pp. 627–643, Sept. 1985.

[60] W. Stark, "Coding for frequency-hopped spread-spectrum communication with partial-band interference-partii: Coded performance." vol. 33, pp. 1045–1057, Oct. 1985.

[61] P. Crepeau, "Performance of FH/BFSK with generalized fading in worst case partial-band gaussian interference." vol. 8, pp. 884–886, June 1990.

[62] K. Teh, A. Kot, and K. Li, "Performance of FFH/BFSK product combining receiver over a Rician-fading channel with partial-band jamming." *Electron. Lett.*, vol. 33, pp. 935–937, May 1997.

[63] J. Padhye, S. Agarwal, V. Padmanabhan, L. Qiu, A. Rao, and B. Zill, "Estimation of link interference in static multi-hop wireless networks." in *Proc. ACM SIGCOMM'06*, 2005, pp. 305–310.

[64] G. Foschini, "Layered space-time architecture for wireless communications in a fading environment when using multi-element antennas." Bell Labs Tech. Journal, Aug. vol. 2, pp. 41-59, 1996.

[65] G. Foschini, G. Golden, R. Valenzuela, and P. Wolniansky, "Simplified processing for high spectral efficiency wireless communication employing multi-element arrays." vol. 17, pp. 1841–1852, Nov. 1999.

[66] H. Dai, A. Molisch, and H. Poor, "Downlink capacity of interference-limited MIMO systems with joint detection." vol. 3, pp. 442–453, Mar. 2004.

[67] R. Blum, "MIMO capacity with interference." vol. 21, pp. 793–801, June 2003.

[68] V. Tarokh, N. Seshadri, and A. Calderbank, "Space-time codes for high data rate wireless communication: Performance criterion and code construction." vol. 44, pp. 744–765, Mar. 1998.

[69] V. Tarokh, H. Jafarkhani, and A. Calderbank, "Space-time block codes from orthogonal designs." vol. 45, pp. 1456–1467, July 1999.

[70] J. Liang, J. Chen, and A. Paulraj, "A two-stage hybrid approach for CCI/ISI reduction with space-time processing." vol. 1, pp. 163–165, Nov. 1997.

[71] D. Gesbert, M. Shafi, D. Shiu, P. Smith, and A. Naguib, "From theory to practice: An overview of mimo space-time coded wireless systems." vol. 21, pp. 281–302, Apr. 2003.

[72] A. Raniwala and T. Chiueh, "Architecture and algorithms for an IEEE 802.11-based multi-channel wireless mesh network." in *Proc. IEEE INFOCOM'06*, 2005, pp. 2223–2234.

[73] J. Tropp and A. Gilbert, "Signal recovery from partial information via orthogonal matching pursuit." vol. 53, pp. 4655–4666, June 2007.

[74] R. Baranuik, "Compressive sensing." vol. 24, pp. 118–121, July 2007.

[75] E. Candés and M. Wakin, "An introduction to compressive sampling." vol. 24, pp. 21–30, Mar. 2008.

[76] R. Baranuik, M. Davenport, R. Devore, and M. Wakin, "A simple proof of the restricted isometry property for random matrices." *Constructive Approximation*, vol. 28, pp. 253–263, Dec. 2008.

[77] E. Candés and J. Romberg, "Sparse and incoherence in compressive sampling." *Inverse problem*, vol. 23, pp. 969–985, June 2007.

[78] P. Boufounos, "Reconstruction of sparse signals from distorted randomized measurements." in *ICASSP, 2010*, 2010, pp. 3998–4001.

BIOGRAPHICAL STATEMENT

Davis Kirachaiwanich was born in Bangkok, Thailand, in 1977. He received his B.S. degree from King Mongkut's University of Technology, Thonburi, Thailand, in 1998, and his M.S. from University of Florida, USA, in 2002, all in Electrical Engineering. From 2003 to 2007, he served as a research assistant in R&D wireless communication section at National Electronics and Computer Technology Center (NECTEC) in Thailand from which he has received a scholarship for pursuing on the doctoral degree. His current research interest is in the areas of compressive sensing, frequency-hopping communication, MIMO systems, and wireless mesh networks.